1962

Cohesion in the intermetallic series Mg2Si, Mg2Ge, Mg2Sn, and Mg2Pb

Henry John Caulfield
Iowa State University

COHESION IN THE INTERMETALLIC SERIES

Mg_2Si, Mg_2Ge, Mg_2Sn, AND Mg_2Pb

by

Henry John Caulfield

A Dissertation Submitted to the

Graduate Faculty in Partial Fulfillment of

The Requirements for the Degree of

DOCTOR OF PHILOSOPHY

Major Subject: Physics

Approved:

Signature was redacted for privacy.

In Charge of Major Work

Signature was redacted for privacy.

Head of Major Department

Signature was redacted for privacy.

Dean of Graduate College

Iowa State University
Of Science and Technology
Ames, Iowa

1962

TABLE OF CONTENTS

I. INTRODUCTION

A. Cohesive Energy

1. Definition

The understanding of the forces which bind large numbers of atoms together as a solid is of fundamental importance in solid state physics. A useful measure of the strength of the bonding is the cohesive energy. The advent of powerful new experimental and theoretical techniques has led to greatly increased activity in the field of cohesion of solids.

The cohesive energy of an elemental solid is defined by Seitz (1) as the difference in energy between an atom of that element in its free ground state and an atom of that element in its normal state within its perfect crystal. Stated more pictorially, the cohesive energy is the work needed to remove an atom from its elemental crystal to a point of isolation from the crystal forces at zero degrees Kelvin. The requirement of zero temperature eliminates the consideration of excitation energies. The extension of the definition of cohesive energy of a one component solid to cover multicomponent solids must be performed with great care. First, a "molecule" or some other convenient unit of the solid must be selected. For the compound magnesium silicide, the "molecule" Mg_2Si is selected. That is the energy of the solid which will be of interest is the total energy, E_s, of two Mg atoms and one Si atom in a perfect, infinite Mg_2Si lattice. The device by which the energy of a piece of solid Mg_2Si may be partitioned in such a way that E_s is uniquely defined is discussed in Section IIB3 and in Appendix A. Second, a

gaseous state for the substance must be defined. In the case of Mg_2Si, the gaseous state which is of primary interest consists of two monomer Mg atoms and one monomer Si atom. The energy associated with this gaseous system if the gaseous atoms are separated sufficiently to eliminate interaction energies is defined as E_G. Finally, the cohesive energy per "molecule" of the solid is defined as $E_G - E_s$. Again the stipulation that E_G and E_s be measured at the absolute zero of temperature must be imposed to exclude excitation energies. In other words, the cohesive energy of Mg_2Si is the heat of the reaction $Mg_2Si(s) \rightarrow 2Mg(v) + Si(v)$ carried out at $T = 0$.

Until recently the theory of cohesion of solids has relied on phenomenological and semi-empirical methods. Promising new methods of calculation may allow the theory to catch up with the great abundance of experimental data now on hand. Experimental observation can be most useful to the theorist if it is made on substances of a similar nature such as the intermetallic series which is the subject of this investigation.

In the following sections a brief survey of the theoretical situation in cohesive energies will be presented.

2. Cohesion in elemental solids

The equilibrium configuration of a solid is determined by minimizing a total energy expression which consists of both attractive and repulsive parts. It is usually useful to think of these interactions as arising among the valence electrons and the ionic cores. The repulsion arises from electron-electron and core-core effects. The

attraction is a result of the electron-core interaction. The form of this latter interaction is called the bonding type of the crystal. Bonding types are seldom embodied in pure form in any real crystal, but the dominant bonding type often determines the crystal structure (2) as well as other important physical properties. It will be seen in a following section that the inverse operation (inferring bonding types from physical properties) is by no means simple.

Many solids follow the 8N rule of Bradley and Hume-Rothery (3) which states that elements in group N of the periodic table tend to form a crystal such that each atom has 8N nearest neighbors. In this case the electrons are being shared between neighboring atoms to complete stable octets of electrons. This sharing of electrons is called covalent bonding. Covalent bonding is not limited to those cases in which the 8N rule is obeyed. Indeed covalent bonding appears to contribute to some degree to the cohesion of most solids.

Atoms in groups I, II, and III do not possess enough valence electrons to share with their neighbors to produce electron octets. In such cases the electrons tend to be shared equally among all of the atoms. These electrons are then relatively free to move about through the crystal. These "free" electrons produce the transport properties which characterize metals. The bonding arises from the attraction between the atomic cores and the swarm of electrons. Metallic bonding places no limit on the number of nearest neighbors, so size considerations may become the limiting factors. Metals form crystals with high coordination numbers; i.e. each atom has a high number of nearest

neighbors -- usually eight or twelve.

Pauling (4) observed that if the covalent bonding sites for a given electron are not limited to two for each electron as in normal covalent bonding but are essentially unlimited, then the bonding is metallic. Thus the difference between covalent bonding and metallic bonding is quantitative rather than qualitative in nature.

Weak bonding can arise from interaction of the electric dipole moment of an atom with the dipole moment it induces in its neighbors. The resulting electrostatic attraction gives rise to the van der Waals forces. The forces predominate among organic solids, but they may be present in inorganic crystals.

It is not proposed to discuss the various bonding types in detail. Such discussions are plentiful in the literature, e.g. covalent by Pauling (4), metallic by Brooks (5), and van der Waal by Born (6) and Bernardes (7).

3. Cohesion in compounds and alloys

The type of bonds formed by any element in its own pure solid or in a compound with other elements is determined (in part) by the tightness with which the valence electron is bound to the ion core. Loosely bound electrons are more likely to form metallic bonds than are tightly bound electrons. The ionization energy of an element is the energy with which the outer electron is bound to the ion core in a free atom of that element; therefore a knowledge of the ionization energies of various elements can be useful in the qualitative explanation of the bonding in the compounds of those elements. This section will describe what can be

predicted about the ionization energy of an element merely from the position of that element in the periodic table.

It is observed that elements of a given column in the periodic table tend to become more metallic (i.e. to have smaller ionization energies) toward the bottom of that column. All of the atoms in a given column have the same number of valence electrons, but the number of inner shells increases toward the bottom of the column. Within a given column the shielding of the nucleus is increased, and the ionization energy is decreased from top to bottom. Similarly the ionization energy increases from left to right along a given row in the periodic table. This is true because all of the valence electrons of atoms in a given row fall in the same shell. Therefore shielding increases only slightly from left to right, while the nuclear charge increases by e as each column is crossed. As expected, the elements at the upper right (helium, neon, fluorine) have the highest ionization energies, and those at the lower left (cesium, rubidium) have the lowest ionization potentials. The elements at the upper right are said to be strongly electronegative. This means that electrons are hard to remove from their cores. Electronegativity is used as a measure of the likelihood of forming covalent bonds. Pauling (4) has proposed a semi-empirical quantitative measure of electronegativity. Elements at the lower left of the periodic table are said to be highly electropositive. They receive large negative designations on Pauling's electronegativity scale. Electrons are comparatively easy to remove from the core of a highly electropositive element, so electropositive elements tend to form metallic bonds.

In a crystal consisting of atoms differing greatly in electronegativity a new type of bonding can arise. The more electropositive atom tends to give electrons to the more electronegative atom. The resulting ions are subject to Coulomb attraction. The bonding produced by this attraction is called ionic bonding. As might be expected from the above considerations, CsFl is the most ionic crystal. The cohesive energy of CsFl contains a covalent energy term of only a few per cent (2). Contributions to bonding from covalent and ionic types seem to be possible in any ratio.

Solid phases between metals with simple stoichiometries are often called intermetallic compounds. These are quite abundant within the "Zintl limit" (8). The Zintl limit limits the possible "negative ions" for intermetallic compounds to only such elements as lie one to four places before the rare gases in the periodic table. The bonding in the intermetallics is nearly always a mixture of ionic, covalent, and metallic. Some van der Waals bonding may also be present.

The systematic study of cohesion in the intermetallics would be facilitated by cohesive energy data on families of compounds keeping the crystal structure and one element constant. The Mg_2X series (X = Si, Ge, Sn, or Pb) is such a series.

4. Calculation of cohesive energies

a. Introduction Two basic types of cohesive energy calculations are in use. The older and more common methods involve approximations based on some assumed bonding mechanism. Two examples of this type of calculation will be discussed - for ionic bonding and for metallic

bonding. These examples of approximate cohesive energy calculation indicate certain limitations which inhere in such approximate calculations. Finally an example of the newer, more exact cohesive energy calculations will be discussed.

b. Ionic bonding The calculation of the cohesive energy of an ionic crystal is particularly simple, but this calculation is typical of approximate methods in many respects. The interaction energy between ions i and j in an ionic crystal is called ϕ_{ij}. Hence the energy of the i'th ion is

$$\phi_i = \Sigma' \phi_{ij},$$

where $\Sigma_j' \phi_{ij}$ is defined as

$$\Sigma_j' \phi_{ij} \equiv \Sigma_j \phi_{ij} - \phi_{ii}$$

The coulomb part of the interaction energy ϕ_{ij} is $\pm e^2/r_{ij}$ is the distance between ions i and j. A repulsive contribution to the interaction energy ϕ_{ij} is assumed in order to assure a stable solid. A convenient and sufficiently accurate approximation for the repulsive contribution to ϕ_{ij} is λ/r_{ij}^n, where λ and n are undetermined parameters. ϕ_i is the same whether i is a positive ion or a negative ion; therefore the total energy of the crystal is

$$U = \tfrac{1}{2}\Sigma_{ij}' \phi_{ij} = N\phi_i,$$

where N is the number of ion pairs. It is convenient to express the distances r_{ij} in terms of some length characteristic of the lattice, say

the lattice parameter. This characteristic distance is called R, and the distance r_{ij} is defined as $r_{ij} = P_{ij}R$. Therefore,

$$\phi_{ij} = \frac{1}{P_{ij}^{n}} \frac{\lambda}{R^{n}} \pm \frac{1}{P_{ij}} \frac{e^2}{R} .$$

Thus,

$$U = N\frac{\lambda A_n}{R^n} - \frac{\alpha e^2}{R} ,$$

where A_n is defined as $\Sigma_j' P_{ij}^{-n}$ and α is defined as $\Sigma_j' (\pm) P_{ij}^{-1}$. The quantity α is called the Madelung constant. The indicated expression for α converges very slowly, so trick methods are used to evaluate α. At equilibrium $\partial U / \partial R = 0$. This condition allows the parameter λ to be evaluated in terms of α, n, and R_o the equilibrium value for R. The equation for U is

$$U = N\frac{\alpha e^2}{R^o}(1 - \frac{1}{n}).$$

The parameter n is determined by comparison of compressibility derived from this expression for U with experimental values of the compressibility. The values of U for alkali halides obtained in this manner are in close agreement with experimentally determined cohesive energies.

c. Metallic bonding A useful method for calculating the cohesive energy of a metal was devised by Wigner and Seitz (9). The metallic crystal is divided into cells which completely fill the lattice. Usually these cells are polyhedra formed by the perpendicular bisector planes of lines joining each atom to its nearest neighbors. In some cases the cells are polyhedra formed by the perpendicular bisector planes

of lines joining each atom to its nearest and next nearest neighbors. The criterion to decide whether the bisectors of the lines to the next nearest neighbor should be included is that the atomic polyhedron should be the more spherical of the two possible polyhedra for any lattice. Near the polyhedron boundary the field due to the ion core at the center of the polyhedron is small. Near the center of the polyhedron the field is spherically symmetric. In the Wigner-Seitz method the field is taken to be V(r) throughout the polyhedron. Wigner and Seitz showed that it is a good approximation to take V(r) as the potential of the free singly-charged positive ion of the metal (9). The wave function, ψ, of the lowest electronic state in the metal must cross smoothly from one polyhedron to another. The requirement of smooth joining imposes the condition that $\partial\psi/\partial n = 0$, where $\partial/\partial n$ means differentiation normal to a bounding plane of the polyhedron evaluated at that bounding plane. Since the polyhedra approximate closely to spheres, it is a good approximation to replace the polyhedron by a sphere of equal volume. The boundary condition $\partial\psi/\partial n = 0$ becomes

$$\left(\frac{\partial\psi}{\partial r}\right)_{r=r_o} = 0,$$

where r_o is the radius of the sphere. This boundary condition can be applied to solutions to the Schroedinger equation

$$\frac{1}{r^2}\frac{d}{dr}\left(r^2\frac{d\psi}{dr}\right) + \frac{2m}{\hbar^2}\left[E - V(r)\right]\psi = 0$$

Here E is the energy of the lowest ground state. The calculation of cohesive energy from the value of E is illustrated in Section VI. The

Wigner-Seitz method of cohesive energy calculation for divalent metals is simply a modification of the Wigner-Seitz method for monovalent metals (10). A critique of the accuracy of the Wigner-Seitz method is available (11).

d. Many electron systems Various methods now exist which allow rigorous solutions to many-electron Schroedinger equations to be derived. These rigorous solutions provide information on the cohesive energy without the necessity of assuming a priori that some particular bond mechanism is involved in the solid under consideration. Indeed the solution of the quantum mechanical problem provides information on the bonding mechanism(s) rather than vice versa.

As a particular example of the rigorous solution of many-electron Schroedinger equations, this section will examine the method due to Ruedenberg (12). Ruedenberg's solutions are expansions of the appropriate atomic orbitals. In the method of Ruedenberg the electron-density operator and electron-pair-density operator of Lowdin (13) and McWeeny (14) are portioned into fragments subject to physical interpretation.

A simple application of the Ruedenberg method to the ion H_2^+ can be used to illustrate the basic features of the method. The atomic orbitals chosen for the two hydrogen are called A and B. The wave function for the electron is defined to be

$$\varphi \equiv \frac{1}{2(1 + S)} (A + B),$$

where the numerical factor S, called the overlap integral, is a dimensionless quantity. The Hamiltonian H is given by

$$H = T - \frac{e^2}{r_A} - \frac{e^2}{r_B} + \frac{e^2}{R_{AB}},$$

where R_{AB} is the distance between the nuclei, r_A is the distance of the electron from nucleus A, r_B is the distance of the electron from nucleus B, T is the kinetic energy of the electron, and e is the electronic charge. The electron density ρ is given by

$$\rho = \varphi^2 = \tfrac{1}{2}(A^2 + B^2) + \frac{1}{1+S}\left[\frac{AB + BA}{2} - \tfrac{1}{2}S(A^2 + B^2)\right].$$

Ruedenberg breaks ρ into a classical part, $\frac{1}{2}(A^2 + B^2)$, and a part which arises from interference, $\frac{1}{1+S}\left[\frac{AB + BA}{2} - \frac{S}{2}(A^2 + B^2)\right]$. The total energy, E, of the electron is given by

$$E = \int \varphi^* H \varphi \, dV = \int \varphi^* T \varphi \, dV - \int \varphi^* \frac{e^2}{r_A} \varphi \, dV - \int \varphi^* \frac{e^2}{r_B} \varphi \, dV + \frac{e^2}{R_{AB}} \int \varphi^* \varphi \, dV.$$

By definition

$$\int \varphi^* \varphi \, dV = 1.$$

The terms in the expression for E can be broken up in a manner analagous to the partitioning of ρ. The result of this partitioning of the terms in the expression for E is

$$E = E_A + E_B + E_{AB}^{Cl} + E^I + E^{II},$$

where each of these quantities is explained below. By definition,

$$E_A \equiv \tfrac{1}{2}(A|T|A) + \tfrac{1}{2}\left(A\left|-\frac{e^2}{r_A}\right|A\right)$$

The quantity E_A is simply the classical hydrogen atom energy $\left(A\left|-\frac{e^2}{r_A}\right|A\right)$

plus a so-called promotion energy $(A|T|A)$. The factor $\frac{1}{2}$ occurs in the formula for E_A because the total energy E arises not only from A but also from B. E_B is defined in exact analogy to E_A. The quantity E_{AB}^{Cl} is called the quasiclassical interaction. By definition,

$$E_{AB}^{Cl} \equiv \tfrac{1}{2}\int dV \left[A^*\left(\frac{-e^2}{r_B}\right)A + B^*\left(\frac{-e^2}{V_A}\right)B \right] + \frac{e^2}{R_{AB}} .$$

The term E_{AB}^{Cl} corresponds to Coulomb interaction between the electron at one nucleus and the positive charge at the other nucleus and to nuclear repulsion. The interference energy, E^I, is, by definition,

$$\frac{1}{1+S}\left[\tfrac{1}{2}(A|H'|B) + \tfrac{1}{2}(B|H'|A) \right] ,$$

where

$$H' = T - \frac{e^2}{r_A} - \frac{e^2}{r_B} .$$

Finally the energy E^{II} is defined as all of the remaining terms in the expression for E, i.e.

$$E^{II} = -\frac{S}{1+S}\tfrac{1}{2}(A|H'|A) + \tfrac{1}{2}(B|H'|B) .$$

The further subdivision and study of the various terms is beyond the scope of this thesis.

The application of the method of Ruedenberg to the Mg_2Sn crystal is now being attempted*. Precise wave functions for Mg_2Si are being sought

*Ruedenberg, Klaus, Department of Chemistry, Iowa State University of Science and Technology, Ames, Iowa, Electronic Structure of Solids. Private communication. 1961.

in a different way by Dr. J. M. Keller**.

B. Cohesion and the Physical Properties of the Mg_2X Series

In this section an attempt will be made to infer as much as possible about the bonding in the Mg_2X series from the known physical properties of Mg_2X. The theory of the electronic structure of compounds is not so well developed that final assertions on the bonding can be made on the basis of the physical properties of the Mg_2X series, but the bonding cannot be inconsistent with the other physical properties.

All four of the Mg_2X compounds are anti-isomorphic to the flourspar (CaF_2) lattice. Figure 1 shows a unit cell of Mg_2X. The structure assumed by the Mg_2X compounds is a common structure for ionic crystals. In Mg_2X and in other cases of intermetallic compounds between substances differing considerably in electronegativity, the electronegative component tends to form a close-packed structure. There may develop van der Waals type of attraction between the anions, as is favored by the close packing. According to Raynor (15) these van der Waals attractions may transform gradually and continuously into the metallic type of bonding by the process of loosely bound electrons becoming effectively under the control, not of one nucleus, but of several. Of the four compounds Mg_2Si, Mg_2Ge, and Mg_2Sn are semiconductors, but Mg_2Pb displays metallic conduction.

**Keller, Joseph M., Department of Physics, Iowa State University of Science and Technology, Ames, Iowa. Electronic Structure of Mg_2Si. Private communication. 1962.

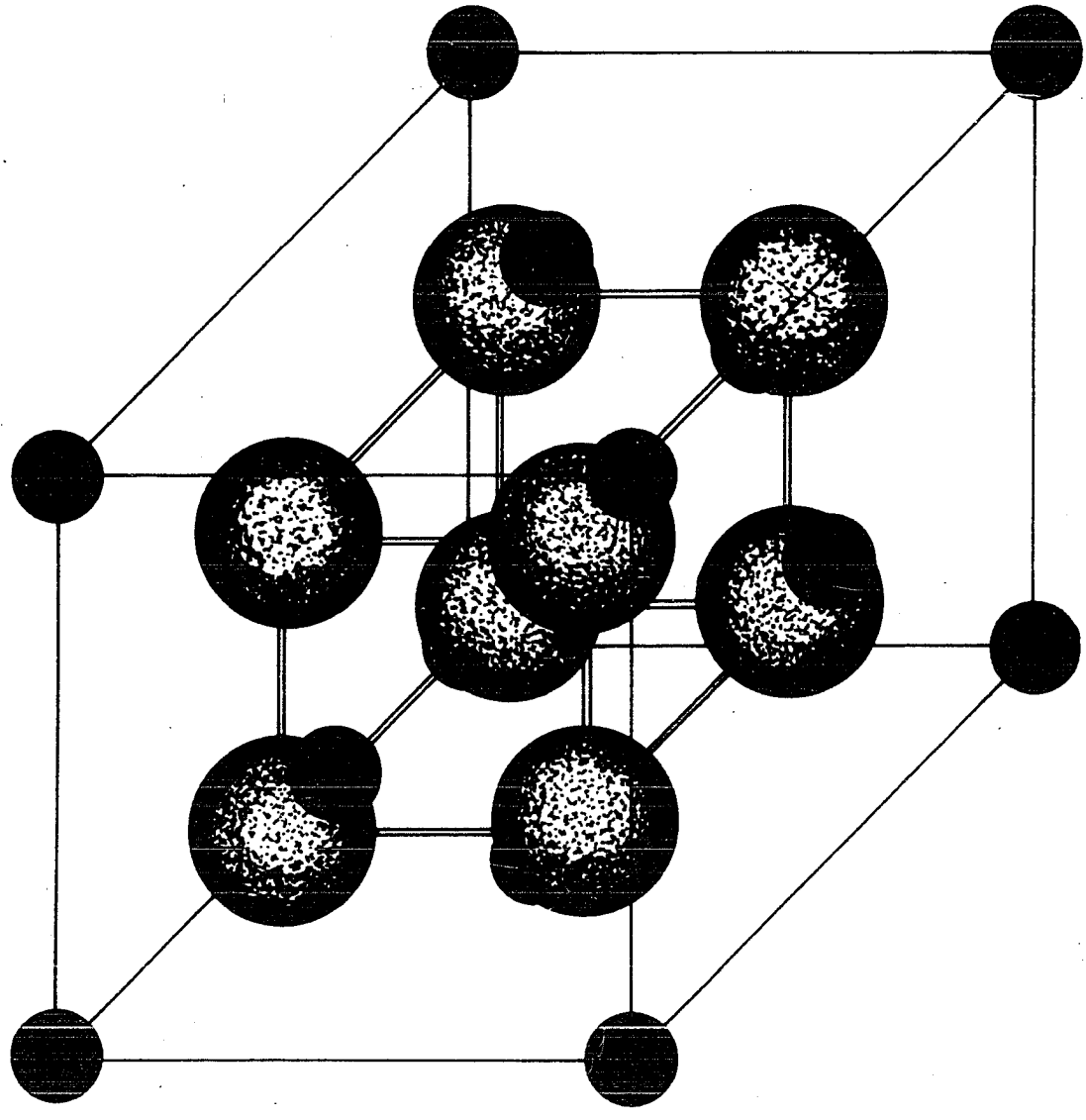

Figure 1. Unit cell of Mg_2X. The larger spheres represent Mg atoms

Boltaks (16) examined the electrical and magnetic properties and the boiling point of Mg_2Sn. He concluded that Mg_2Sn involves metallic as well as ionic bonding. Boltaks' conclusion seems to support the theory of gradual transition from largely ionic Mg_2S; to largely metallic Mg_2Pb. Robertson and Uhlig (17) also believe that the physical properties of Mg_2Sn and Mg_2Pb indicate vast differences in their bonding mechanisms.

The interpretation of the electrical properties of the Mg_2X series as resulting from a gradual change from ionic to metallic bonding is not the only possible explanation. The semiconductivity of Mg_2Si, Mg_2Ge, and Mg_2Sn may arise from filled Brillouin zones rather than from ionic bonding. Mg_2Pb can then be viewed as having the same bonding type as the other compounds of the series but so low an energy gap that at room temperature it is a degenerate semiconductor. The Brillouin zone picture of the conduction properties of various crystals was formulated by Mott and Jones (18). Let W be the volume of a Brillouin zone and let V be the average atomic volume. Then there are 2WV states per atom in each energy band. If, on the average, each atom has R valence electrons, then the number of filled bands is $N = R/2WV$. If the cell edge dimension of the Mg_2X unit cell is a, then $V = a^3/12$ and $W = 4/a^3$. In Mg_2X one can regard the valences as -2 for Mg and -4 for X, so $\bar{R} = 1/3(2+2+4) = 8/3$. Then $N = 8/3/(2)(a^3/12)(4/a^3) = 4$. Thus Mg_2X has four filled energy bands. Thus Mg_2X might be expected to be a semiconductor. In fact Mg_2Si, Mg_2Ge, and Mg_2Sn are semiconducting. The systematic decrease in energy gap with electronegativity (Table 1) suggests the possibility that Mg_2Pb may indeed be degenerate. Further evidence that the conduction properties

Table 1. Energy gaps of the Mg_2X series

Mg_2X	Energy gap by conductivity (ev)	Energy gap by Hall effect (ev)
Mg_2Si	0.76[a]	0.77[a] 0.78[b]
Mg_2Ge	0.74[a]	0.74[a] 0.69[b]
Mg_2Sn	0.36[a]	0.36[a]
Mg_2Pb	0?	0?

[a]Data from Raynor (19). [b]Data from Morris, Redin, and Danielson (72,73).

of Mg_2X are due to zone considerations rather than bonding types is given by Raynor (19). Melting of Mg_2Sn destroys the zone structure and thus removes zone restrictions on the excitation of electrons. Upon melting, Mg_2Sn shows a great rise in conductivity. If melting also destroyed the ionic bonding, this experiment could be explained by either of the two hypotheses mentioned so far; however such dissociation of salts on melting is not common. The conductivity σ of a dissociated melt should be given by $\sigma \cong \sigma_o e^{-B/kT}$ with no discontinuity at the melting point, where B is a constant of the material, k is the Boltzmann constant, and T is the absolute temperature. Such a discontinuity has been found experimentally.

A third approach to the relation of semiconductivity to bonding is also possible. Jaffe (20) attributes semiconductivity to the bonding rather than to the periodic character of the lattice. Mooser and

Pearson (21) trace the evolution of Jaffe's rough formulation in 1951 (22). This theory views bonding in semiconductors as essentially covalent. All that is required for semiconductivity is that at least one of the elements have its s and p bands filled and that the bonding not connect states with unfilled s and p bands. The covalent nature of the bonding may explain the Zintl limit (Section IA). For covalent bonding it is obvious that at least one member of the compound must lie within the Zintl limit. Let n_v be the number of valence electrons per molecule. Let n_Z be the number of atoms per molecule within the Zintl limit. And let b be the number of bonds between the atoms within the Zintl limit per molecule. In order that the energy bands be filled, it must follow that $n_v/n_Z + b = 8$. For Mg_2X we have $n_v = 8$, $n_Z = 1$ and $b = 0$ for X = Si, Ge, or Sn. Each X employs all of its valence electrons in forming covalent sp^3 bonds which, by virtue of empty orbitals on Mg, are free to undergo resonance among eight positions. Thus the s and p shells of X are filled. Mg uses its two valence electrons in the covalent bonds with the X. Even though Mg contains empty orbitals, Mg_2X is semiconducting, because there are no electrons left to form Mg-Mg bonds. According to Mooser and Pearson the transition from semiconducting Mg_2Sn to conducting Mg_2Pb may involve a sort of band overlap. The next highest orbital of Pb other than the first s and the first three p states may lie close enough to these to allow considerable occupation. In this case the s and p shells of Pb will not be filled, so metallic conduction will occur even though there are no Mg-Mg bonds.

A direct approach to the problem of bonding types in Mg_2Si was

taken by Ageev and Guseva (23). Ageev and Guseva measured the electron distribution within the Mg_2Si lattice by x-ray analysis. The charge density between atoms and the directional variation in charge density lead them to attribute considerable covalent bonding to Mg_2Si. The known physical properties of Mg_2Si suggested to Krebs (24) that its bonding is essentially a resonance between $Mg^{++}(Si\text{-}Mg)^{--}\ Mg^{++}$. This bonding mechanism appears to differ little from the bonding mechanism suggested by Mooser and Pearson (22). Kubaschewski and Slowman (25) list Mg_2Si as having large ionic and covalent bonding terms. In Mg_2Sn the covalent term is less than those due to ionic and metallic bonding. The increasing part played by the metallic bonding as the electronegative element X in Mg_2X moves down column IV in the periodic table suggests strong metallic bonding in Mg_2Pb.

If, as assumed earlier, some of the crystalline bonding persists after melting, the internal friction of the melt can be made to yield some indication of the nature of that bonding. Gebhardt et al. (26) found evidence of strong ionic bonding in Mg_2Sn and Mg_2Pb in this manner.

The physical properties of the Mg_2X series which were examined in this section are manifestations of the electronic structure of Mg_2X. The bonding type is an incomplete characterization of the electronic structure; therefore the bonding type does not determine the other physical properties uniquely. The insufficiency of bonding mechanism to account for the other physical properties of a solid accounts for the ambiguities reported in this section in deriving bonding mechanisms from the known physical properties. Another complication which is illustrated

in this section is that the physical properties of the Mg_2X series are so complex that a mixture of several different bonding types is likely.

C. Experimental Methods

1. Introduction

The cohesive energy is an especially useful quantity to obtain if one wishes to study the cohesion of a particular solid. Section IIE3 will discuss a method whereby the cohesive energy can be obtained from calorimetry experiments. This section will duscuss the measurement of the heat of sublimation of a solid.

The heat of sublimation (or enthalpy of sublimation) is obtained from vapor pressure by the Clausius-Clapeyron equation (Section IIB),

$$\Delta H_T = -R \frac{d \ln P}{d (1/T)}$$

where ΔH_T is the heat of sublimation at the temperature T, R is the universal gas constant, and P is the saturated vapor pressure at the temperature T. Therefore ΔH_T can be derived from a knowledge of the temperature dependence of the vapor pressure. Fortunately, the temperature dependence of ΔH_T is such that a plot of lnP vs. 1/T will appear linear over a considerable temperature range. To within experimental accuracy, ΔH_T is the slope of the lnP vs. 1/T plot multiplied by the factor -1/R. The slope of the lnP vs. 1/T graph is unaffected if P is replaced by the quantity $P' = CP$, where C is some number independent of temperature. A quantity P' which differs from the true saturated vapor pressure only by a multiplicative constant is called the relative vapor

pressure. Since reasonable measurements of temperature are not especially difficult, this section will discuss the measurement of vapor pressures (actual or relative).

2. Direct measurement of vapor pressures

If the vapor pressure of a substance is sufficiently large, a direct measurement of the vapor pressure is possible. A substance under pressure P and at temperature T will boil if and only if P is less than or equal to the saturated vapor pressure at temperature T. Baur and Brunner (27) made highly accurate vapor pressure measurements on many common metals by observing the temperatures at which the metals boiled under known pressures of an inert gas. Other methods of direct measurement of saturated vapor pressures are abundant (11); however these methods are impractical for substances with vapor pressures as low as the pressures observed for Mg_2X.

3. Indirect measurement of vapor pressures

The direct manifestations of pressure (the boiling point of the substance, the height of a column of mercury, etc.) are very difficult to observe for extremely low vapor pressures. For materials too involatile to subject to direct pressure measurements, it is necessary to measure some quantity which can be measured more easily and which depends on the pressure in a known way. The extraction of vapor pressures from data on some pressure dependent quantity is called an indirect pressure measurement. Clearly the distinction between direct and indirect measurements is not sharp, but the distinction provides a useful insight into

measuring techniques.

The rate, dN/dt, at which atoms sublime from the surface of a solid is given by a formula derived from thermodynamics and the kinetic theory of bases (Sections IIA and IIC):

$$\frac{dN}{dt} = \frac{\beta P_e A}{\sqrt{2\pi mkT}}, \quad (1)$$

where P_e is the saturated vapor pressure at absolute temperature T, A is the surface area of the solid, m is the mass of subliming particle, and k is the Boltzmann constant. The quantity β ($\beta \leq 1$) is a unitless factor called the evaporation coefficient. The evaporation coefficient is a constant of the particular solid. In principle all of the quantities in Equation 1 are measurable, so P can be determined. The only temperature-dependent terms in the expression for dN/dt are P and T. Therefore the relative vapor pressure can be obtained by assigning an arbitrary value to the quantity $A/\sqrt{2\pi mk}$ in Equation 1. The expression for the pressure at temperature T then becomes

$$P = C \frac{dN}{dt} \sqrt{T}, \quad (2)$$

where C is a constant. Vapor pressure measurements using Equation 2 to relate P to the sublimation rate dN/dt are called Langmuir effusion measurements (28).

---

*The equations used in this thesis are independent of the units employed, so long as the units are consistent. For example if P is in dynes/cm^2, A is in cm^2, m is in gms, and k is in ergs/^{o}k, then dN/dt is in particles/sec.

If the solid sample is placed in a cell which is closed except for a single small orifice, the factor β in Equation 1 is absent in the expression for the rate at which atoms escape the cell through the orifice. In this case the rate dN/dt at which atoms escape (effuse) from the orifice is given by

$$\frac{dN}{dt} = \frac{P\ a}{\sqrt{2\pi\, mkT}} , \tag{3}$$

where P is the pressure at the temperature T, a is the orifice area, and m is the mass of the escaping (effusing) vapor. Vapor pressure measurement by observation of the rate of effusion from a hot cell is called the Knudsen effusion method (29). Again Equation 2 applies, i.e. relative vapor pressures are independent of everything but dN/dt and T.*

Three distinct methods of measuring the rate of effusion (Langmuir or Knudsen) from a cell are currently employed. These three methods will be discussed briefly. One effusion rate measurement method involves the condensation of the effusing atoms on a cold target. The deposition is allowed to continue until the amount of material which has condensed is sufficient to be determined accurately by weighing, by quantitative chemical analysis (30) or by counting experiments on radioactive isotopes (31). A second method for measuring effusion rates was described by Daane (32). In this method the rate of weight loss of the cell is measured directly,

*Actually a small correction must be made for the temperature dependence of the orifice area (Section IVC).

a value for the average mass of an effusing particle is assumed, and the effusion rate is found. The third method for determining effusion rates is to transform some portion of the stream of neutral particles effusing from the cell into ions. The ions produced are then detected as a current. If a constant fraction of the effusing particles is ionized, the ion current is proportional to the effusion rate. Taylor and Langmuir (33) used surface ionization at a hot tungsten wire in their experiments on effusion from cells containing cesium. The use of surface ionization in modern effusion studies is discussed by Fox (34). Complex molecules tend to break up into their constituent atoms during surface ionization, so other ionization methods are preferred for the study of solids from which complex molecules might sublime. Ionization of molecules with little accompanying dissociation can be accomplished with electron bombardment. An electron bombardment ionization source is described in Section IIIB2. Further details on ionization by electron bombardment are given by Jackson and Hudson (35).

The cold target method and the weight-loss method have the advantage of measuring the saturated vapor pressure rather than the relative vapor pressure, but both methods require large samples and precise temperature controls to regulate temperature over long periods of time. Furthermore the most sensitive and accurate of the three effusion-rate methods is the ionization method. The work reported in this thesis employed a particular type of ionization-detection method called the mass spectrometric method.

4. The mass spectrometric method

In the mass spectrometric method used in this laboratory, the vapors effusing from a heated cell are ionized (in this experiment by electron bombardment) and analyzed with a mass spectrometer. The sole purpose of the mass spectrometer in this experiment is to separate ion beams corresponding to different masses. The obvious advantage of the mass analysis is that inferences as to the content of the vapor effusing from the cell can be made on the basis of the various masses observed with the mass spectrometer. Furthermore the mass spectrometric method has the advantage of separating the material of interest from the slight impurities which may also effuse from the cell. If a surface ionization source is used, enormous errors may result from a slight contamination of the sample (11). The particular instrumentation used in this experiment (Section III) allowed high precision to be obtained without the sublimation of a considerable portion of the solid. This great sensitivity proved to be especially useful because the thermodynamics of sublimation from binary compounds is simplified considerably by the assumption that the vapor pressure measurement does not necessitate the sublimation of great quantities of the vapor (see Section IIC).

II. THEORY OF THE EXPERIMENT

A. Knudsen Effusion

1. Introduction

Since Knudsen's paper in 1909 (29) the problem of Knudsen effusion has been under continual investigation. A solid sample is placed in a Knudsen effusion cell, i.e. a container whose only opening is a small orifice. If the cell is heated to a uniform temperature the rate of escape (effusion) from the orifice is a function of the cell geometry, the solid sample, and the temperature. The approach to the problem of the explicit exhibition of the dependence of effusion rate on these factors which will be followed in this thesis is iterative. That is, as a first approximation the cell will be considered closed. The vapor within the cell will become saturated. Under these conditions the rate at which atoms strike a unit area of the wall can be calculated. The effusion rate can be approximated by the rate at which atoms strike a unit area of the cell wall multiplied by the orifice area. Then a correction will be made for the fact that not all atoms reaching the orifice escape the cell. Finally, corrections will be made for the fact that the actual steady-state system is not at thermodynamic equilibrium (Section IID).

2. The closed cell

The pressure within a closed cell at temperature T is simply the saturated vapor pressure of the solid sample at temperature T (the vapor pressure due to the cell material is assumed to be negligible). It is

easy to derive the rate (in particles per second) at which the particles of the gas strike a unit area of the cell wall if the following properties hold for the gas:

1) the gas has a uniform mean density n (particles per unit volume) throughout the cell,

2) the gas particles move in random directions (all directions are equally probable), and

3) there is a velocity distribution function f(v) such that the average number of particles with velocities between v and v+dv is given by f(v)dv.

The rate at which atoms strike a unit area of the wall can be obtained by integrating the number striking the area from the solid angle $d\omega$ during one second over the total solid angle from which atoms can reach the wall. This integration is performed in most kinetic theory books, e.g. Kennard (36). The result is that the rate at which atoms strike a unit area of the wall, J, is given by

$$J = \tfrac{1}{4} n\bar{v},$$

where v is the average velocity, i.e.

(4) $$\bar{v} = \frac{\int_0^\infty v\, f(v)\, dv}{\int_0^\infty f(v)\, dv}$$

If the orifice area is a, the effusion rate, dN/dt, is given by

(5) $$\frac{dN}{dt} = \tfrac{1}{4} n\bar{v}a.$$

Equation 5 can be transformed into a more useful form if the vapor

assumed to be ideal and if the velocity distribution function is assumed to be Maxwellian:

$$f(v) = A \exp(-\frac{\frac{1}{2}mv^2}{kT}),$$

where A is a constant, m is the mass of the particle, and k is the Boltzmann constant. The use of this f(v) in Equation 4 gives the mean velocity

$$v = \sqrt{\frac{8kT}{\pi m}} . \tag{6}$$

The ideal gas law expression for the particle density is

$$n = \frac{P}{kT} . \tag{7}$$

Expressions 8 and 9 can be used to transform Equation 5 into the form

$$\frac{dN}{dt} = \frac{Pa}{\sqrt{2\pi mkT}} . \tag{8}$$

3. Correction for finite orifice thickness

Since the orifice of the Knudsen cell is of finite thickness, some of the particles passing into the orifice from within the cell are returned again to the cell as a result of collisions with the walls of the orifice and with other gas molecules. For low pressure gases it is safe to neglect particle-particle collisions in comparison with particle-wall collisions. If in addition it is assumed that particles rebound from the wall with a directional probability distribution proportional to the cosine squared of the angle with the normal, an exact treatment of the problem is possible using integration techniques devised by Clausing (37).

if the orifice is a cylinder, then the effusion rate is that indicated in Equation 8 multiplied by a constant factor, W, called the Clausing factor. The Clausing factor can be made greater than 95% by the techniques described in Section B2.

The method used by Clausing (37) to calculate W, was applied to the cell as a whole by Carlson (38). This treatment is discussed in Section IID. A similar calculation for a multicomponent gas was made by Schrage (39).

4. Pressure limitation

Equation 5 does not hold for arbitrarily large pressures. Knudsen (29) studied the pressure limitation in detail. His investigation showed that Equation 5 applies if and only if the pressure is such that the mean free path is at least ten times the orifice diameter. At higher pressures the escape rate (not called effusion rate at these pressures) is somewhat greater than would be predicted by Equation 5. The escape takes place by means of a hydrodynamic streaming process.

B. The Thermodynamics of the Sublimation of Two Component Systems

1. Introduction

The sublimation of one component solids and the sublimation of one component from a multicomponent solid are governed by the Clapeyron equation

$$\frac{dP}{dT} = \frac{\Delta S}{\Delta V}, \tag{9}$$

where ΔS is the entropy increase per mole of the subliming component

during sublimation, $\Delta \bar{V}$ is the increase in molar volume experienced by the subliming components, P is the pressure, (see the immediately following section for a derivation and further discussion). Not all sublimation from a two component system is governed by the Clapeyron equation. The most general type of sublimation which will be considered in this section involves a binary compound A_nB_m. The sublimation is assumed to take place within a closed cell (e.g. a Knudsen effusion cell), so the number of atoms necessary to fill the cell with gas is quite small, in general, compared with the number of atoms that are contained in the solid sample. It is assumed that both components, A and B, sublime. However the solid may become slightly depleted with respect to one of the components if the sublimation is not stoichiometric. It is also assumed that only monomer A and B vapors sublime. The reaction of interest is

$$(10) \qquad A_nB_m(s) \rightarrow \alpha nA(v) + \beta mB(v) + A_{n(1-\alpha)}B_{m(1-\beta)}(s).$$

The volatilities α and β are assumed to be much less than unity.* Also α and β are assumed to be constants over the temperature range of interest. The equilibrium within a closed cell is then

$$(11) \qquad A_{n(1-\alpha)}B_{m(1-\beta)}(s) \rightleftharpoons \alpha nA(v) + \beta mB(v).$$

*In this section α and β will mean the volatilities of A and B, not the adsorption and evaporation coefficients. Both uses of α and β are useful and standard. The usage of α and β in any section will be clearly stated and also will be clear from context.

The system contains one solid phase, $A_{n(1-\alpha)}B_{m(1-\beta)}(s)$, and one vapor phase, $\alpha\, nA(v) + \beta\, mB(v)$. If $\alpha = \beta$, the sublimation is stoichiometric, and the solid phase is just $A_nB_m(s)$. In the more general case $\alpha \neq \beta$, the solid is slightly depleted in one of the components. It is assumed, without loss of generality, that the more volatile component is A; i.e. $\alpha > \beta$. It will be demonstrated in Appendix A that this general reaction can be treated in a straightforward manner. The case in which $\beta = 0$ will be discussed in Section IIB3. The solution presented in Section IIB3 is often confused with the Clausius-Clapeyron equation which is discussed in Section IIB2 (40,41).

2. The Clausius-Clapeyron equation

Equilibrium of a two phase system at constant T and P requires that the molar Gibbs free energy, g, of the two phase be equal, i.e.

$$g^s = g^v$$

Here s and v denote the solid and vapor phases respectively. If small changes dT and dP in the temperature and pressure of the system are to maintain the equilibrium, the resulting changes in g^s and g^v must be such that

(12) $$dg^s = dg^v$$

For those cases in which

(13) $$dg = -SdT + VdP$$

for both phases, Equation 11 reduces to

$$-S^S dT + V^S dP = -S^V dT + V^V dP$$

Therefore

(14) $$\frac{dP}{dT} = \frac{S^V - S^S}{V^V - V^S} \cong \frac{\Delta S}{\Delta V}$$

Equation 14 is called Clapeyron's equation. For reactions at constant T and P

(15) $$\Delta H = T\Delta S,$$

where ΔH is the molar enthalpy of the vapor minus the molar enthalpy of the solid. The quantity ΔV can be approximated by

(16a) $$\Delta V = V^V - V^S \cong V^V$$

For an ideal gas

(16b) $$V^V = \frac{RT}{P}$$

where R is the universal gas constant. Equations 14 and 15 are used to transform Equation 14 to the form

(17) $$\frac{dP}{dT} = \frac{P\Delta H}{RT^2}, \text{ or } \frac{d\ln P}{d(1/T)} = \frac{-\Delta H}{R}$$

Equation 17 is called the Clausius-Clapeyron equation.

3. Sublimation of one component of a binary solid

The reaction to be considered in this section is of the form of Expression 11 for the case $\alpha \neq 0$, $\beta = 0$. For the solid phase (two components) the change in total Gibbs free energy is given by

$$dG = -SdT + VdP + \Sigma \mu_i dn_i, \tag{18}$$

where the chemical potential μ_i is given by

$$\mu_i = (\partial G/\partial n_i)_{T,P,n_j \atop j \neq i} \tag{19}$$

The condition for equilibrium of a two phase multicomponent system can be expressed

$$\mu^a{}_i = \mu^b{}_i, \tag{20}$$

where $\mu^a{}_i$ is the chemical potential of component i in phase a, etc. Equation 20 requires that the chemical potential of any component in one phase must equal the chemical potential of the same component in the other phase. Small changes dT and dP which maintain the equilibrium must be such that

$$d\mu_i{}^a = d\mu_i{}^b, \tag{21}$$

where the $d\mu_i$'s arise from changes dP, dT, and any accompanying changes in the composition of either phase. For a vapor phase consisting of n_A^v moles of A vapor, $G^v = n_A^v g_A^v$, so $\mu_A^v = g_A^v$. Therefore

$$d\mu_A^v = -S_A^v dT + V_A^v dP, \tag{22}$$

where $\bar{S}_A^V$ and $\bar{V}_A^V$ are the molar entropy and volume of A vapor. The two component solid offers a different situation. Suppose the volume of one mole of solid A_nB_m is V^S. The volume of t moles of A_nB_m is tV^S. That is V^S is homogeneous of order one in n and m. But by Euler's theorem a function f(n,m) which is differentiable and homogeneous of order q can be written

$$qf(n,m) = n(\partial f/\partial n)_m + m(\partial f/\partial m)_n$$

Therefore

(23a) $$V^S = nV_A^S + mV_B^S,$$

where $V_A^S = (\partial V^S/\partial n_A)_{nB}$ and $V_B^S = (\partial V^S/\partial n_B)_{nA}$. Similarly one can show that

(23b) $$S^S = nS_A^S + mS_B^S \text{ and}$$

(23c) $$H^S = nH_A^S + mH_B^S$$

Equations similar to Equations 23a, 23b, and 23c hold for any function which is differentiable and homogeneous of order one in n and m in any phase. The quantity $d\mu_A^S$ can be written

(24) $$d\mu_A^S = (\partial \mu_A^S/\partial n_A)_{T,P,n_B} dn_A + (\partial \mu_A^S/\partial n_B)_{T,n_A,n_B} dP +$$
$$(\partial \mu_A^S/\partial n_A)_{T,P,n_B} dn_A + (\partial \mu_A^S/\partial n_B)_{T,P,n_A} dn_B$$

Equation 19 can be used to obtain

$$(25) \qquad \left(\partial \mu_A^s / \partial T\right)_{P,n_A,n_B} = \frac{\partial}{\partial T}\left[\left(\partial G^s / \partial n_A\right)_{T,P,n_B}\right]_{P,n_A n_B}$$

$$= \frac{\partial}{\partial n_A}\left[\left(\partial G^s / \partial T\right)_{P,n_A,n_B}\right]_{T,P,n_B}$$

$$= -\left(\partial S / \partial n_A\right)_{T,P,n_B}$$

$$= -S_A^s$$

The operations performed in Equation 25 apply if G^s is continuous in T and n_A^s. Similarly

$$\left(\partial \mu_A^s / \partial P\right)_{T,n_A,n_B} = V_A^s$$

By hypothesis $dn_B = 0$. The quantity $\left(\partial \mu_A^s / \partial n_A\right)_{T,P,n_B}$ is the partial derivative of an intensive variable (μ_A^s) with respect to an extensive variable (n_A). Therefore $\left(\partial \mu_A^s / \partial n_A\right)_{T,P,n_B}$ is a quantity which decreases as n_A and n_B are increased in the stoichiometric ratio $n_A/n_B = n/m$. If it is assumed that n_A^s is large enough, the term $\left(\partial \mu_A^s / \partial n_A\right)_{T,P,n_B} dn_A$ in Equation 24 is negligible and Equation 24 reduces to

$$(25) \qquad d\mu_A^s = -S_A^s dT + V_A^s dP$$

Equations 21, 22, and 25 can be used to obtain

$$\frac{dP}{dT} = \frac{S_A^v - S_A^s}{V_A^v - V_A^s} = \frac{\Delta S_A}{\Delta V_A},$$

where $\Delta S_A = S_A^v - S_A^s$ and $\Delta V_A = V_A^v - V_A^s$. The pressure is due entirely to component A, i.e. $P = P_A$, so

$$(26) \qquad \frac{dP_A}{dT} = \frac{\Delta S_A}{\Delta V_A}$$

Equation 26 is the desired analogue of the Clausius equation.

4. Final working equation

This thesis involves the use of Equation 26 to describe the sublimation of Mg out of Mg_2X (X = Si, Ge, Sn, or Pb). In this case A = Mg and X = B. It will be demonstrated in Appendix B that $\alpha >> \beta$, so Equation 26 is a good approximation to the physical situation. By the methods of the previous section Equation 26 can be written in the form

$$\frac{d\ln P_{Mg}}{d(1/T)} = \frac{-\Delta H_{Mg}}{R}, \tag{27}$$

where the various symbols have the meanings assigned to them in Section IIB3. In Section IVD Equation 26 will be transformed into the form

$$\Delta H_{Mg} = -R\frac{d\ln I}{d(1/T)}, \tag{28}$$

where I is the recorder current. The present experiment consists of the experimental determination of I as a function of T. The quantity ΔH_{Mg} is then found from Equation 28.

C. Corrections for Non Equilibrium Situations

1. Introduction

Section IIA discussed the effusion from a Knudsen cell on the assumption that calculations made for the equilibrium situation (zero orifice area) applied for sufficiently small orifices. It is the purpose of this section to examine the extent to which that assumption is justified.

2. Standard corrections

The complication of the various processes which produce the effect we call effusion has delayed exact treatment until quite recently. However a very simple approximate correction for the non equilibrium situation was devised. The present section will discuss the older correction, and the following section will describe the new correction.

In Section IIC3 the expression for the evaporation rate from a solid with area A and evaporation coefficient β was found to be

$$\frac{dN}{dt} = \frac{\beta P_e A}{\sqrt{2\pi mkT}} \tag{1}$$

In Equation 1 the term P_e is the saturated vapor pressure of the solid at temperature T. The pressure in the vapor near the solid is not P_e but is some value P_s because the cell is not in thermodynamic equilibrium. By Equation 8 the rate $(dN/dt)_s$ at which atoms from the gas strike the solid sample is

$$\left(\frac{dN}{dt}\right)_s = \frac{P_s A}{\sqrt{2\pi mkT}}$$

It is assumed that of the particles which strike the solid, a fraction α is reassimilated into the solid and a fraction $1-\alpha$ is reflected back into the gas. The quantity α is called the adsorption coefficient or the accommodation coefficient by various authors. At this juncture a distinction should be made between P_s, the pressure in the gas near the surface of the solid, and P, the pressure near the orifice. The standard correction is based on the assumption that $P = P_s$. Then the previous

equation becomes

$$\left(\frac{dN}{dt}\right)_s = \frac{PA}{\sqrt{2\pi mkT}}$$

The net rate at which atoms leave the surface is

(29) $$\frac{\beta P_e A}{\sqrt{2\pi mT}} - \frac{\alpha PA}{\sqrt{2\pi mkT}}$$

Also by Equation 8 the rate at which atoms effuse from the orifice is

(30) $$\frac{Pa}{\sqrt{2\pi mkT}}$$

The steady state occurs when Expressions 29 and 30 are equal, or

(31) $$\frac{Pa}{\sqrt{2\pi mkT}} = \frac{\beta P_e A}{\sqrt{2\pi mkT}} - \frac{\alpha PA}{\sqrt{2\pi mkT}}$$

Equation 31 holds if and only if

(32) $$P = P_e \frac{\beta}{\alpha + a/A}$$

As a approaches zero, P must approach its equilibrium value P_e.

Therefore at equilibrium

(33) $$\alpha = \beta$$

Equation 33 reduces Equation 32 to the commonly-used expression

$$P = P_e \frac{\alpha}{\alpha + a/A}$$

For most substances α is unity or only slightly less, so the criterion

for equilibrium is

$$\frac{a}{A} \ll 1$$

Some evidence exists for cases in which although $\alpha \approx 1$, $\beta \ll 1$ for the steady state (42, 43). Complications involving α are discussed in Section IIC5. The cases in which the criterion of equation 68 is not reliable must be considered exceptional.

3. Modified Carlson correction

Carlson (38) has devised a method for correcting for the non equilibrium method without making the assumption that the vapor pressure is uniform throughout the cell. Carlson treated the case of a right circular cylindrical cell of radius R_1 and height L. The solid sample filled the bottom of the cell, and at the top of the cell was an orifice of radius R_o. He described the particle distribution by applying the methods devised by Clausing to describe the "conductivity" of the Knudsen cell orifice (see Section IIA3). The significant parameters are $H = L/R_1$ and $P = R_o/R_1$. In all cases Carlson assumed $\alpha = 1$. For $H = 2$ and $P = 0.1$ he obtained $P_{observed} = 0.946\ P_{equilibrium}$. For $H = 2$ and $P = 0.01$ he got $P_{observed} = 0.99\ P_{equilibrium}$. Carlson suggests the way in which these solutions can be modified to allow $\alpha < 1$. This has been done in Appendix C. The approximations employed were chosen such that the observed pressure, P_o, is really closer to the equilibrium pressure, P_e, than is indicated in the following equations:

$$P_o = P_e\left[0.946-0.02(1-\alpha)\right] \text{ for } H = 2 \text{ and } P = 0.1 \text{ and}$$

$$P_o = P_e\left[0.99-0.02(1-\alpha)\right] \text{ for } H = 2 \text{ and } P = 0.01.$$

Carlson's geometry is convenient for calculation, but it was not so convenient for application in this experiment. However it should be useful to indicate some general features of Knudsen effusion. For any real use, experiment must provide validity checks. There is experimental evidence to indicate that P_o/P_e is a function of the cell geometry rather than the classical $P_o/P_e = \frac{\alpha}{\alpha + a/A}$ of the previous section (43). In either case a proper choice of the orifice area can eliminate the dependence.

4. Diffusion

In some binary solids the diffusion of the volatile constituent to the surface is not fast enough to allow sublimation of that constituent to occur at its equilibrium rate. In such cases the sublimation is said to be diffusion limited. The diffusion rate is temperature dependent, so the temperature dependence of a diffusion limited effusion rate involves not only the $\exp(-\Delta H/RT)$ term from the pressure but also an $\exp(-\Delta E/RT)$ term from the diffusion constant where ΔE is the diffusion activation energy. Extensive discussions of diffusion limitation in Knudsen effusion experiments are given by Boteler (44) and Peavler and Searcy (45). The effect of diffusion limitation in the experiments reported in this thesis is examined in Section IIE.

5. Sublimation mechanism

The effusion rate can lead to incorrect ΔH values if there is a temperature dependent adsorption coefficient α which is not eliminated from the equation governing the effusion rate. This matter is discussed

by Knacke, Stranski, and Wolff (46, 47, 48, 49). They show that if the sublimed molecules must break primary bonds in becoming reassembled into the lattice a temperature dependent adsorption coefficient of the form $\alpha = \alpha_0 e^{-E/RT}$ will result, where α_0 = 0.1 to 1.0 and E is an energy of the order of Δ H. For such cases the sublimation rate depends on the $e^{-E/RT}$ from $\alpha(T)$ as well as the $e^{-\Delta H/RT}$ from P(T). Clearly this is a phenomenon exclusive to rather complicated compounds. These undesirable variations of observed Δ H with orifice area are not to be expected if the orifice area is small enough to satisfy $a/A \ll 1$.

6. Temperature gradients

In the discussions so far the possibility of temperature gradients along the cell, within the gas, within the solid, or along the solid-gas interface has been ignored. Temperature gradients can arise from faulty heating techniques or from surface cooling produced by the sublimation. The effect of temperature gradients is particularly difficult to evaluate empirically, because the temperatures of interest may be unmeasurable in principle (50). Appendix C contains two analyses of the error possible from temperature gradients based on the irreversible thermodynamics of DeGroot (51).

D. Interpretation as Cohesive Energy

1. Surface and interior energies

Sublimation occurs from the surface and from the first few monolayers (50), but the atoms on or near the surface have different binding

energies from an atom in the interior (46, 47, 48, 49). The problem is how to interpret energies measured in sublimation processes in terms of the energy of an interior atom. This section will present a highly pictorial solution to this problem. Figure 2 is an idealized potential diagram for the atoms near the surface of a solid. The potential, ψ_1, of the atom nearest the surface is less than the potential, ψ, of an atom deep within the solid, because the surface atom has fewer nearest neighbors, next nearest neighbors, etc. than does the interior atom. If it is supposed that the surface atom gains enough energy, ψ_1, to escape, sublimation may occur. If the surface atom is removed, the potential, $\psi_1+\psi_2$, of its former neighbor is reduced because that atom has lost a nearest neighbor. Similarly atoms further into the solid have lost a next nearest neighbor or a next next nearest neighbor, etc. Therefore the potentials of all other atoms are affected by the removal of one atom from the surface. The net effect of these potential changes is to restore the potential diagram to the form of Figure 2. In this process one atom has been given an additional energy ψ_1, another particle has gained energy ψ_2, another has gained, ψ_3, and so forth. The total change of energy is $\psi_1+\psi_2+\cdots=\psi$, but ψ is the energy with which an interior atom is bound. The energy, Δ H, supplied to the solid must be sufficient to produce all of these energy changes, so Δ H = ψ.

2. Extrapolation to T = 0

In Section IA1 it was shown that the cohesive energy of a substance can be obtained by extrapolating the heat of sublimation to T = 0. This section will present an equation whereby that extrapolation can be

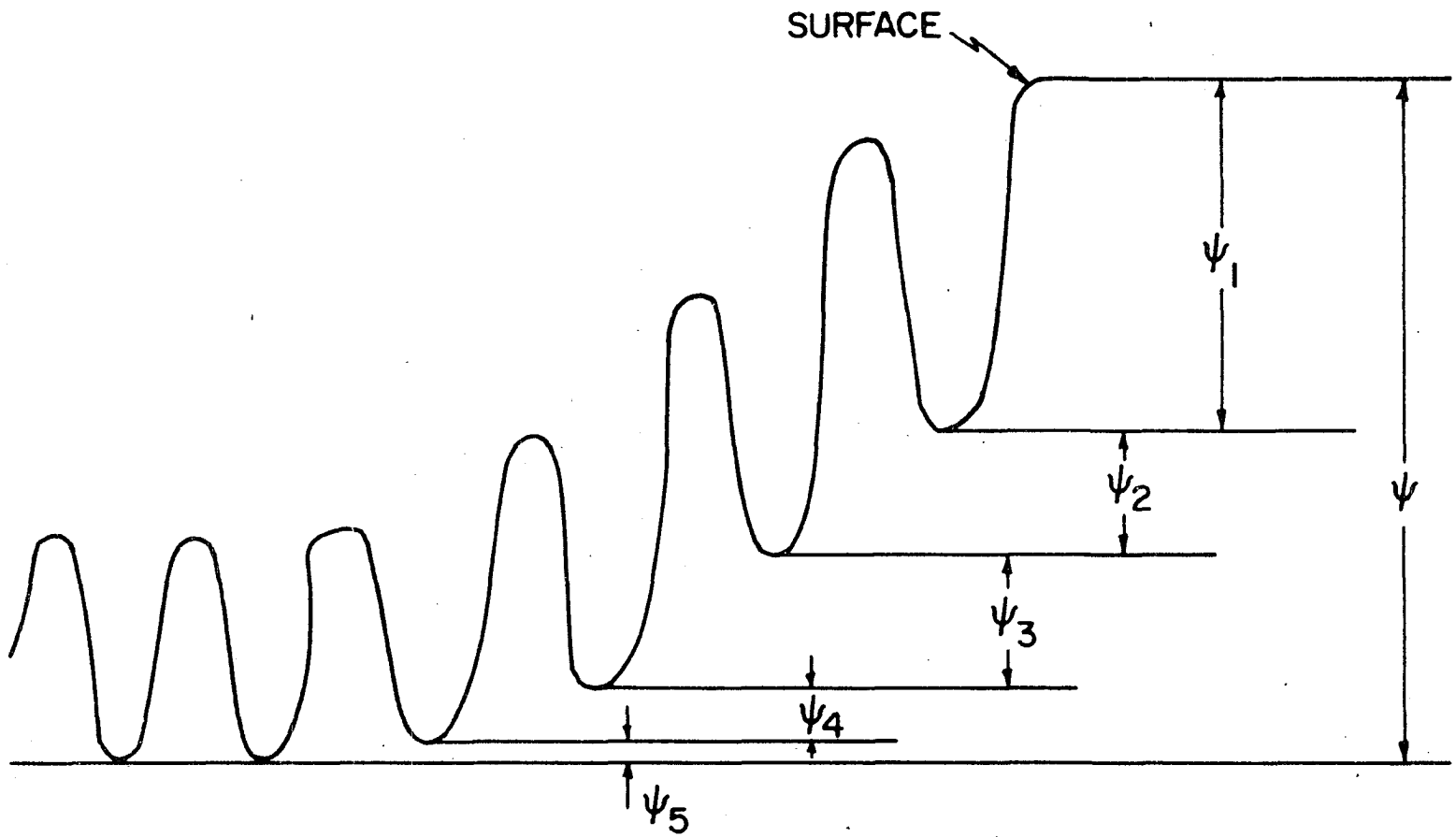

Figure 2. Schematic representation of the potential of a solid near the surface

accomplished.

ΔH at temperature T and pressure P is the difference between $H^S(T,P)$ and $H^V(T,P)$. The cohesive energy ΔH_o is the difference between $H^S(T=0,P_o)$ and $H^V(T=0,P_o)$. Here P_o is the pressure at T = 0. For either phase the enthalpy change can be calculated from the elementary formula

$$dH = \left(\frac{\partial H}{\partial T}\right)_P dT + \left(\frac{\partial H}{\partial P}\right)_T dP = C_p dT + \left[V - T\left(\frac{\partial V}{\partial T}\right)_P\right] dP$$

If the vapor phase is ideal

$$V - T\left(\frac{\partial V}{\partial T}\right)_P = 0 ,$$

so $H^V(T,P) - H^V(T=0,P_o) = \int_o^T C_p^V \, dT$. The quantity $H^S(T,P) - H^S(T=0,P_o)$ is calculated along a path such that

$$H^S(T,P) - H^S(T,P_o) = \int_{P_o}^{P} V^S \, dP + \int_o^T C_p^S \, dT$$

The pressure integral is negligible at low pressures, so

$$\Delta H_o - \Delta H = \int_o^T (C_p^S - C_p^V) \, dT \qquad (34)$$

The application of Equation 34 to any real case necessitates the specification of the solid and vapor phases at temperature T. In this thesis the solid is Mg_2X and the vapor phase to be considered is a mixture of Mg and X in the ratio 2:1 (Section IA1). The C_p^V to be employed was given by

$$C_p^V = 2C_p^V(Mg) + C_p^V(X) ,$$

where it is assumed that both gases are monomer and ideal. Therefore

$C_p^v = 3(5R/2) = 7.5R$. The value for C_p^s at atmospheric pressure can be used in Equation 56, because C_p^s is extremely insensitive to pressure.

3. Connection with heats of formation

It was shown in Section IA that the cohesive energy was the enthalpy change ΔH_R during the sublimation

(35) $$Mg_2X\ (s) \rightarrow 2Mg(v) + X(v)$$

extrapolated to T = 0. It does not matter for the purpose of this section that the reaction of expression 35 is not the reaction which occurs in practice. The quantity of interest is the enthalpy change, ΔH_R which would occur if the reaction of Expression 35 did occur. Using Equation 23 and the similar equation for H^s, ΔH_R is found from the special case n = 2, m = 1:

(36) $$\Delta H_R = 2\Delta H_{Mg} + \Delta H_X ,$$

where it is considered to use the partial molar quantities as described in Section IIB.

$$\Delta H_{Mg} = H_{Mg}^v - H_{Mg}^s \text{ and}$$

$$\Delta H_X = H_X^v - H_X^s$$

The reaction of Expression 35 can be accomplished in a three step process

(37a) $$Mg_2X(s) \rightarrow 2Mg(s) + X(s) ,$$

(37b) $$2Mg(s) \rightarrow 2Mg(v), \text{ and}$$

(37c) $$X(s) \rightarrow X(v).$$

The heat of reaction for Expression 37a is, by definition, the heat of formation, ΔH_f. The heat of reaction for Process 37b is given by $2L_{Mg}$, where L_{Mg} is the latent heat of sublimation of pure magnesium. The heat of reaction for Expression 37c is the heat of sublimation of pure X, L_x. By the state property of enthalpy the heat of reaction for the reaction of Expression 35 is independent of how the reaction occurs. Therefore

$$\Delta H_R = 2L_{Mg} + L_x + \Delta H_f \tag{38}$$

The quantities L_{Mg}, L_x, and ΔH_f have been measured by other investigations, so ΔH_R can be determined for all of the Mg_2X compounds. The quantity measured in this work is ΔH_{Mg}.

If ΔH_x could be determined in the present work, a value of ΔH_R could be found from Equation 36. Actually, ΔH_x could not be determined for experimental reasons. However, we feel that <u>accurate</u> measurements of the quantity ΔH_{Mg} alone should be very useful in a systematic study of the cohesion of the <u>series</u> Mg_2X.

At the present it is felt that the known experimental values of ΔH_f are so unreliable that values of ΔH_R found from Equation 38 are of doubtful use in a cohesion study (52) of the Mg_2X series.

It should be noted that some workers (53, 54) appear to equate ΔH_x with L_x in carrying out energy cycles. Since these energies arise physically from different crystals, such calculations should be considered qualitative.

E. Critique of the Experiment

In this section the possible sources of experimental error in ΔH_{Mg} are enumerated and discussed. The possible errors due to the mathematical analysis of the experimental raw data are discussed in Appendix E. The areas of particular concern in this section are: (1) diffusion effects, (2) the temperature dependence of the adsorption coefficient, (3) temperature gradients, (4) the surface chemistry of the solid sample, and (5) instrumental uncertainties. These areas will be examined consecutively.

1. Diffusion effects

The problem of diffusion limitation was discussed in Section IIC. The diffusion limitation process is discussed in detail by Boteler (44). The results quoted in this paragraph are from Boteler or are easily derived from Boteler's work. The time dependence of the Knudsen effusion rate dN/dt is given by

$$\frac{dN}{dt} = AG\, N_{Mg}\,(0,0)\; h\; (t/\tau)^{\frac{1}{2}} ,$$

where

A = sample area,

G = surface conductance of Mg_2X $\left(= \dfrac{aP_e}{AN_{Mg}(0,0)\sqrt{2\pi mkT}}\right)$

$N_{Mg}\,(0,0)$ = the concentration of Mg at the surface of the Mg_2X(x=0) at the beginning of the diffusion process (t=0),

$h(x) = \text{erfc}\,(x)\, \exp\,(x^2)$,

$\text{erfc}\,(x) = 1-\text{erf}(x)$,

$$\text{erf}(x) = \frac{2}{\sqrt{\pi}} \int_0^x e^{-y^2} dy,$$

t = time elapsed since diffusion began, and

τ = decay time ($=D/G^2$).

For D $\approx 10^{-9}$ cm^2/sec (a typical intermetallic value for T $\approx$ 700°C) and for G $\approx 10^{-2}$ cm/sec (a typical value for $P_e \sim 10^{-3}$ mm and T $\approx$ 700°C), $\tau \approx 10^{-9}$ $cm^2/sec \times 10^{24}$ $sec^2/cm^2 = 10^{15}$ sec or 3×10^{11} hours. The estimates just quoted are based on the work of Boteler (44). The Mg^+ beam from Mg_2Ge in a cell with a 30 mil orifice was monitored for two hours. No decay with time was observed. According to Boteler's equation either $\tau > 2 \times 10^4$ hours or $\tau < 2 \times 10^{-4}$ hours, because $h\left[(t/\tau)^{\frac{1}{2}}\right]$ is rapidly varying for $10^2 \gg (t/\tau)^{\frac{1}{2}} \gg 10^{-2}$. Therefore if the possibility of very severe diffusion limitation ($\tau < 2 \times 10^{-4}$ hours) is excluded, diffusion limitation is negligible and dN/dt is independent of orifice area and of the diffusion constant. The ion current was steady from the beginning of the run. That is any decay in ion current that occurred must have happened during the first ten minutes of the heating during which the beam was found and adjusted. Therefore $(t/\tau) > 10^4$ for t = 10 minutes, or $\tau < 10^{-3}$ minutes. The quantity τ estimated for typical intermetallic values for D and G is $\tau \approx 10^{13}$ minutes (44). Therefore the value τ less than 10^{-3} seems unlikely on the basis of the best available approximations. The weight loss data on Mg Ge taken by Novotny (Appendix F) showed that the number of atoms subliming from the cell

during a typical run was about 10^{18} particles.* If each atom occupies an area of about 10^{-15} cm^2 and if the surface area of the crystal is about 1000 cm^2, then the subliming particles could form about one monolayer. For the more reasonable estimate A = 100 cm^2, only ten monolayers are involved. That is only atoms which were originally very near the orifice eventually sublimed over the period of one run, so very little diffusion was necessary. Therefore diffusion limitation appears to be of negligible importance for this work.

Some contribution to the effusion flux may arise from Mg atoms which have diffused along the inner surface of the cell to the outside of the cell through the orifice and which sublime from the outside of the cell near the orifice. The Mg atoms can be considered to be bound to the tantalum cell with some average energy ΔE, which may differ markedly from ΔH_{Mg}. If adsorbed-desorbed atoms contribute significantly to the Mg flux leaving the cell, the energy obtained by the methods of this thesis will be some linear combination of ΔE and ΔH_{Mg} rather than just ΔH_{Mg}. For materials such that sufficient information on surface diffusion rates, adsorption coefficients, and ΔE values was available the errors in ΔH_{Mg} arising from desorption have been calculated, by Winterbottom and Hirth (55). Unfortunately the relevant data for Mg_2X is not available, so an experimental test for desorption

*Novotny, Donald B., Department of Metallurgy, Iowa State University of Science and Technology, Ames, Iowa, Sublimation of Mg_2Ge. Private communication. 1961.

difficulties was devised. The atom flux effusing from the orifice is proportional to the orifice area a. The atom flux diffusing through the orifice is proportional to the orifice perimeter. Therefore the ratio of effusive to surface diffusive flow varies with $\sqrt{a}$. If the desorption process is surface diffusion limited, a variation of ΔH_{Mg} with orifice area will result. This variation is not observed. By the arguments of the previous paragraph, the desorption is unlikely to be diffusion limited. Therefore it was assumed that diffusion limited desorption did not contribute to the measured ΔH_{Mg} values. If the desorption process was sublimation limited, a deposit of Mg should have been found on the orifice of a cell. No deposits were found on most of the cells used. Occasionally a thin uniform film was found on the entire cell. This film was attributed to oxidation of the cell. No deposit was found to be concentrated near the orifice, so no sublimation limited desorption appears to have contributed to the apparent effusion rate.

In some cases diffusion limitation may result in errors of other types. Kay and Gregory (56) measured water pressures resulting from the reaction.

$Mg(OH)_2$ (s) $\rightleftharpoons$ MgO (s) + H_2O (v). The apparent ΔH of the reaction from the Knudsen effusion data was 58% larger than the thermodynamic value which had been measured under equilibrium conditions. A possible kinetic explanation of the discrepancy is that sublimation from $Mg(OH)_2$ can occur from either of two bonding sites -- one with bonding energy ΔH and the other with bonding energy $1.58\Delta H$. Initially sublimation occurs from the sites most favored energetically, so the apparent ΔH is the

thermodynamic value. Eventually, however, these favorable sites may become depleted if diffusion of H_2O cannot replace molecules at these sites fast enough. In this case the sublimation occurs largely from the sites of tighter bonding. This effect could also be related to the relative areas occupied by the various types of bonding effects. If this is true, the area effect may be more important than the diffusion limitation. This phenomenon should be sensitive to a/A. In particular it should have resulted in systematically lower than average ΔH_{Mg} results for powdered samples, but no such effect was observed (Section VB). It was concluded that the Kay and Gregory phenomenon was not present. Furthermore the number of particles within the cell ($\sim 10^{18}$ at any one time) should have been sufficient to supply Mg to the depleted sites. That is the Kay and Gregory phenomenon should not occur for pressures as large as those encountered in this experiment.

2. Adsorption coefficient effects

The contribution to ΔH_{Mg} which might arise from temperature dependent adsorption coefficients is discussed in Section IIC. Section IIC also demonstrates that for sufficiently small orifice areas the error from adsorption coefficients is negligible. The observed independence of ΔH_{Mg} to changes in orifice area is evidence that no significant contribution from temperature dependent adsorption coefficient existed.

3. Temperature gradient effects

Temperature gradients at various places within the Knudsen cell can cause considerable error. It is demonstrated in Appendix C that a temperature difference of 1.6°K between the gas and the solid within the cell could result in about 1% error in ΔH_{Mg}. However the effect described in Appendix C could be described in terms of a temperature dependent evaporation coefficient. However such an effect would be sensitive to orifice area changes, so ΔH_{Mg} as measured in this work must have been unaffected by temperature gradients between the solid and the gas. All other temperature gradients are considered to be even less important than the one discussed. In any case the temperatures of interest occur within such a few monolayers that they are unmeasurable with any currently known device (50).

4. Surface condition effects

The measured H_{Mg} is sensitive to the condition of the Mg_2X surface. However since surface conditions must change during the course of several consecutive runs, the effect of surface conditions on ΔH_{Mg} should change systematically from run to run so long as the runs are made consecutively and without pause between runs. Such runs are Mg_2Ge: 1B-1E; Mg_2Sn: 1A-1E, 2A-2C; and Mg_2Pb: 2A-2C (Section VB). The lack of chronological correlation among these runs is taken as evidence of a negligible error due to surface effects. Also surface condition effects can be considered as causes of temperature dependent adsorption and evaporation coefficients, so for the reasons stated previously in this

section no effect due to surface conditions was detected.

5. Instrumental effects

Instrumental errors certainly contribute an uncertainty to the quoted value of ΔH_{Mg}. In Section III experimental tests for the linearity of each component of the apparatus are described. The numerical evaluation of instrumental error is discussed in Section IVE.

III. APPARATUS AND INSTRUMENTATION

A. Introduction

The instrumentation of this work was designed to yield information on the rate of change of pressure with temperature for a solid sample. Hence the primary locale for the physically significant processes is the Knudsen cell in which the solid is contained. The balance of the equipment serves to maintain the cell at a uniform temperature, to measure the cell temperature, and to measure the pressure of the gas in the cell. The apparatus can be seen in Figure 3. The bulk of the apparatus consists of the mass spectrometer and associated equipment, but it should be remembered that the process being studied takes place within the Knudsen cell. The mass spectrometer is of interest only in so far as it enables us to study what happens within the cell. System parameters of interest to specialists only are not described in detail but are itemized in Appendix D.

B. The Mass Spectrometer

1. Introduction

The components of the mass spectrometer are shown schematically in Figure 4. In Figure 4 the source chamber, A, contains a source of neutral particles, an ionizing device, and a system of slits and associated electrostatic potentials. These components combine to produce a well-defined beam of ions of a uniform velocity. This beam passes into the mass tube, B. The mass tube is simply a shell that allows a vacuum to be produced along the ion trajectory. The ions are deflected by a

Figure 3. Photograph of mass spectrometer

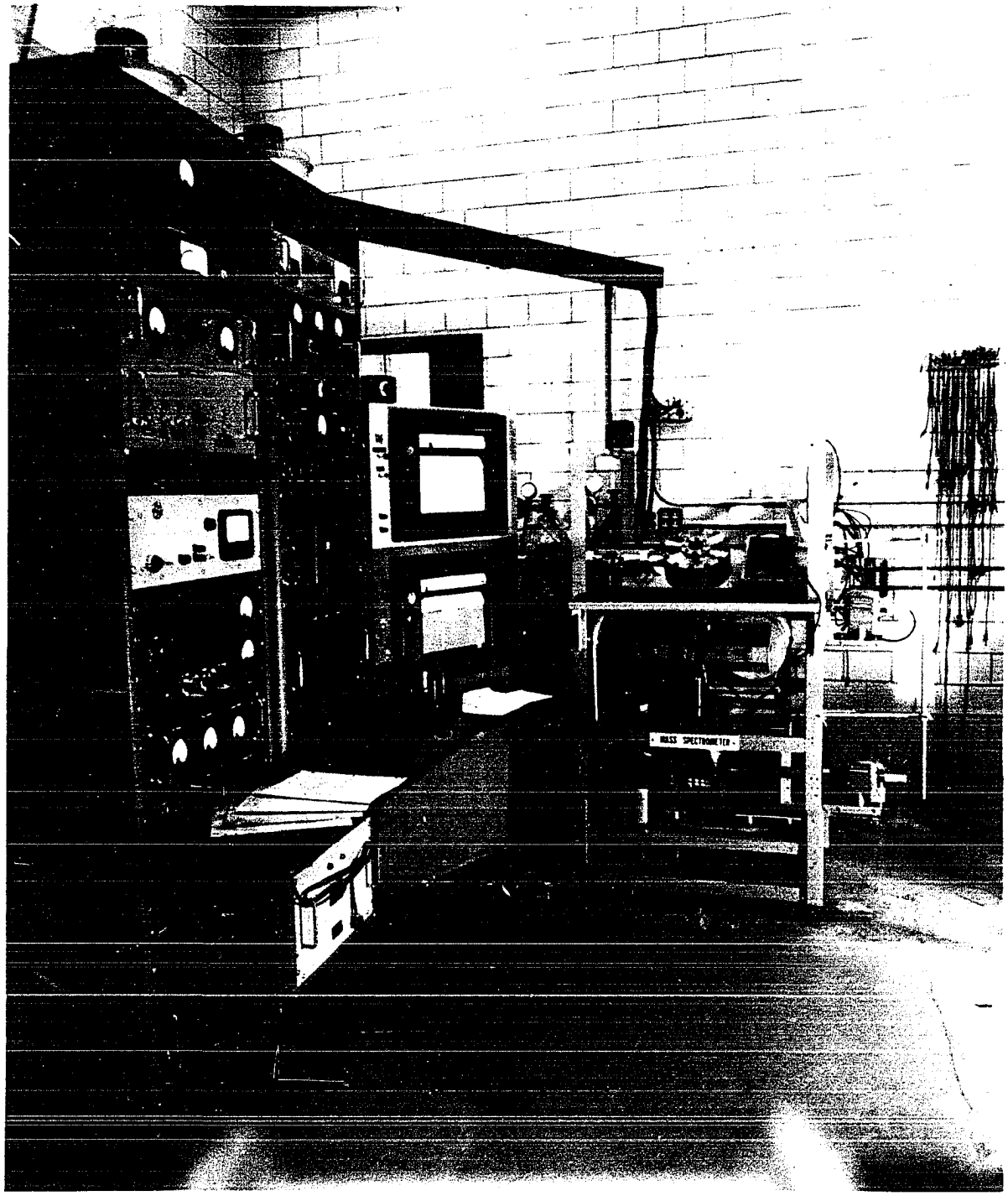
MASS SPECTROMETER

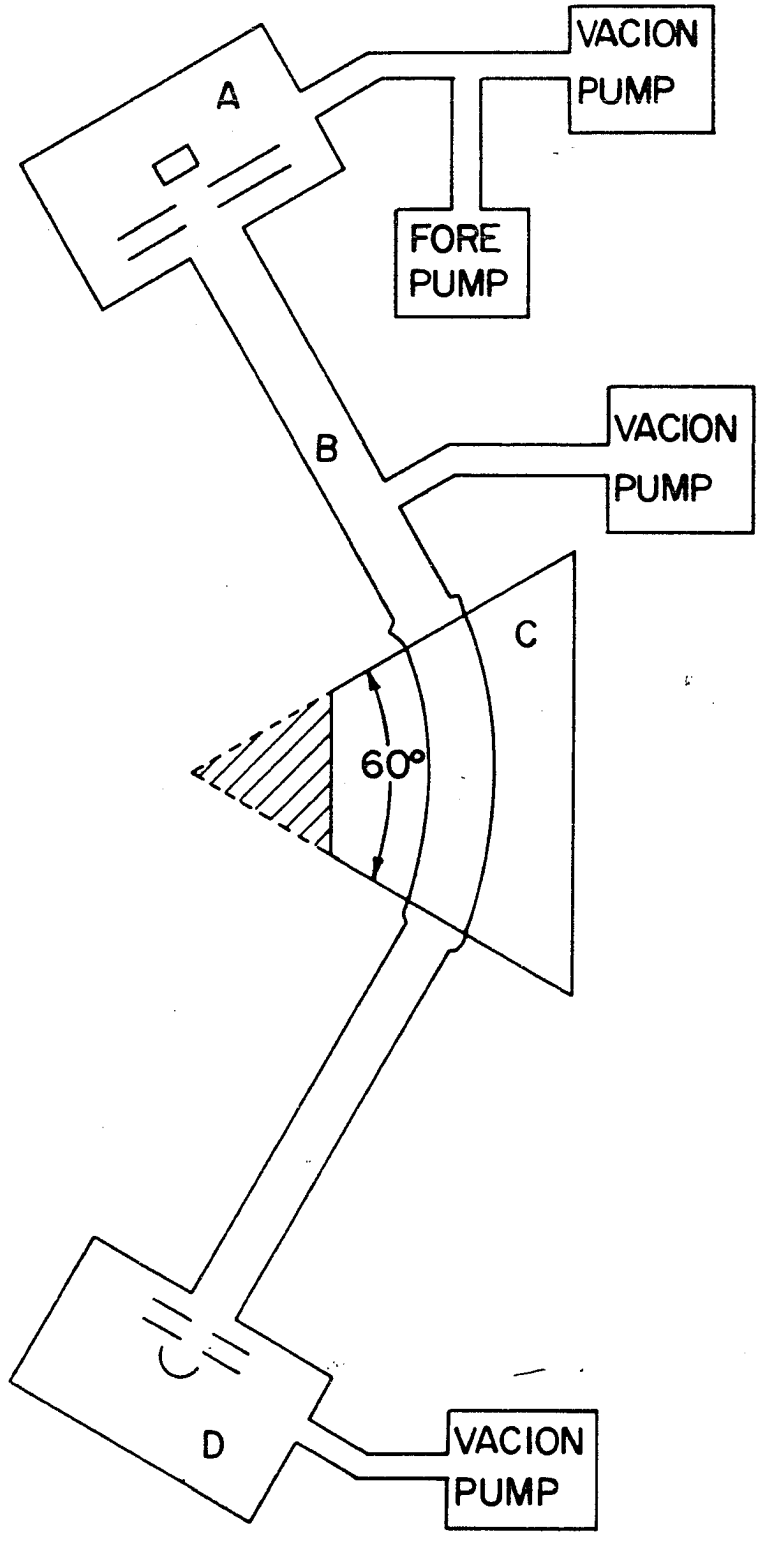

Figure 4. Block diagram of the mass spectrometer

60° sector electromagnet, C, which produces a magnetic field which is continuously variable. The magnet is adjusted until it is of the precise strength to bend the ions of interest through such an angle that they continue to pass freely down the mass tube and into the collection chamber, D. Ions bent through any other angle strike the sides of the mass tube and are conducted away to ground. After definition by slits in the collection chamber, the ion beam strikes an electron-multiplier ion detector. The multiplier feeds a vibrating reed amplifier which in turn causes a deflection on a strip recorder.

The balance of this section will describe each component of the mass spectrometer and the part that component plays in the measurement of the quantities of interest - the temperature and vapor pressure within the Knudsen cell.

2. Ion source

a. Introduction The term "ion source" will be used to mean those devices which are involved in the production of a neutral gas and its subsequent conversion into a well-defined ion beam of fixed high energy. A schematic diagram of the ion source is given in Figure 5. The neutral particles effuse from the Knudsen cell, A, and follow the indicated path. In the electron bombardment ionization source, B, these particles become ionized. The ions are pulled out by a voltage between the ion chamber, B, and the draw out plate, C. The beam is accelerated from B to D by a total voltage of 1900 volts. The beam is defined by slits at D and E. The Knudsen cell itself is heated by radiation from a hot tungsten filament arrangement, F. The neutral atoms from the Knudsen

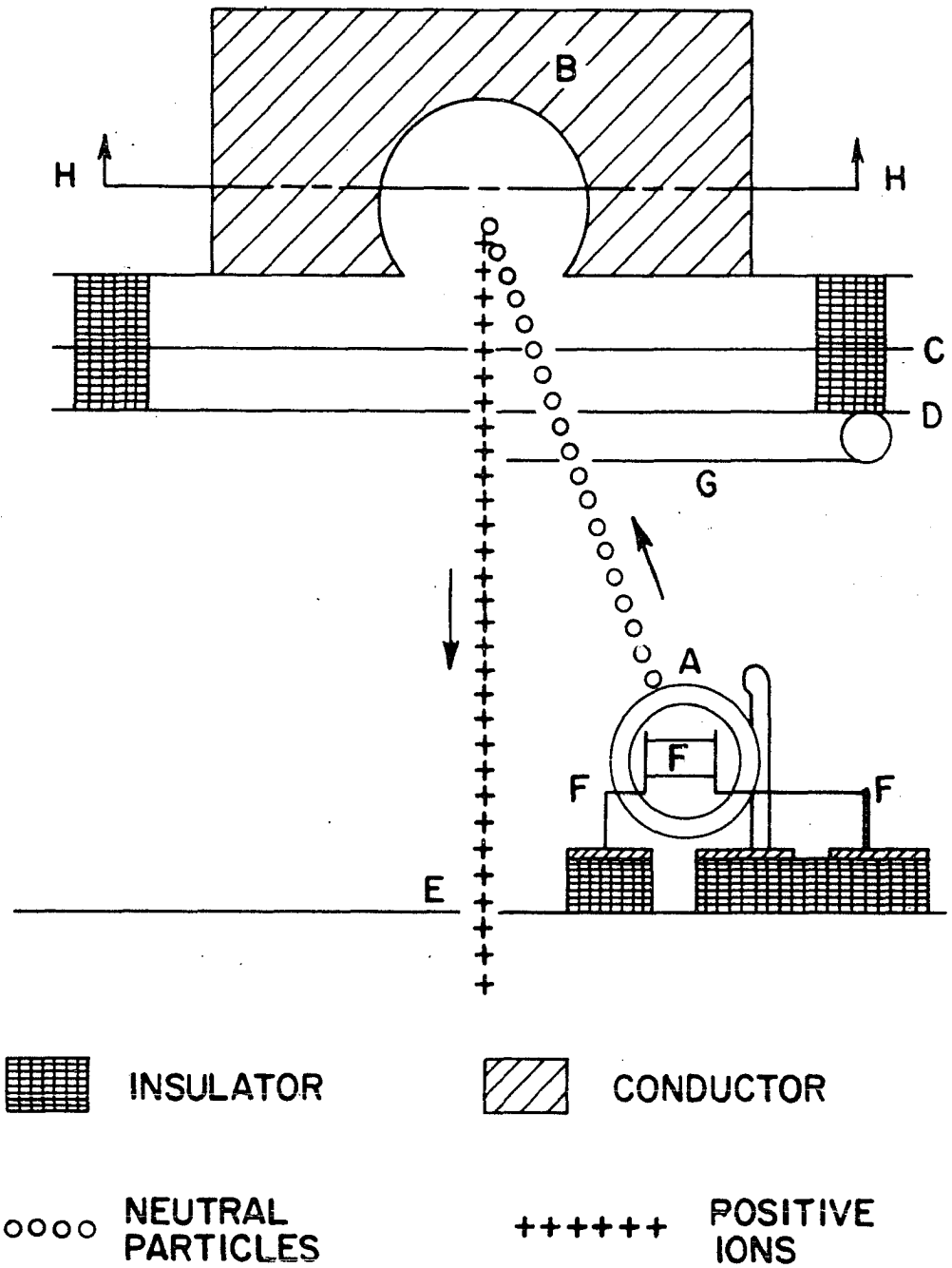

Figure 5. Schematic diagram of the ion source

cell may be prevented from reaching the ionization chamber by closing a shutter, G.

b. Knudsen cell The Knudsen cells used in this work were made from 0.250 inch diameter tantalum rod according to the dimensions shown in Figure 6. Orifices of the desired diameter were drilled in a guide hole made by a number 31 drill as indicated in figure. This procedure assured thin-edged orifices, so Clausing factors were always near unity. A 20 mil hole (T in Figure 6) was drilled roughly 30 mils into the cell opposite the orifice, and a thermocouple was then peened into this hole. The sample was introduced into the cell. Finally the cell was closed by compression-fitted end caps cut from 20 mil tantalum sheet. The cell was held in position by molybdenum wire supports as shown in Figure 7. Since all that is required of the Knudsen cell is that it introduce neutral particles into the ionization region at a rate proportional to the vapor pressure within the cell, run-to-run variations in cell position do not effect the result so long as the alignment is good enough to allow a significant fraction of the atoms which escape the cell to enter the ionization chamber.

c. Electron bombardment ionization source The design and construction of this device have been described by Jackson and Hudson (35). Figure 8 is a diagram of the system. The plane of the figure is perpendicular to Figure 6 at the line HH. Electrons are emitted by a hot tungsten filament and are accelerated to an adjustable energy eV_A. Note that the entire ionization chamber is at a uniform potential. The electrons are drawn out of the ionization chamber and into the trap by

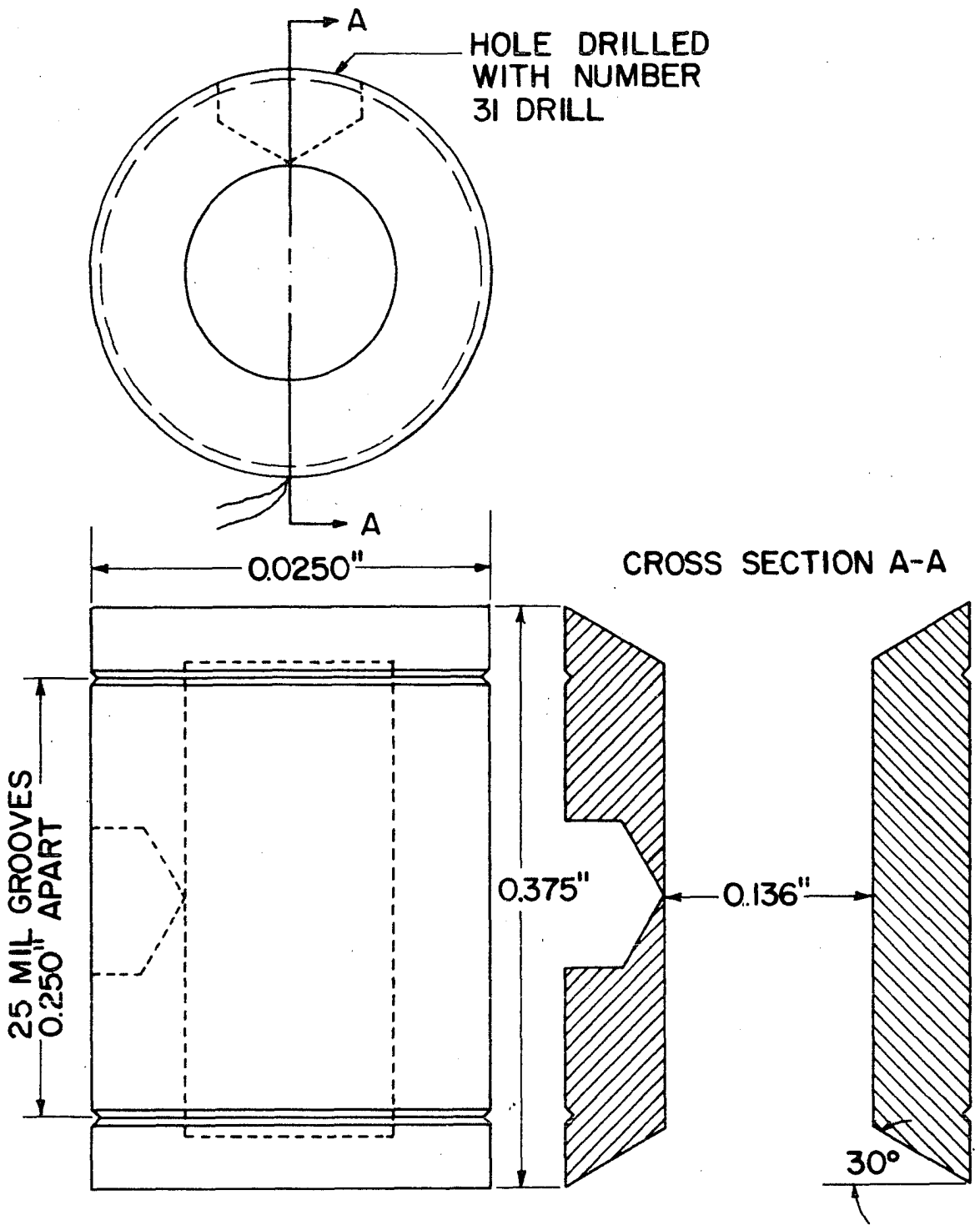

Figure 6. Drawing of the Knudsen cell

Figure 7. Photograph of the cell and cell mounting

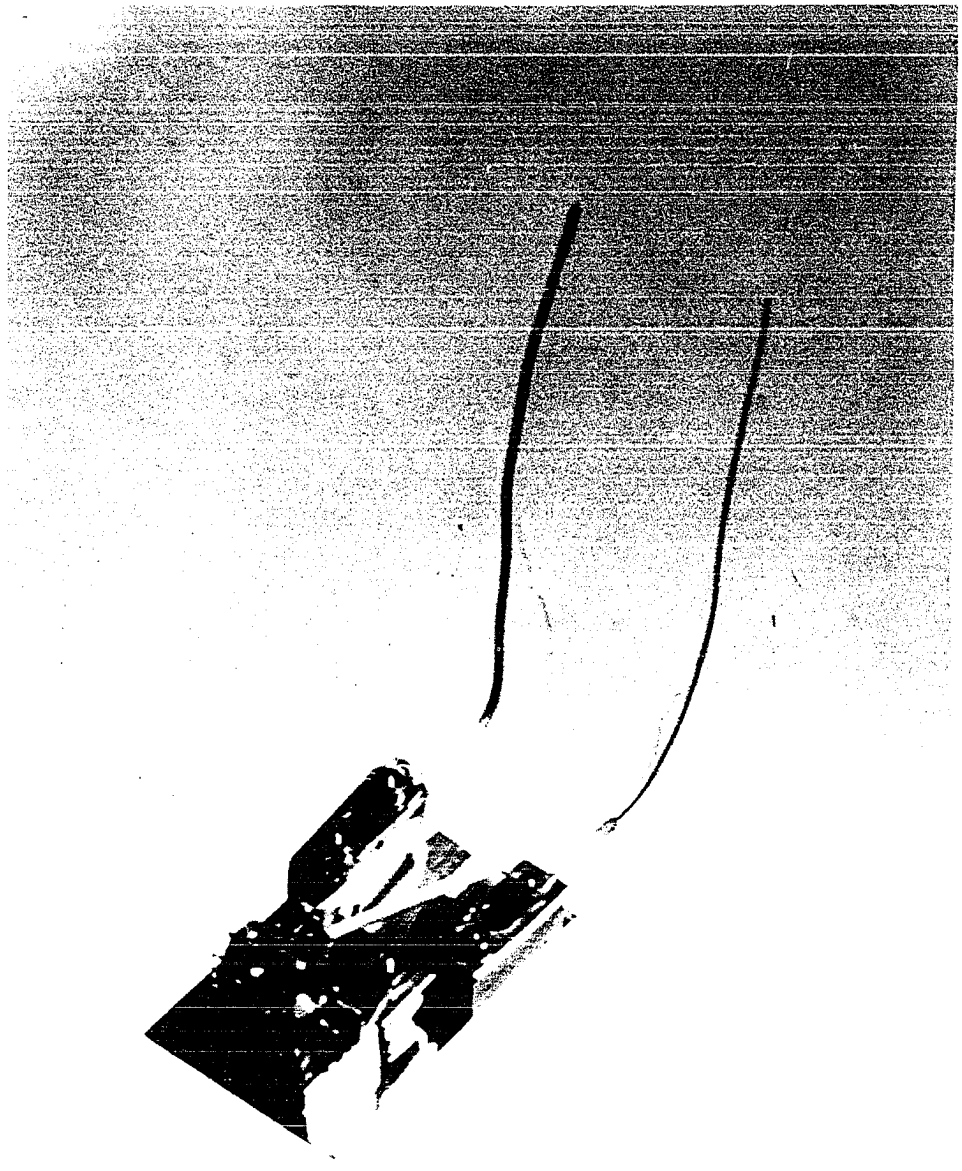

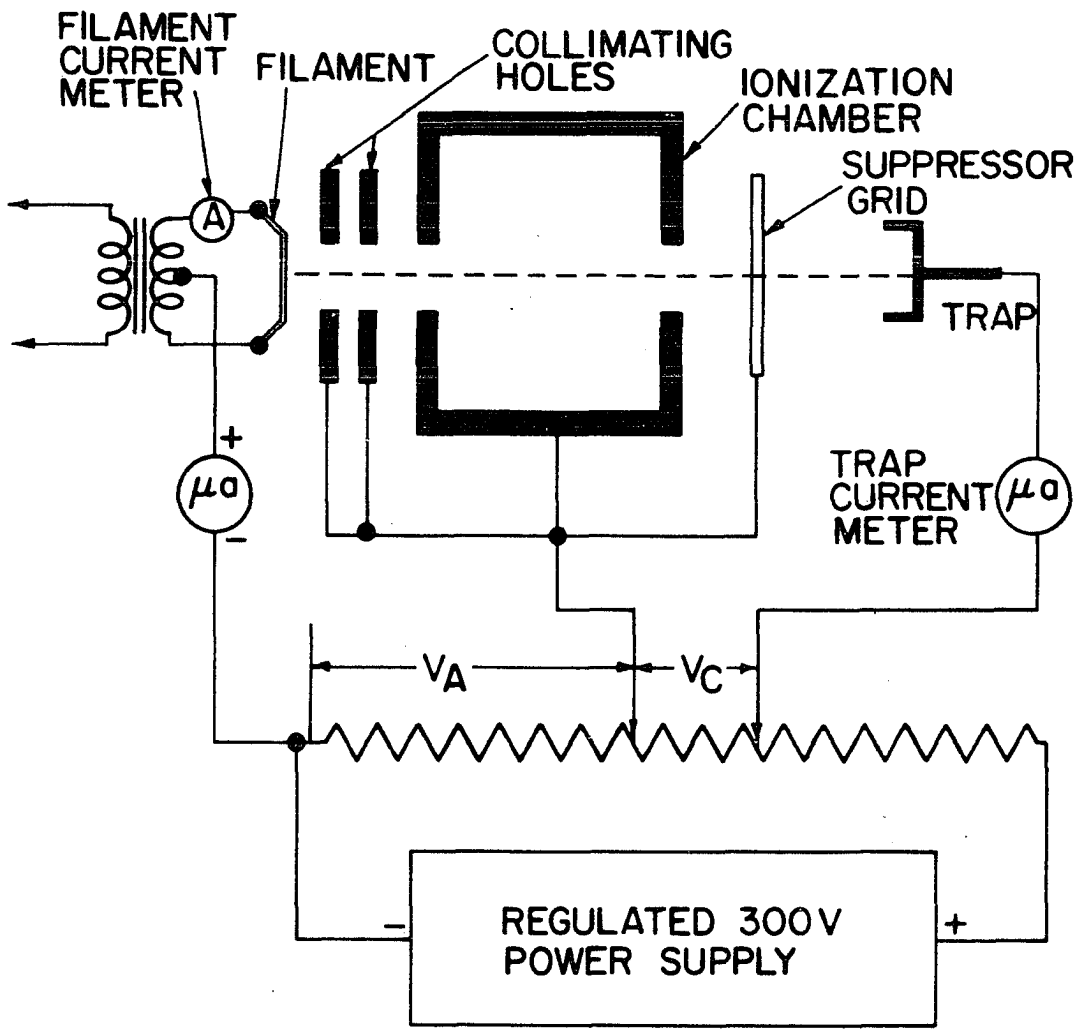

Figure 8. Schematic drawing of the electron bombardmant ionization source (EBIS)

the voltage V_C. The ionization efficiency for a given atom varies with V_A and with the trap current. The electron bombardment ionization source will be referred to hereafter as EBIS.

The ionization device is assumed to convert a constant fraction of the incoming particles into ions. Thus the ion current drawn out of the ionization chamber is proportional to the vapor pressure within the Knudsen cell. The stability of the filament power supply and of the 300 volt accelerating power supply is critical, and details of the circuits designed to produce that stability are given by Jackson and Hudson (35).

d. Ion optics It is generally true that in a mass spectrometer the intensity of the beam increases as the beam-defining slits are widened. However the ability of the mass spectrometer to resolve adjacent mass peaks decreases as the slits are widened. The slit system used in this work is shown in Figure 5 and is described in detail in Appendix D. The ion energy was determined by a potential of 1900 volts between points B and E of Figure 5. This potential was maintained by an electronic voltage regulator. A 200 volt potential between points B and C of Figure 6 drew the ions out of the ionization chamber.

Experiments indicate that the resolution and intensity of the ion beam with the 1900 volt accelerating potential depends strongly on the values and stability of the voltages between B and C and between C and D of Figure 6 (Appendix D). For this purpose the 200 volt B-C potential was supplied by a battery. The success of the experiment depends on the proportionality between the ion current leaving the slit system and the pressure within the Knudsen cell. This proportionality is insensitive to

the particular (constant) values of the voltages between the various slits.

e. Cell heater The cell (A, Figure 5) was heated by radiation from hot tungsten filaments (F) situated at both ends of the cell. Within the precision of the optical pyrometer no temperature gradient existed along the cell at temperatures four or five hundred degrees higher than those used in this experiment. It was assumed that this also held true for temperatures too low to be measured with the optical pyrometer.

The only critical feature of the heater system is that the filament power supply must be regulated sufficiently well to minimize temperature drift over the one minute during which data on any point was taken. Experiments indicated that temperature drift during a five minute period was usually much less than 1°C.

f. Shutter The shutter (G, Figure 5) was a thin tungsten plate mounted on a steel bar. The bar was supported at both ends within sections of glass tubing. Current could be passed through wire coils wrapped around either of these insulating supports and the magnetic field thus produced served to draw the shutter toward the support on that side. Thus, the path to the ion chamber could be completely closed or completely unobstructed by the shutter. This situation could be checked visually through a window in the top of the source chamber.

3. Magnetic analyzer

The mass analyzer (C, Figure 5) was a 60° sector electromagnet. The selection of the ion peak was accomplished by variation of the magnetic

field, so controls were employed which allowed slow, continuous variation of the magnetic field from about 2 to 8 kilogauss. Once an ion peak was selected, it was important that the magnetic field be stable enough to prevent drifting off peak. The circuits designed to assure this stability are discussed elsewhere (11).

The atomic mass, M, of an ion is related to the magnetic field, B, which brings that mass into focus by the formula

$$M = A B^2 ,$$

where A is a constant of the mass spectrometer. The constant A was determined empirically by recording B for a known M in an auxiliary experiment. Pure Mg was placed in the Knudsen cell, and the isotopes were identified by shutter sensitivity (see Section IIIB) and by the isotopic abundance of the three Mg isotopes. The B values were measured on a Marion Type TS-15A/AP flux meter.

4. Collection and detection system

The ions had access to the collection chamber (D, Figure 5) through a narrow entrance slit. The resolution and intensity depend strongly on the size of this slit once the defining slip in the source has been fixed. For the slit system employed, the spectrometer was capable of resolving adjacent masses at masses around 200 amu. The beam intensity also was sufficient for the required measurements.

The ions passing through the final slit were incident upon a converter dynode which produced several secondary electrons for each impinging ion. These secondaries were accelerated to a second stage

where further multiplication occurred in the same manner. Thirteen such stages were employed. The voltage for each stage was supplied by an NJE Corporation Model S-325 500-2500 VDC regulated power supply operating across a voltage divider designed to supply equal voltage at each stage. The regulation of this voltage was sufficient to eliminate drift due to variation in multiplier gain. Typically, voltages in the 2000-2500 volt range were used. Details of this multiplier have been reported by its designer, Dr. O. C. Trulson (57). Trulson reports the gain to be of the order of magnitude of 10^4.

The multiplier output was fed directly to a vibrating reed electrometer which amplified the signal and recorded it continuously on a Brown moving-strip recorder. If the multiplication and amplification were linear, then the recorder current was proportional to the incident ion current which, in turn, was proportional to the vapor pressure of the sample.

5. Instrumental linearity

The overall linearity of the complete mass spectrometer system was verified by the experiment described in Appendix B. The linearity of the various components of the collector-detector systems was checked experimentally. The linearity of the detection system (electrometer and recorder) was tested by observing the response on the recorder to known voltages applied directly across measuring resistor of the electrometer. The voltages were battery-supplied. The impressed voltage was read simultaneously on the recorder and on the potentiometer (see Section IIIC for description of the potentiometer). The recorder had three

sensitivity scales. The linearity of all three scales was confirmed in this experiment to within 0.1%.

Trulson (11) tested the linearity of the multiplier by collecting the ion current from a given source both by direct collection in a Faraday cup and by collection with the multiplier system. To within the accuracy of the experiment, the linearity of the multiplier system was confirmed.

C. Auxiliary Equipment

1. Thermocouple and potentiometer

The temperature of the cell was measured by Pt - Pt 13% Rh thermocouples installed as described in Section IIIB2b. The reference temperature, 0^{o} C, was maintained by an ice bath. The thermocouple emf was measured on a Leeds and Northrup Type K potentiometer. Calibration of the thermocouple used against a secondary standard (a Pt - Pt 13% thermocouple calibrated by the National Bureau of Standards) was performed by imbedding both thermocouples within one quarter of an inch of each other in a copper block, heating the copper block in an oven, and comparing the voltages read on the potentiometer. The thermocouples used in all of the experiments reported in this thesis were made from the same rolls of 6 mils diameter, high quality Pt and Pt 13% Rh wires (obtained from the American Platinum Works, Newark, New Jersey), so the calibration was assumed to be valid for all of the experiments reported in this thesis. An auxiliary experiment was performed to test the accuracy of the thermocouple as a device to measure the cell temperature. A closed but empty

cell was placed in the source chamber. As usual the Knudsen cell was grounded. A modification of a device used by Trulson (11) was used to obtain high temperatures. That is the filaments were placed at a potential of about -450 volts. This potential caused cell heating to arise from electron bombardment as well as from radiation. The cell was thoroughly outgassed for temperatures up to 1300° K. The temperature of the cell was allowed to reach a steady value which was read as 1213° K by the thermocouple. The apparent temperature of the orifice was read with an optical pyrometer. The orifice was treated as a black body and window absorption was evaluated by the method described by Trulson (11). The corrected values of the cell temperature as determined by the optical pyrometer were 1217° K, 1217° K, 1215° K, and 1216° K. Even with an experienced operator of the optical pyrometer these values (average 1216° K) must be considered to agree within the experimental accuracy with the value 1213° K obtained with the thermocouple. The inexperience of this operator was assumed to have played some part in the 3° K difference between thermocouple and optical pyrometer temperature values. A net error of $\pm$ 2° K was assumed for all thermocouple temperature measurements.

2. Vacuum system

The entire unshaded region in Figure 4 was maintained at a high vacuum. The vacuum was obtained and monitored by three 5 liter/second VacIon pumps. At all times during data taking the pressure was between $2X10^{-7}$ and $10X10^{-7}$ mm. Auxiliary experiments indicated no sensitivity of results to this residual background pressure over this range of pressures.

IV. PROCEDURE

A. Introduction

In Section IC it was shown that the information of interest in a sublimation experiment was the temperature dependence of the vapor pressure. This section will describe the technique by which the mass spectrometric analysis of the vapor effusing from a Knudsen cell has been used to obtain data on ΔH_{Mg}.

B. Preliminary Operations

Before useful data were taken on an Mg_2X sample, certain preliminary operations were performed. The sample was placed in the cell, and the cell was placed in position in the source chamber of the mass spectrometer. Once the sample was in position a suitable vacuum was developed. Finally, the ion current of interest was focused on the collector-detector system (see Section III4). It is the purpose of this section to describe the manner in which these preliminary operations were carried out for the experiments reported in this thesis.

The loading of the sample into the cell and of the cell into the source chamber of the mass spectrometer was performed by an operator wearing clean plastic gloves and working with clean tweezers on a cleaned work area. The samples were filed with a new clean file to remove any surface impurity contamination. Where the individual Mg_2X member required unusual handling techniques, those techniques are described in the subsection of Section V which deals with that particular compound. In all cases the loading operations were performed as quickly as

practicable.

The forevacuum on the mass spectrometer was obtained by a mechanical fore pump operating in conjunction with a liquid nitrogen cold trap between the pump and the mass spectrometer. Within 30 minutes after the fore pump was started, the VacIon pumps were started. The VacIon pumps were allowed to operate one day before outgassing was begun. In order to assure a good vacuum, outgassing of various parts of the system was required. The electron emission filament in EBIS (Figure 8) was heated at operating temperature for about 24 hours before data were taken. During this period, the Knudsen cell heater (F, Figure 6) was operated at reduced temperatures so that the cell warmed to about 200° C-300° C. This operation required about eight hours. The cell heater was flashed at the maximum operating current periodically during the rest of the outgassing period. During the outgassing, the Knudsen cell temperature was never allowed to exceed about 400° C to minimize surface oxidation and to avoid depletion of Mg from the sample. Data were taken at pressures around $8X10^{-7}$ mm. Hg.

After the system was outgassed as described, the ion beam of interest was focused on the collector-detector system by varying the field of the magnetic analyzer. The most abundant isotope of magnesium, Mg^{24}, was used.

C. The Sublimation Run

It will be recalled that the raw data to be obtained in this experiment consist of the ion current I as a function of the cell temperature T (See Equation 28). The value of I is displayed on a moving-strip

recorder and T is derived from a potentiometric thermocouple measurement.

A sublimation run consisted of from 10 to 20 measurements each of the recorder current and the corresponding thermocouple voltage reading. The first point (recorder current and thermocouple voltage) was at the highest temperature of the run. Subsequent points corresponded to systematically lower temperatures. The final point, or "check point", of a run was at a temperature near that of the initial point. A single "point" of a run consists of values for three quantities - the recorder current with the shutter open, the recorder current with the shutter closed, and the thermocouple voltage. The shutter-open and shutter-closed positions were marked O and X respectively on the recorder strip, and the thermocouple voltage was recorded on the recorder strip. Figure 9 is a facsimile of a portion of the record of a typical run.

D. Data Analysis

This section will discuss the techniques by which the raw data of a run were used to obtain a value of ΔH_{Mg} (Section IIB) for that run.

The first step in the analysis of a run was the conversion of the raw data into more usable forms. The current, I, for any point is the difference between the recorder current with the shutter open and the recorder current with the shutter closed (Section IVC). The conversion from thermocouple voltage to absolute temperature T, is discussed in Section IIIC.

The next step in the analysis is the numerical reduction of the data to ΔH_{Mg} values. According to Section IIA the ion current, I, is proportional to the effusion rate:

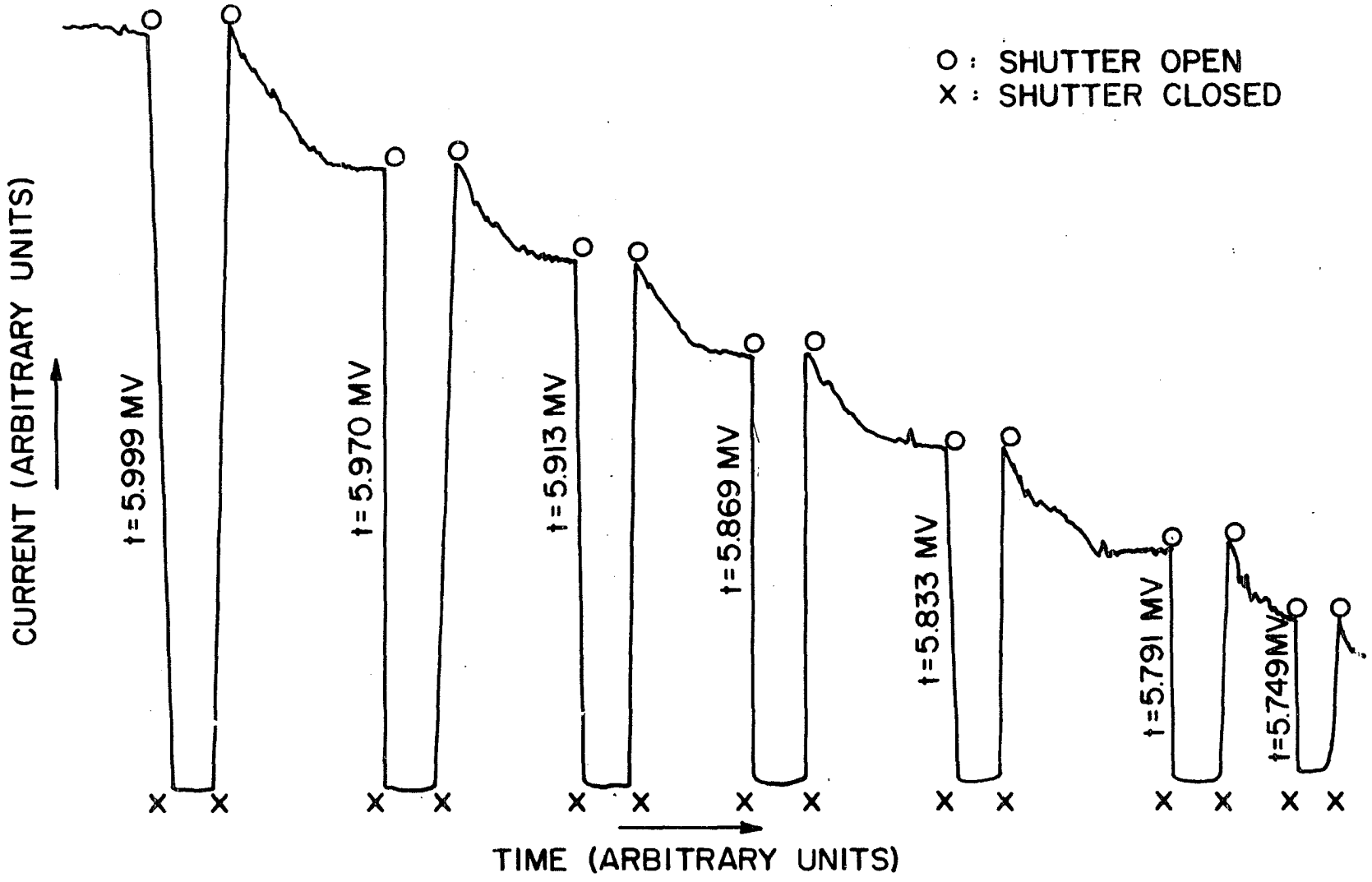

Figure 9. Drawing of typical recorder output during a run

(8) $$\frac{dN}{dt} \doteq \frac{Pa}{\sqrt{2\pi mkT}}$$

Also according to Sections IC, IIA, IIB, IIE, IIIB many factors enter into determining I. The formula for I can be written

(39) $$I = ng\left(\frac{Pa}{\sqrt{2\pi mkT}}\right)\sigma f(i)\bar{t}\, M\, W ,$$

where the various factors are as follows:

n = a numerical factor to make the units consistent

g = a geometrical factor involving transmission probabilities for the various steps in the history of an ion

P = the pressure

a = the orifice area

m = the mass of the ion

k = the Boltzmann constant

T = the absolute temperature of the cell

σ = the ionization cross section for Mg in the EBIS

f(i) = a function of the EBIS trap current, i, for a given ionizing energy (Sections IC, IIIB)

$\bar{t}$ = the average time a neutral atom spends in the EBIS ionization chamber (Section IC, and below)

M = the collection and multiplication efficiency (Section IIIB)

W = the Clausing factor (Section IIA)

Of the quantities on the right hand side of Equation 39, only $\bar{t}$, P, T, and a are temperature dependent; therefore

(40) $$I = C\, P\, T^{-\frac{1}{2}}\, \bar{t}\, a ,$$

where C is a constant such that $dC/dT = 0$.

The quantity $\bar{t}$, the mean time an atom spends in the ionization region of EBIS, is inversely proportional to the velocity of the particle; therefore if the average particle velocity is given by Equation 6, then $\bar{t}$ is proportional to $T^{-\frac{1}{2}}$. Thus Equation 40 can be replaced by

$$I = DPT^{-1}a \quad , \tag{41}$$

where D is a constant such that $dD/dT = 0$. The change in the orifice area a with temperature can be calculated from the linear expansion coefficient, $\bar{\alpha}$, of the cell material by the formula

$$\frac{d\ln a}{d(1/T)} = -2\bar{\alpha}T^2$$

Let H be any enthalpy change described by either Equation 17 or Equation 27. Both equations have the form

$$\frac{d\ln P}{d(1/T)} = -\frac{\Delta H}{R}$$

Using Equation 41 one can demonstrate that

$$\Delta H = -R\frac{d\ln I}{d(1/T)} + RT + R\frac{d\ln a}{d(1/T)} \tag{42}$$

For ΔH in kilocalories/mole and for a tantalum crucible,

$$R\frac{d\ln a}{d(1/T)} = -2.66T^2 \times 10^{-8*} \quad ,$$

where T is in ^{o}K and where the $\bar{\alpha}$ for tantalum has been used. The

*Throughout this thesis the ideal gas constant R is taken to be 1.9869×10^{-3} kcal/mole-^{o}K.

dlnI/d(1/T) was obtained by a least squares straight line fit of the lnI vs. 1/T plot for any run. The terms RT and R dlna/d(1/T) in Equation 42 were evaluated at the midpoint of the 1/T range, i.e. at

$$T_M = \frac{2T_{MAX}\ T_{MIN}}{T_{MAX} + T_{MIN}} ,$$

where T_{MAX} and T_{MIN} were the maximum and minimum temperatures represented by points in that particular run.

E. Error Analysis

This section will present the method by which uncertainties in ΔH_{Mg} have been assigned. The uncertainties to be listed are the so-called standard errors. That is the number to be quoted as the final uncertainty in ΔH_{Mg} should be such that there is a 68% probability that the true ΔH_{Mg} lies in the range of $\overline{\Delta H_{Mg}} \pm$ the quoted uncertainty. Here $\overline{\Delta H_{Mg}}$ is a quantity to be defined later in this section. For convenience the subscripts Mg will be omitted on the ΔH values. This section will discuss errors in ΔH arising from uncertainties in the measured current and temperature values as well as an uncertainty derived statistically from run-to-run variations in ΔH. Errors which arise from nonlinearity of the apparatus will be neglected for reasons discussed in the section on apparatus and equipment. Note that since the quantity of interest is the variation of lnI with (1/T) any constant multiplicative error in I will not affect the results. The various sources of error discussed in the critique but not discussed in this section were assumed to have a negligible effect on the experimental uncertainty in ΔH.

For each run (i) the following quantities are defined (the subscript i's are omitted for convenience):

$b = d\ln I/d(1/T)$

S_b = standard deviation in b (from least-squares analysis)

e_b = instrumental error in b (from errors in measurement of I and T)

e'_T = instrumental error in T_m (from inaccuracies in measurement of T)

e_n = net experimental error in ΔH for the run (from e_b and e'_T)

The value of ΔH (Equation 42) for the i'th run is called ΔH_i. A quantity W_i is defined by

$$W_i = 1/S_{bi}^2$$

for run i. The quantity W_i is called the weight of run i. The error in b due to uncertainty in T is called e_T. The instrumental error in b associated with errors in I is called e_I. The errors e_T and e_I are assumed to be equal for all points of all runs because they are due to constant instabilities and inaccuracies of the apparatus. The instrumental error in ΔH_i is given by

$$e_n^2 = R^2(e_b^2 + e'^2_T) ,$$

where error in the very small orifice correction has been neglected. Furthermore since $Rb >> RT_m$ and since the errors in b are greater than those in T_m,

$$e_n^2 \cong R^2 e_b^2 .$$

The instrumental error in b is given by

$$e_b^2 = e_I^2 + e_T^2 ,$$

but the great linearity of the collector-detector (Section IIIB) and the instrumental uncertainty in T to within $\pm$ 2°K (Section IIIC), assure

$$e_T^2 >> e_I^2 , \text{ so}$$

$$e_b^2 \cong e_T^2 .$$

The quantity e_T can be calculated from an examination of the evaluation of the formula b = dlnI/d(1/T),

$$b = \frac{\ln I_1 - \ln I_2}{1/T_1 - 1/T_2}$$

If T_1 and T_2 are both in error by ΔT, the apparent value b' of b will be given by

$$b' = \frac{\ln I_1 - \ln I_2}{1/(T_1 \pm \Delta T) - 1/(T_2 \pm \Delta T)}$$

$$= \frac{\ln I_1 - \ln I_2}{\frac{T_2 - T_1}{T_1 T_2 \left(1 \mp (\Delta T/T_1) \mp (\Delta T/T_2)\right)}}$$

$$= \frac{b}{1 \mp 2\Delta T/T_M}$$

$$\cong b \left(1 \pm 2\Delta T/T_M\right) .$$

That is

$$e_T = 2B \Delta T/T_M \ .$$

If it had been assumed that ΔT was proportional to T, the resulting error e_T would have been

$$e_T = b \Delta T/T_M \ .$$

The choice of constant ΔT seems more reasonable physically, and the factor of two difference between the e_T values makes the constant ΔT choice safer. Therefore the net instrumental error e_n in each run is

$$e_n = 2Rb(\Delta T/T_M) \ .$$

The instrumental error in the net ΔH for the substance is assumed to be e_n.

For reasons to be discussed in greater detail in Appendix E, $\overline{\Delta H}$, the net ΔH for all runs on a given substance, is given by

$$\overline{\Delta H} = \frac{\Sigma W_i \Delta H_i}{\Sigma W_i}$$

The quantity K_i, called the normalized weight of the i'th run, is defined by

$$K_i = \frac{W_i}{\Sigma W_i} \ .$$

Expressed in terms of K_i, the previous formula becomes

$$\overline{\Delta H} = \Sigma K_i \Delta H_i \ .$$

The observed standard deviation in ΔH is by definition

$$S_h^o \equiv \left[\Sigma K_i \, (\overline{\Delta H} - \Delta H_i)^2\right]^{\frac{1}{2}},$$

where n is the number of runs. Topping (58) suggests a second expression for the standard deviation, S_h^e called the expected standard deviation and given by

$$S_h^{e\,2} = \Sigma \, K_i^2 \, S_{bi}^2 R^2,$$

where S_{bi} is the standard deviation of b for the i'th run. One can show, using the equations for K_i, W_i, and S_{bi}, that

$$S_h^e = \left(\frac{1}{\Sigma W_i}\right)^{\frac{1}{2}} R.$$

The expected standard deviation S_h^e depends only on the internal consistency of the individual runs. The observed standard deviation S_h^o depends largely on run-to-run variations. In any real case $S_h^o > S_h^e$, but ratios of S_h^o to S_h^e much greater than unity indicate that there are errors from run to run which are in excess of the errors that would be expected if the scatter of points within each run were the only source of run-to-run variation. The net error in ΔH is

$$E_h = \left[S_h^{o2} + e_b^2\right]^{\frac{1}{2}} \text{ or}$$

$$E_h = \left[\frac{1}{n-1} \Sigma \, K_i \, (\overline{\Delta H} - \Delta H_i)^2 + \left(\frac{2Rb \, \Delta T}{T_M}\right)^2\right]^{\frac{1}{2}}.$$

F. Numerical Calculations

The numerical calculations outlined in this section were carried out by an IBM 650 digital computer using two programs written by Mr. D. M. Jackson of this laboratory. The I and T values for each run served as the input for a program which calculated ΔH, T_M and W_i for each run. The output of this run analysis program served as the input to a program which calculated $\overline{\Delta H}$, average T_M, S_h^o and S_h^e. The quantities K_i were hand calculated with a desk calculator. The numerical results of Jackson's programs were checked against the hand calculated results of Trulson (11). The hand calculations confirmed the computer results to within the accuracy of the hand calculations (five significant digits).

V. EXPERIMENTAL RESULTS

A. Introduction

This section will describe some aspects of this experiment which are common to all of the Mg_2X compounds used in this experiment.

All Mg_2X samples employed in this work were furnished by Experimental Physics Group VI under the leadership of Dr. G. C. Danielson. The crystals used were formed from a melt of stoichiometric proportions of pure Mg and X in a graphite crucible. The melt was slowly cooled to room temperature. The samples used in this work were from parts of the crystals which were never in contact with the graphite. No carbon impurities appeared in any of the samples tested (VB). Details on the preparation Mg_2X compounds studied by Dr. Danielson are available (59).

It was shown in Section IIB that if the subliming vapor is largely Mg, then ΔH_{Mg} is given by

$$\Delta H_{Mg} = -R \frac{d\ln P_{Mg}}{d(1/T)}$$

The application of this formula for this experiment is discussed in Section IV. Appendix B describes several auxiliary experiments which show the predominance of Mg over X in the vapor over Mg_2X. These experiments involved direct search for X with the mass spectrometer, analysis for X in the deposit of vapor from Mg_2X which adhered to a cold target, comparison with previous results, analysis of weight-loss data on Mg_2X on the assumption that Mg dominates the vapor, and application of the Duhem-Margules equation to the Mg_2X crystal. All of these experiments confirmed the great predominance of Mg over X in the vapor over Mg_2X.

Another auxiliary experiment was performed in order to test the overall operation of the mass spectrometer as a device for measuring Δ H values. This experiment was the measurement of ΔH for the sublimation of europium metal by the methods and equipment of this thesis. The results of this experiment agree quite well with previous results (Appendix B). It was concluded that the method used in this work was adequate to yield reasonable H values.

The Knudsen cell temperature range employed for each compound was not chosen arbitrarily. Instrumental factors (especially the recorder noise level) limited the measurements for sufficiently low temperatures. The low temperature for each compound is that temperature for which the current is so low that instrumental noise causes fluctuations of a few percent in the apparent ion current. The high temperature was so chosen that several runs could be taken before plating of Mg on the window of the source chamber was noticeable. It was felt that significantly higher temperatures might lead to depletion of the Mg in the solid with a consequent inapplicability of the thermodynamics of Section IIB. A few runs were taken over temperature ranges as large as about 100°K. The data on Mg_2Sn and on Mg_2Pb showed the largest run-to-run variations of temperature ranges. For Mg_2Sn Run 1A had a temperature range of 104°K while Run 1B had a temperature range of 66°K. The ratio of the high to the low temperature ranges was 1.58. No systematic variation with temperature range was observed. If the final ΔH_{Mg} were calculated by weighting the ΔH_{Mg} of each run by the temperature range of that run, a value ΔH_{Mg} = 43.8 kcal/mole would result. The ΔH_{Mg} value quoted in

Section VB is 44.0 $\pm$ 1.2 kcal/mole. A significant systematic variation of ΔH_{Mg} with temperature range would be expected to result in a temperature-range-weighted ΔH_{Mg} noticeably different from the value 44.0 $\pm$ 1.2 kcal/mole obtained in Section VB. For Mg_2Pb the temperature ranges varied from 100°K (Run 1C) to 63°K (Run 1J). The ratio of ranges was 100°K/63°K = 1.59. No systematic variation of ΔH_{Mg} with temperature range was noticed. The ΔH_{Mg} obtained from weighting each run according to its temperature range was 34.32 kcal/mole as compared with ΔH_{Mg} = 33.6 $\pm$ 0.6 obtained in Section VB. The data on temperature ranges are found in Appendix F.

For each compound results have been calculated from the formulas of Sections IIB, IVD, and IVE. The calculations were carried out numerically to a point which is absurd on the basis of the estimated errors involved. It was no extra trouble to do this, and it was considered desirable to defer any rounding off until the final figures for ΔH_{Mg}, E_h, and T_M were quoted. Therefore the tables contain data stated to more significant figures than the physics justified. The value of E_h was considered to be accurate to within $\pm$ 30%. Errors whose first two significant digits were less than 35 were quoted to two significant digits. All other errors were quoted to one significant digit. A result whose error term has its last quoted digit n places to the right (left) of the decimal place was quoted such that its last significant digit was n places to the right (left) of the decimal place.

Typical data plots have been included for all of the substances studied. It is of interest to note that the points show very little

scatter about the indicated straight line and that no systematic deviations (e.g. with 1/T) appear to be present.

Techniques involved in the handling of the various compounds are described in Section IVB if they are common to all of the compounds and in Section VB if they are peculiar to one compound.

The various compounds were analyzed spectrographically in the Ames Laboratory Spectroscopy Group under Dr. V. A. Fassel. In each case there was a faint trace of Ca and there were no other impurities. No shutter sensitive Ca^{+} or Ca^{++} was observed mass spectrometrically.

Each run was designated by a code consisting of a number (the loading number) and a letter (the order of that run within the runs on that loading). Therefore the first run on any material was called 1A. The second run made with that sample and cell without reopening the source chamber was called 1B. The first run made after the cell used in loading 1 was removed and another cell was inserted was called 2A. This information should assist the reader in examining the data for systematic trends. No such trends were detected by this author (VB). The conclusions to be drawn from their absence are discussed in Section IIE and in Appendix B.

B. Results for Individual Compounds

1. Mg_2Si

A total of fourteen sublimation runs was taken on five loadings from two samples of Mg_2Si. All Mg_2Si samples were polycrystalline. Quantitative chemical analysis of one of the samples (number 24-B) indicated

63.25% Mg by weight as opposed to 63.40% Mg in pure Mg_2Si. If all of the Mg exists as Mg_2Si, there are 0.0056 moles of excess Si for every mole of Mg_2Si.

Loadings 1, 2, and 3 involved small chunks of sample 24-B. The Knudsen cell orifice diameters were 30 mils, 20 mils, and 30 mils, respectively. Loadings 4 and 5 were of batch 16-B. Loading 4 had chunks of the sample in a cell having a 30 mil orifice. Loading 5 used a powdered sample in a cell having a 20 mil orifice. Only one run was taken on loading one, because a heater filament broke in heating the cell for the second run.

A typical run (number 1A) is shown in Figure 10. For run 1A $\Delta H_{Mg} = 45.10 \pm 0.34$ kcal/mole at $T_M = 863^oK$. The data on Mg_2Si are summarized in Table 2. The experimental value of ΔH_{Mg} at 864^oK was 44.41 ± 0.34 kcal/mole.

Appendix E discusses a method for assessing the statistical significance of the effect on ΔH_{Mg} of certain experimental parameters. In this way it was determined whether or not ΔH_{Mg} was sensitive to orifice diameter, to the sample of Mg_2Si employed, or to the fineness of the granulation of the sample employed. The test is to determine whether the observed variations in ΔH_{Mg} due to these parameters can be accounted for as statistical variations in values picked at random from a normal population or whether additional sources of variation must be postulated. All of the tests gave the negative result. That is, the observed ΔH_{Mg} did not appear to depend on the orifice area, nor upon whether or not the sample was powdered, nor upon which sample of Mg_2Si was being studied.

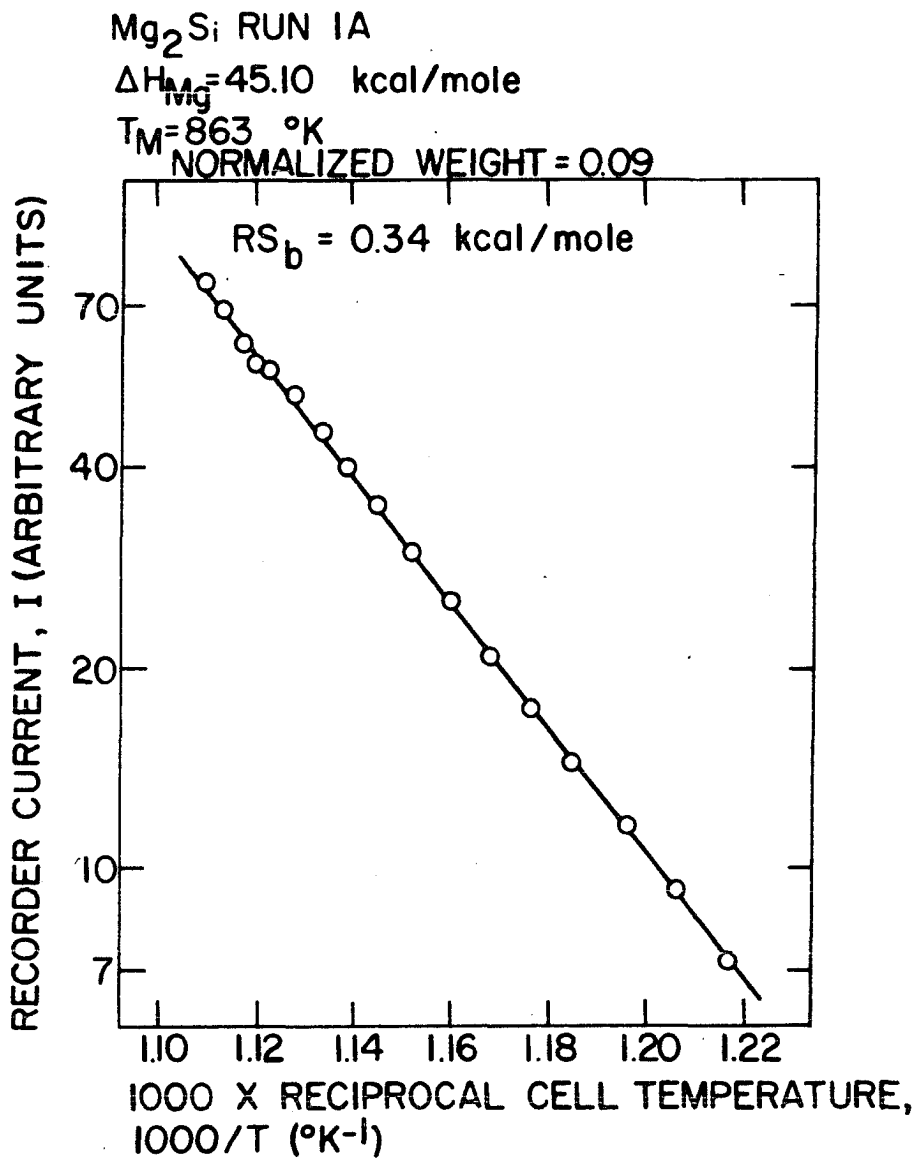

Figure 10. A typical Mg_2Si data plot

Table 2. Data compilation on Mg_2Si

Run	Number of points	ΔH_{Mg} (kcal/mole)	Midrange temperature (°K)	Normalized weight (K_i)
1A	19	45.10	863	0.098
2A	11	44.99	867	0.227
2B	11	43.35	866	0.041
2C	10	44.56	868	0.163
3A	10	39.62	864	0.004
3B	10	40.81	864	0.009
3C	11	44.47	863	0.075
3D	11	44.68	866	0.141
4A	11	40.99	864	0.003
4B	11	44.07	864	0.004
5A	10	43.13	860	0.005
5B	10	41.56	861	0.185
5C	10	42.78	864	0.003
5D	10	42.42	865	0.042
Mean	11	44.43	864	0.071

$S_{bi}^2 = 2948/K_i(°K^2)$

Expected standard deviation of mean, S_h^e	0.12 kcal/mole
Observed standard deviation of mean, S_h^o	0.26 kcal/mole
Instrumental error, e_n	0.21 kcal/mole
Net experimental error, E_h	0.34 kcal/mole
Orifice correction	-0.02 kcal/mole

Experimental result: $\Delta H_{Mg} = 44.41 \pm 0.34$ kcal/mole at 864°K.

The cohesive energy of Mg_2Si can be evaluated from known thermodynamic data. The heat of sublimation of Mg metal has been reported by Smith and Smythe (54) and by Kubaschewski and Evans (60). The respective values are 34.99 $\pm$ 0.63 kcal/mole and 35.6 $\pm$ 0.8 kcal/mole, both at 298°K. The value of Smith and Smythe will be used because it is more recent. The heat of sublimation of elemental Si at 298°K as reported by Brewer (61) is 90 kcal/mole. Honig (62) lists the heat of sublimation of Si as 105 $\pm$ 2 kcal/mole. The value of Honig will be used because it involves only the sublimation of the monomer Si. The heat of formation of Mg_2Si is 18.6 $\pm$ 1.5 kcal/mole (52). The cohesive energy, except for the small correction in extrapolation to T = 0, is given by $\Delta H_R = 2L_{Mg} + L_{Si} + \Delta H_f = 2(34.99) + (105) + (18.6) = 193.6 \pm 2.8$ kcal/mole (Section IID). Using the methods of Section IID, one can extrapolate ΔH_R to the cohesive energy H_o of Mg_2Si using the known (63) Cp values for Mg_2Si. The final cohesive energy value is ΔH_o = 194.6 $\pm$ 2.8 kcal/mole. This author feels that the 2.8 error estimate is too conservative, because ΔH_f itself could be in error by that amount (Section IID). Furthermore the difference in measured L_{Mg} between the results of Smith and Smythe (54) and those of Kubaschewski and Evans (60) suggests a slight increase in the error attached to L_{Mg} above the value 0.63 assigned to it in the calculation of ΔH_o.

2. Mg_2Ge

A total of fourteen sublimation runs was taken on two loadings from a single sample of Mg_2Ge. The Mg_2Ge used in this work was polycrystalline. The Analytical Chemistry Group found the sample to be 39.58% Mg by weight,

whereas pure Mg_2Ge would be 40.1% Mg. If all of the Mg existed as Mg_2Ge, then there were 0.023 moles of excess Ge for every mole of Mg_2Ge.

Run 1A had to be discarded, because the check point indicated unusual current drift. Run 2B was discarded, because some unknown phenomenon caused half of the points to be displaced by a fairly constant lnI from the other points.

A typical Mg_2Ge data plot (Run 2H) is given in Figure 11. For Run 2H, $\Delta H_{Mg} = 53.09 \pm 0.38$ kcal/mole at $T_M = 869^{\circ}K$. The results of the twelve Mg_2Ge runs are summarized in Table 3. The experimental results are $\Delta H_{Mg} = 54.4 \pm 1.1$ kcal/mole at $875^{\circ}K$.

In loading 1 (Runs 1B, 1C, 1D, 1E) the orifice diameter was 20 mils. In loading 2 (Runs 2A, 2C, 2D, 2E, 2F, 2G, 2H, 2I) the orifice diameter was 30 mils. The ratio of orifice areas for the two runs was $(20/30)^2 = 0.44$. The factorial analysis of Appendix E suggests no significant dependence of ΔH_{Mg} on orifice area.

A cohesive energy estimate can be obtained from published data. The heat of sublimation of Mg as determined by Smith and Smythe (54) is 34.99 $\pm$ 0.63 kcal/mole at $298^{\circ}K$. The error as quoted arises from purely statistical effects. Kubaschewski and Evans (60) list the heat of sublimation of Mg as 35.6 $\pm$ 0.8 kcal/mole. Honig (64) lists the heat of sublimation of Ge as 89 $\pm$ 2 kcal/mole. This compares poorly with the value 78.4 kcal/mole listed by Brewer (61). The heat of formation of Mg_2Ge has been measured with an undetermined accuracy as 18.3 kcal/mole (52). A crude guess as to the error is $\pm$ 3 kcal/mole. This author does not feel competent to choose between conflicting listed values, but for

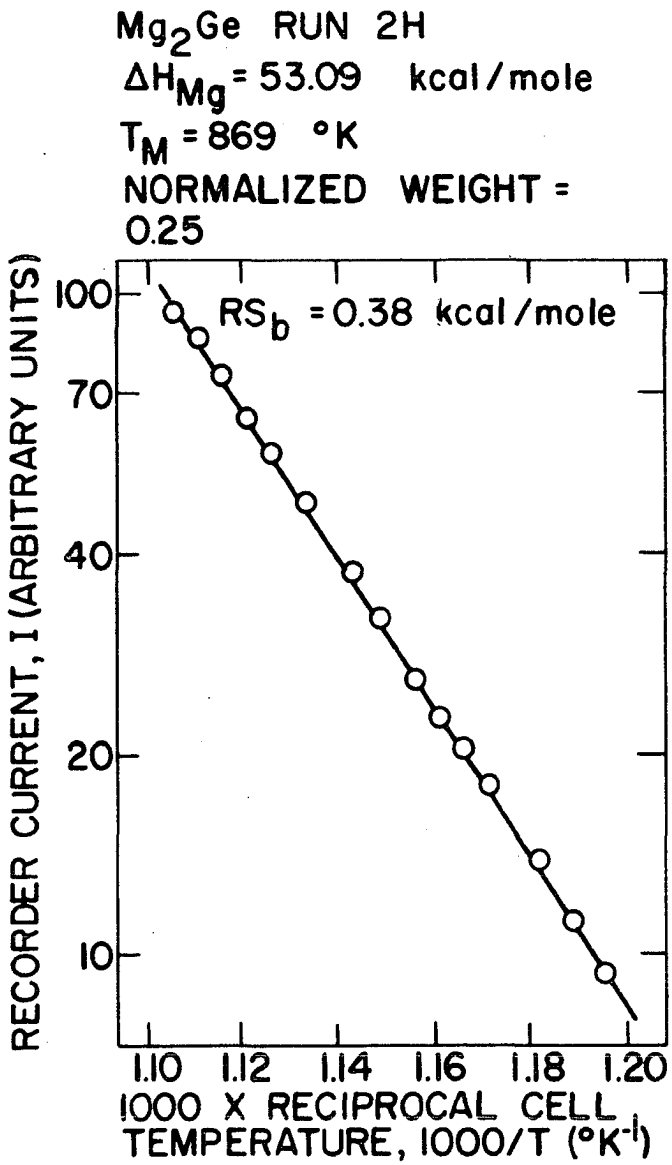

Figure 11. A typical Mg_2Ge data plot

Table 3. Data compilation on Mg_2Ge

Run	Number of points	ΔH_{Mg} (kcal/mole)	Midrange temperature (^oK)	Normalized weight (K_i)
1B	22	53.70	887	0.035
1C	21	60.58	883	0.008
1D	15	53.81	880	0.019
1E	36	58.79	883	0.033
2A	15	58.34	875	0.020
2C	16	51.71	869	0.046
2D	15	50.47	874	0.067
2E	15	54.58	867	0.021
2F	21	57.72	869	0.017
2G	16	49.52	869	0.073
2H	17	53.09	869	0.257
2I	18	54.27	870	0.343
Mean	19	54.38	875	0.083

$S_{bi}^2 = 9423/K_i$

Expected standard deviation of mean, S_h^e	0.19 kcal/mole
Observed standard deviation of mean, S_h^o	1.12 kcal/mole
Instrumental error, e_n	0.25 kcal/mole
Net experimental error, E_h	1.14 kcal/mole
Orifice correction	-0.02 kcal/mole

Experimental result: $\Delta H_{Mg} = 54.4 \pm 1.1$ kcal/mole at $T = 875^oK$.

calculation purposes the latest values will be employed. Thus ΔH_R (see Section IID) for Mg_2Ge at 298°K is 2(34.99) + (89) + (18.3) = 177.3 ± 3.8 kcal/mole. Cp for solid Mg_2Ge has not been measured. If the correction for Mg_2Si were applied, the resulting cohesive energy for Mg_2Ge would be 178 ± 4 kcal/mole. Again the error term should exceed 4 kcal/mole, especially since L_{Ge} might be 78.4 rather than 89 kcal/mole. A more reasonable value would be ΔH_o = 178 ± 15 kcal/mole.

3. Mg_2Sn

Thirteen sublimation runs were taken on three loadings from a single sample of polycrystalline Mg_2Sn. Quantitative chemical analysis showed the solid to be 28.05% Mg by weight, compared to 29.07% for pure Mg_2Sn. Enough excess Sn was present to form 0.051 moles of Sn for every mole of Mg_2Sn, if all of the Mg existed as Mg_2Sn.

A typical data plot for Mg_2Sn (Run 3D) is shown in Figure 15. For Run 3D ΔH_{Mg} = 42.29 ± 0.14 kcal/mole at 825°K. The data on Mg_2Sn are compiled in Table 4. The experimental result is ΔH_{Mg} = 44.0 ± 1.2 kcal/mole at 821°K.

The orifice area dependence was checked with the aid of the methods of Appendix E. The orifice diameters for loading 1, 2, and 3 were 20 mils, 30 mils, and 40 mils, respectively. The orifice area of the cell did not appear to be correlated with ΔH_{Mg}.

The cohesive energy of Mg_2Sn was calculated from published data by the formula $\Delta H_R = 2L_{Mg} + L_{Sn} + \Delta H_f$ (Section IID). Smith and Smythe (54) obtained L_{Mg} = 34.99 ± 0.63 kcal/mole. Kubaschewski and Evans (60) list L_{Mg} = 35.6 ± 0.8 kcal/mole. Brewer (61) found L_{Sn} = 70 ± 5 kcal/mole.

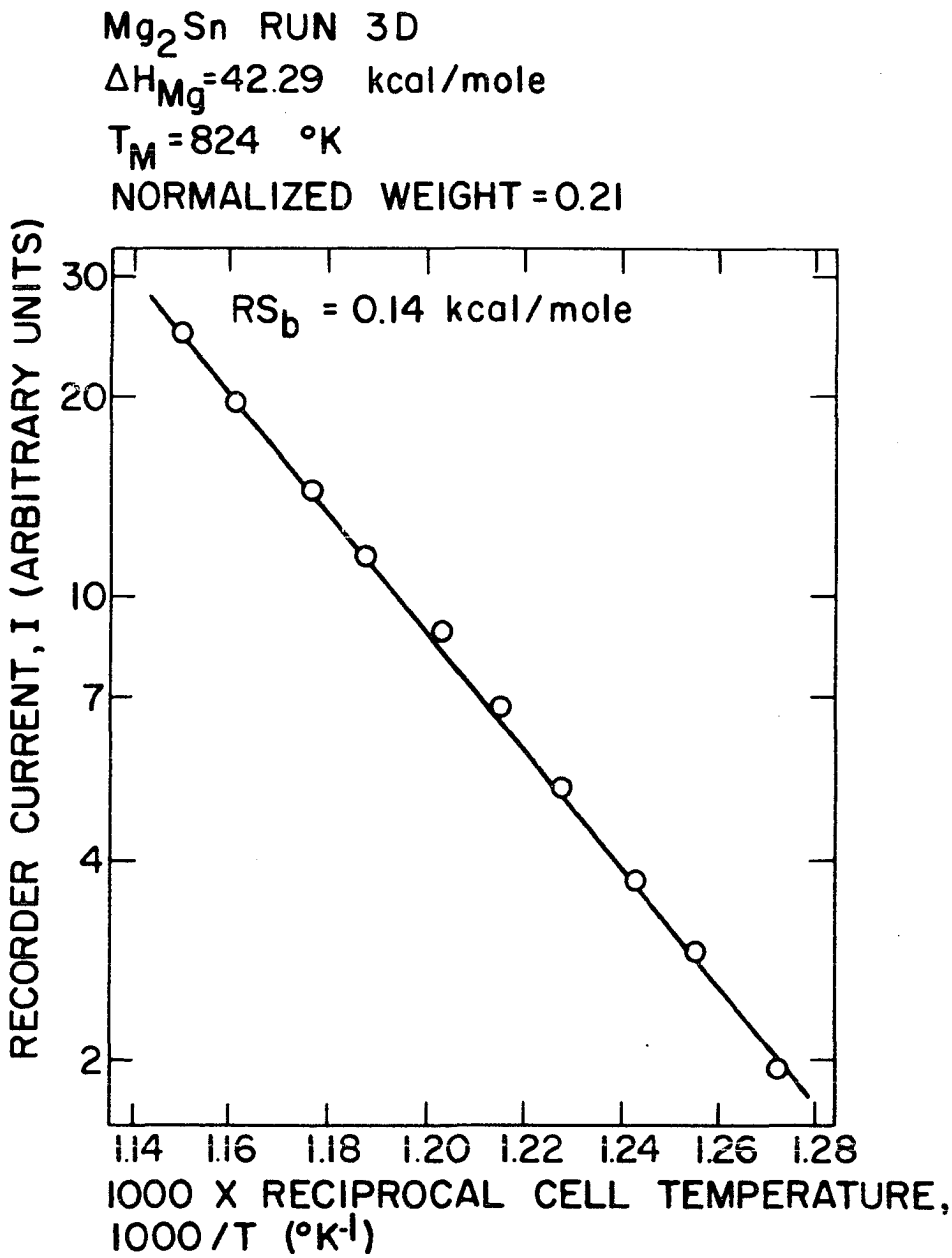

Figure 12. A typical Mg_2Sn data plot

Table 4. Data compilation on Mg_2Sn

Run	Number of points	ΔH_{Mg} (kcal/mole)	Midrange temperature (^oK)	Normalized weight (K_i)
1A	22	54.57	825	0.089
1B	17	47.71	816	0.071
1C	18	46.26	827	0.072
1D	17	50.84	825	0.035
1E	10	39.50	821	0.039
2A	10	41.26	815	0.030
2B	10	41.16	811	0.065
2C	10	38.62	814	0.028
3A	10	41.40	825	0.073
3B	10	38.38	824	0.002
3C	10	43.92	824	0.061
3D	10	42.29	825	0.216
3E	10	41.85	822	0.220
Mean	13	44.00	821	0.077

$S_{bi}^2 = 1014/K_i (^oK^2)$

Expected standard deviation of mean, S_h^e	0.20 kcal/mole
Observed standard deviation of mean, S_h^o	1.20 kcal/mole
Instrumental error, e_n	0.21 kcal/mole
Net experimental error, E_h	1.22 kcal/mole
Orifice correction	-0.02 kcal/mole

Experimental result: $\Delta H_{Mg} = 44.0 \pm 1.2$ kcal/mole at $T = 821^oK$.

The heat of formation, ΔH_f, listed by Sullivan et al. (52) is 18.3 ± 1.2 kcal/mole. All of these quantities are at 298°K. If the value L_{Mg} = 34.99 ± 0.63 kcal/mole is used, ΔH_R = 158 ± 5 kcal/mole. No data on Cp for Mg_2Sn are available. If Cp for Mg_2Sn is assumed to be the same as Cp for Mg_2Si, the cohesive energy of Mg_2Sn is found to be ΔH_o = 159 ± 5 kcal/mole.

4. Mg_2Pb

Thirteen sublimation runs were taken on two loadings of a single, polycrystalline sample of Mg_2Pb. Mg_2Pb decomposes and oxidizes very rapidly in normal air. Therefore it had to be stored under oil. All handling of Mg_2Pb was done in a dry box in a dry nitrogen atmosphere. The oil was removed with trichloroethylene followed by acetone. The material was then filed with a file used only for that purpose until only a metallic color appeared. The cleaning with acetone was then repeated. The sample was inserted into the cell and the cell was loaded into the ion source. The transfer of the ion source to the mass spectrometer and the connection of the various leads took about two minutes. At that time the spectrometer was closed and the fore pump was turned on. Examination of the Mg_2Pb in the cell after each run gave no indication of oxidation or decomposition. The decomposition product was black and powdery. The necessity for special handling techniques prevented the spectoscopic and quantitative analyses performed on the other compounds. The Mg_2Pb was made from the same pure Mg as the other compounds, and the Pb employed was as pure as possible. No shutter-sensitive peaks were found with the

mass spectrometer except for Mg.

A typical data plot for Mg_2Pb (Run 1C) is given in Figure 13. For this run ΔH_{Mg} = 31.98 kcal/mole at Tm = 753°K. The data on Mg_2Pb are summarized in Table 5. The best value for ΔH_{Mg} is 33.6 $\pm$ 0.6 kcal/mole at 770°K.

Loading 1 used a 30 mil diameter orifice. Loading 2 involved a 20 mil diameter orifice. Tests for systematic variation of ΔH_{Mg} with orifice area (see Appendix E) gave the negative result, i.e. ΔH_{Mg} did not appear to be sensitive to the cell orifice area.

Using the heat of sublimation of Mg obtained by Smith and Smythe (54), 34.99 $\pm$ 0.63 kcal/mole; the heat of sublimation of Pb listed by Brewer (61), 46.48 $\pm$ 0.50 kcal/mole; the heat of formation of Mg_2Pb given by Sullivan *et al.* (52), 12.60 $\pm$ 1.0 kcal/mole; and the specific heat data on Mg_2Si (63), one obtains the cohesive energy of Mg_2Pb, ΔH_o = 128.1 $\pm$ 1.6 kcal/mole. The 1.6 kcal/mole error is suspect for the reasons noted in the previous parts of Section VB.

C. Summary

This section consists of a tabulation of measured values of ΔH_{Mg} and derived values for ΔH_o and ΔH_X. The quantity ΔH_X was calculated from the formula $\Delta H_X = \Delta H_R - 2\Delta H_{Mg}$. The errors in ΔH_X and ΔH_o are not listed, because it was felt that the calculated errors for these quantities were misleading (VB). Table 6 is this tabulation.

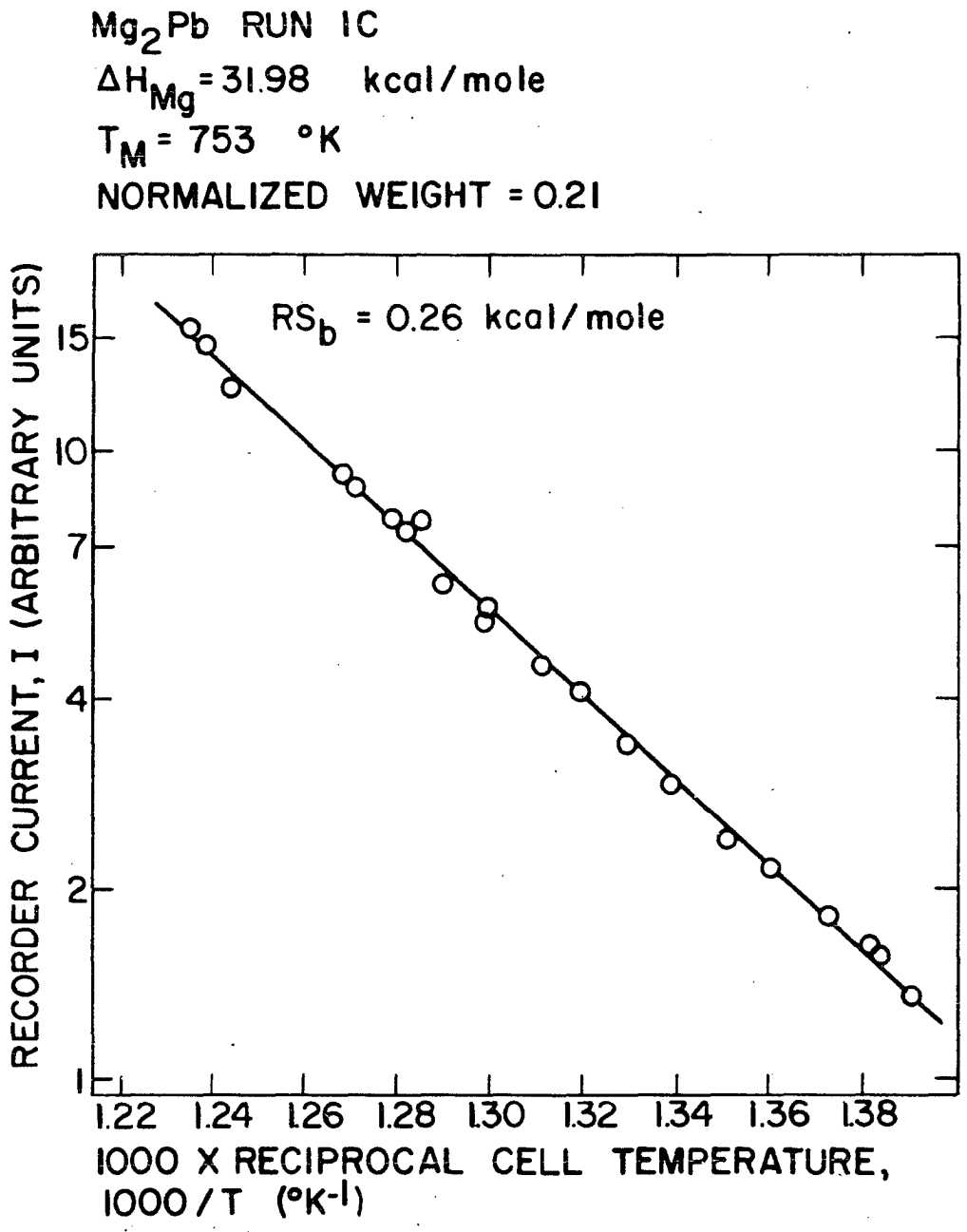

Figure 13. A typical Mg_2Pb data plot

Table 5. Data compilation on Mg_2Pb

Run	Number of points	ΔH_{Mg} (kcal/mole)	Midrange temperature (^oK)	Normalized weight (K_i)
1A	15	39.34	751	0.065
1B	16	32.70	770	0.127
1C	22	31.98	753	0.216
1D	17	34.67	746	0.125
1E	15	32.68	774	0.120
1F	17	32.30	776	0.131
1G	17	35.98	778	0.045
1H	21	31.49	776	0.012
1I	16	35.27	776	0.040
1J	16	33.30	776	0.038
2A	18	36.78	778	0.044
2B	14	32.54	775	0.019
2C	11	36.21	774	0.016
Mean	17	33.62	770	0.077

$S_{bi}^2 = 3770/K_i (^oK^2)$

Expected standard deviation of mean, S_h^e	0.12 kcal/mole
Observed standard deviation of mean, S_h^o	0.60 kcal/mole
Instrumental error, e_n	0.18 kcal/mole
Net experimental error, E_h	0.62 kcal/mole
Orifice correction	-0.02 kcal/mole

Experimental result: $\Delta H_{Mg} = 33.6 \pm 0.6$ kcal/mole at $T = 770^oK$.

Table 6. Tabulation of data on Mg_2X

Compound	ΔH_{Mg} at T_M (kcal/mole)	T_M (^oK)	ΔH_o (kcal/mole)	ΔH_X (kcal/mole)
Mg_2Si	44.41 $\pm$ 0.34	864	195	104
Mg_2Ge	54.4 $\pm$ 1.1	875	178	68
Mg_2Sn	44.0 $\pm$ 1.2	821	159	71
Mg_2Pb	33.6 $\pm$ 0.6	770	128	60

VI. DISCUSSION OF RESULTS

A. Introduction

In this section the experimental results listed in VC will be discussed in relation to the cohesion in the Mg_2X series. Also the results will be evaluated in their relationships to current and future theoretical calculations.

B. Qualitative Considerations

Actual cohesion calculations on the Mg_2X series would be an especially difficult undertaking (Section IA4), but several approximate cohesion calculations can be made with much less difficulty. These approximate calculations are not substitutes for a rigorous calculation, but they can yield some insight into the cohesion mechanisms involved.

Pauling (4) proposed a simple formula for the heat of formation, ΔH_f, of an ionic compound between two substances, A and B. This formula is $\Delta H_f = 23.07\ z(X_A-X_B)^2$ kcal/mole. Here z is the number of A-B valence links, four for Mg_2X, and X_i is the electronegativity of substance i. The electronegativities can be determined to within an additive constant by applying this formula to ionic compounds for which ΔH_f is known. The electronegativities involved in Mg_2X are listed by Pauling (4) and Kubaschewski and Sloman (25). The predicted and measured ΔH_f values are listed in Table 7. The measured values are those listed by Sullivan et al. (52). According to Kubaschewski (65) errors in ΔX values attach an error of about $\pm$ 9 kcal/mole to the predicted ΔH_f values.

Table 7. Measured and predicted values of ΔH_f for Mg_2X

Compound	ΔX	$23.0\ z\ (\Delta X)^2$ (kcal/mole)	ΔH_f MEAS. (kcal/mole)
Mg_2Si	0.6	33.1	18.6 ± 1.5
Mg_2Ge	0.5	23.0	18.3
Mg_2Sn	0.5	23.0	18.3 ± 1.2
Mg_2Pb	0.4	14.7	12.6 ± 1.0

Pauling (4) also derived a semiempirical formula for estimating the percentage of the heat of formation which arises from ionic bonding for those compounds in which the bonding is mixed covalent and ionic bonding. His formula for relative ionicity is $1-\exp(-\Delta X^2/2)$. Despite the many cases in which Pauling's analysis fails, the formula remains a useful guide (66). The percent ionic contributions to ΔH_f predicted by the Pauling formula are Mg_2Si, 8%; Mg_2Ge, 6%; Mg_2Sn, 6%; and Mg_2Pb, 4%. Thus Pauling's formula predicts that all of the Mg_2X series members are largely covalent, in agreement with the theory of Mooser and Pearson (22).

Kubaschewski (65) proposed a formula for ΔH_f based on the assumption that the strength of an A-A bond in a compound is proportional to the strength of an A-A bond in elemental A solid and to a factor C^*_A/C_A where C^*_A and C_A are "effective coordination numbers" for A in the compound and in the elemental solid respectively. The effective coordination number involves not only the number of nearest and next-nearest neighbors but also the distances involved. It was assumed by

Kubaschewski that the strength of an A-A bond varied inversely proportional to the A-A distance. The calculation of ΔH_f with the Kubaschewski formula is long and not especially enlightening. The result of precise ΔH_f calculations based on Kubaschewski's formula was of the wrong sign. That is, Kubaschewski's assumption that bonding arises from increased effective coordination does not apply to the Mg_2X series.

C. Wigner-Seitz Calculations

1. Introduction

The quantity measured in this experiment was ΔH_{Mg}, the energy with which Mg is bound in the Mg_2X series. If the bonding of Mg in Mg_2X is largely metallic, then an estimate of ΔH_{Mg} should be possible by a Wigner-Seitz calculation (IA). Strictly speaking, the Wigner-Seitz calculation applies only to elemental metals, but an extension of this method to cover Mg in the Mg_2X lattice will be made in this section. Rather than performing the Wigner-Seitz calculation "from scratch," the author based his calculation on the Wigner-Seitz calculation for pure Mg performed by Raimes (10).

2. The work of Raimes on Mg metal

The Wigner-Seitz calculation was described in some detail in Section IA. Raimes (10) devised a form for the radially symmetric potential V(r) which excludes two electrons of the same spin from occupying the same atomic polyhedron. The self consistent field chosen was $V(r) = v(r) + A$, where v(r) is the ion-core field and A is the field due to electrons of the opposite spin within the polyhedron. The quantity A

depends on ψ_o, the lowest wave function of the Schoedinger equation

$$\frac{1}{r^2}\frac{d}{dr}\left[r^2\frac{d\psi}{dr}\right]+\frac{2m}{\hbar^2}\left[\epsilon - v(r) - A\right]\psi = 0.$$

Here ϵ is the energy associated with the wave function ψ. Note that the equation for ψ_o already involves ψ_o in the term A. Therefore an iterative solution was performed by Raimes. Raimes calculated ψ_o and ϵ_o numerically for spheres whose radii (r_s) were in the range $r_s = 3.28$ to $r_s = 4.56$ Bohr radii. For values of r_s in this range, ϵ_o was effectively constant at -0.66 Rydberg units.* Raimes evaluated the total energy and cohesive energy of Mg quantum mechanically. His result reduced to the cohesive energy of Mg (L_{Mg}) given by

$$L_{Mg} = \epsilon_o + E_F + E_x + E_c .$$

Here E_F is the Fermi energy and E_x and E_c are correction factors which must be added to account for spin correlation energy, E_c, and for exchange energy, E_x. E_F is estimated from the free electron model. These quantities have been worked out by Raimes and are given by the formulas $E_F = 3.51/r_s^2$, $E_x = -1.154/r_s$, and $E_c = -0.576/(0.79r_s+5.1)$.

Using the method just outlined, Raimes calculated the heat of sublimation of Mg to be 43 kcal/mole as compared with the measured value 34.99 ± 0.63 kcal/mole (54). Thus the Wigner-Seitz calculation for Mg metal was in error by about 8 kcal/mole. This is considered reasonable in view of the many approximations involved.

*Throughout this section energies will be given in Rydberg units and lengths will be given in Bohr units, except where other units are clearly specified.

3. Application of the work of Raimes to Mg_2X

If it is assumed that electrons in the vicinity of an Mg^{++} ionic core in the Mg_2X lattice are relatively free, and if the electronic wave functions are assumed to be small and flat everywhere except in the vicinity of the ionic cores, then the Wigner-Seitz approximation should be applicable to Mg in Mg_2X. Note that no assumption on the nature of the bonding of the X atoms is necessary.

The first step in a Wigner-Seitz calculation is the construction of a polyhedron centered around the ionic core of interest by erecting planes which bisect perpendicularly lines connecting the central atom with its nearest and next-nearest neighbors. Each Mg atom has six nearest neighbor Mg atoms in the Mg_2X lattice. The perpendicular bisector planes for the lines between the central Mg atom and its nearest neighbors form a cube of side $\ell/2$, where ℓ is the lattice parameter. The next-nearest neighbors are four X atoms arranged on the corners of the cube in such a way that each face of the cube contains exactly two X atoms diagonally across from each other on the face. The erection of the perpendicular bisectors of the lines connecting these X atoms with the central Mg atom cut off four corners of the cube. The resulting polyhedron is shown in Figure 14.

In the Wigner-Seitz method, this polyhedron is replaced by a sphere with the same volume. Even though the polyhedron is far from spherically symmetric, there is reason to believe that the approximation involved in replacing the polyhedron by a sphere is acceptable. The reasoning is based on the fact that the wave functions flatten out considerably before

Figure 14. Photograph of the atomic polyhedron in Mg_2X

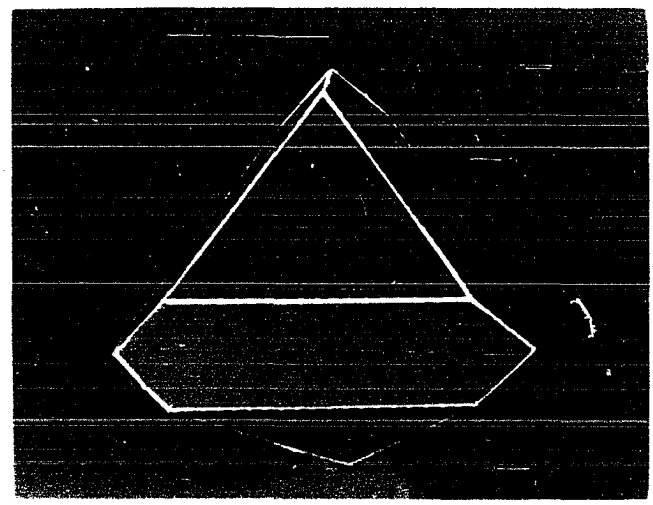

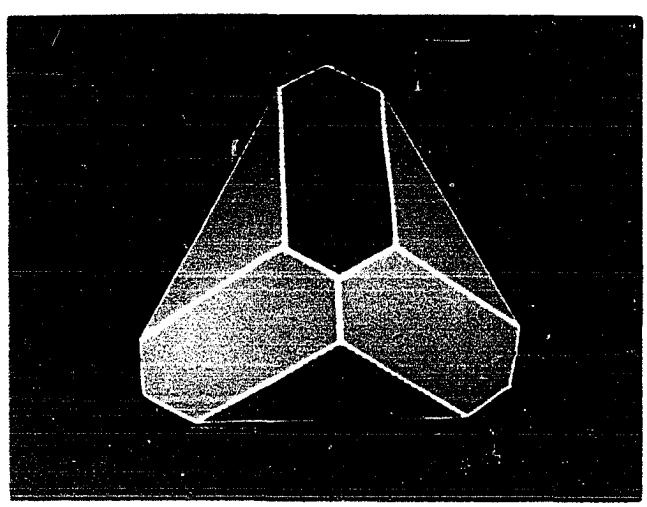

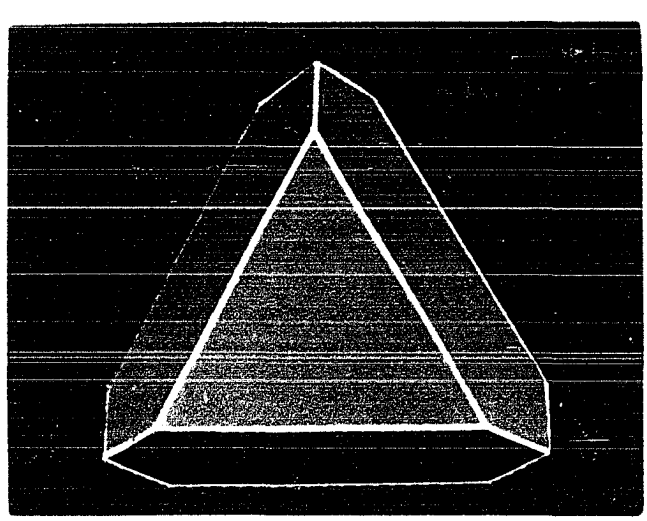

they reach the polyhedron walls. Thus the Wigner-Seitz calculation has worked well in cases with equally complicated polyhedra. The volume of the polyhedron is $0.0898\ell^3$, where ℓ is the lattice parameter. The radius of a sphere of the same volume as the polyhedron is $r_s = 0.278\ell$.

The sphere radii (r_s) for all of the Mg_2X compounds fall within the range of r_s's calculated by Raimes. Therefore the value $\epsilon_o = -0.66$ is a good approximation for all of the Mg_2X series. The only terms in the expression for ΔH_{Mg} which are sensitive to r_s are E_F, E_x, and E_c. The quantities E_F, E_x and E_c can be calculated from the formulas of Raimes which were just presented. Table 8 lists r_s, E_F, E_x, E_c, and ΔH_{Mg} for the Mg_2X series as calculated by the Wigner-Seitz approximation.

Table 8. Wigner-Seitz calculations for Mg in Mg_2X

Mg_2X	r_s	E_F	E_x	E_c	ΔH_{Mg}	ΔH_{Mg} (kcal/mole)
Mg_2Si	3.3275	0.317	-0.347	-0.107	0.078	24.4
Mg_2Ge	3.3485	0.313	-0.345	-0.107	0.080	25.0
Mg_2Sn	3.5491	0.279	-0.325	-0.107	0.094	29.4
Mg_2Pb	3.5669	0.276	-0.324	-0.107	0.096	30.0

The Wigner-Seitz results are compared with the measured ΔH_{Mg} values in Table 9. Note that the only Mg_2X compound for which the Wigner-Seitz approximation yields reasonable results is Mg_2Pb. This agreement will be discussed below.

Table 9. Wigner-Seitz values of ΔH_{Mg} compared with measured values

Mg_2X	ΔH_{Mg} calculated (kcal/mole)	ΔH_{Mg} measured (kcal/mole)
Mg_2Si	24.4	44.41 $\pm$ 0.34
Mg_2Ge	25.0	54.4 $\pm$ 1.1
Mg_2Sn	29.4	44.0 $\pm$ 1.2
Mg_2Pb	30.0	33.6 $\pm$ 0.6

D. Conclusions

1. Thermodynamic significance of ΔH_{Mg}

Although the primary aim of this thesis was the examination of the bonding in the Mg_2X series, it is important to note that the quantity measured, ΔH_{Mg}, is a primary thermodynamic quantity which governs the rate of sublimation of Mg under equilibrium conditions. By the use of published results of other workers, another primary thermodynamic quantity, ΔH_X, was estimated. Neither of these quantities has been measured previously.

2. Bonding in Mg_2X

The previously known information on bonding in the Mg_2X series was summarized in Section IB. The results of this thesis (Sections VC and VIB) indicate that the conducting properties of Mg_2Pb may arise from metallic bonding near the Mg lattice sites. Also the bonding in Mg_2Si, Mg_2Ge, and Mg_2Sn is too strong to have arisen from metallic bonding.

The conclusion of this author is that the bonding in Mg_2Si, Mg_2Ge, and Mg_2Sn is covalent with a small ionic contribution (Section VIA). The bonding of Mg_2Pb is probably metallic near the Mg sites and covalent and ionic elsewhere. These conclusions differ little from those reached by Mooser and Pearson (22).

3. The use of ΔH_{Mg} by theorists

Until recently the calculation of the cohesive energy, ΔH_o, of Mg_2X appeared to be too ambitious for the existing methods of calculation, but recent developments have made the calculation of ΔH_o entirely feasible (Section IA). In many experimental situations (e.g. the experiments reported in this thesis), the quantity of primary interest is H_{Mg}, not ΔH_o. A fully adequate treatment of the electronic structure of Mg_2X must involve the calculation of both ΔH_{Mg} and ΔH_o. It seems entirely possible that the approach of Ruedenberg (Section IA) can be modified to accomplish the desired results. It is hoped that the results tabulated in Section VC will serve as a stimulus and a check for theorists interested in the electronic structure of intermetallic compounds.

VII. LITERATURE CITED

1. Seitz, Frederick. The Modern Theory of Solids. New York N. Y., McGraw-Hill Book Company, Inc. 1941.

2. Saker, E. W. and F. A. Cunnell. Intermetallic Semi-conductors. Research 7:114. 1954.

3. Home-Rothery, W. The Structure of Metals and Alloys. London, Institute of Metals. 1954.

4. Pauling, Linus. Nature of the Chemical Bond. 2nd ed. Ithaca, N. Y., Cornell University Press. 1945.

5. Brooks, Harvey. Accomplishments and Limitations of Solid State Theory. In Goldman, J. E., ed. The Science of Engineering Materials. pp. 44-81. New York, N. Y., John Wiley and Sons, Inc. 1957.

6. Born, Max. Atomic Physics. New York, N. Y., Hafner Co. 1951.

7. Bernardes, Newton. Theory of Solid Ne, A, Kr, and Xe at 0° K. Phys. Rev. 112:1534. 1958.

8. Zintl, E. Intermetallische Verbindungen. Angew. Chem. 52:1. 1939.

9a. Wigner, E. and Frederick Seitz. On the Constitution of Metallic Sodium. I. Phys. Rev. 43:804. 1933.

9b. _____ and _____. On the Constitution of Metallic Sodium. II. Phys. Rev. 46:509. 1934.

9c. _____ and _____. The Theoretical Constitution of Metallic Lithium. Phys. Rev. 47:400. 1935.

10. Raimes, S. The Cohesive Energy of Metallic Magnesium. Phil. Mag. 41:568. 1950.

11. Trulson, Olof Conrad. Cohesive Energies of Some Rare Earth Metals. Unpublished Ph.D. thesis. Ames, Iowa, Library, Iowa State University of Science and Technology. 1959.

12. Ruedenberg, Klaus. The Physical Nature of the Chemical Bond. U. S. Atomic Energy Commission Report IS-106. [Iowa State University of Science and Technology, Ames, Inst. for Atomic Research.] 1961.

13. Lowdin, Per-Olof. Quantum Theory of Many Particle Systems. I. Physical Interpretation by Means of Density Matrices. Phys. Rev. 97:1474. 1955.

14a. McWeeny, R. On the Basis of Orbital Theories. Proc. Roy. Soc. A232:114. 1956.

14b. _____. The Density Matrix in Self Consistent Field Theory. I. Iterative Construction of the Density Matrix. Proc. Roy. Soc. A235:496. 1956.

15. Raynor, G. V. Crystal Structure and Bond Mechanism of Intermetallic Phases. In The Physical Chemistry of Metallic Solutions and Intermetallic Compounds. Vol. 1. Chap. 3A. London, Her Majesty's Stationery Office. 1958.

16. Boltaks, B. I. O Prirode Elektricheskih sroystv Magnitnoi Vosprimchivosty Intermetallicheskogo Soyedineniya Mg_2Sn. Zhur. Tekn. Fiz. 20:180. 1950. Original available but not translated; cited in Kubaschewski, O. and H. A. Slowman. Relations between Physical Properties and Bond Mechanism of Intermetallic Compounds. In The Physical Chemistry of Metallic Solutions and Intermetallic Compounds. Vol. 2. Chap. 3B. London, Her Majesty's Stationery Office. 1958.

17. Robertson, W. D. and H. H. Uhlig. Electrical Properties of the Intermetallic Compounds Mg_2Sn and Mg_2Pb. Trans. Amer. Inst. Min. Engr. 180:345. 1949.

18. Mott, N. F. and H. Jones. The Theory of the Properties of Metals and Alloys. London, Oxford University Press. 1936.

19. Raynor, G. V. The Physical Metallurgy of Magnesium and Its Alloys. New York, N. Y., Pergammon Press. 1959.

20. Jaffe, A. F. Isvest. Akad. Nauk SSSR Ser. Fiz. 15:477. 1951. Original not available for examination; cited in Mooser, E. and W. P. Pearson. The Chemical Bond in Semiconductors. Can. J. Phys. 34:1369. 1956.

21. Mooser, E. and W. B. Pearson. The Chemical Bond in Semiconductors. Can. J. Phys. 34:1369. 1956.

22a. Mooser, E. and W. B. Pearson. The Chemical Bond in Semiconductors. Phys. Rev. 101:1608. 1956.

22b. _____ and _____. Chemical Bond in Semiconductors. J. Electronics 1:629. 1956.

23. Ageev, N. V. and L. N. Guseva. Experimental Study of the Electron Density in Crystals. Communication 5. Electron Density of Mg_2Si. Bulletin Acad. of Sciences USSR. Division of Chemical Sciences. 1:31. 1952.

24. Krebs, H. Chemische Bindung und Halbleterungenschaften. Physica 20:1125. 1954.

25. Kubaschewski, O. and H. A. Slowman. Relations between Physical Properties and Bond Mechanism of Intermetallic Compounds. In The Physical Chemistry of Metallic Solutions and Intermetallic Compounds. Vol. 1. Chap. 3B. London, Her Majesty's Stationery Office. 1958.

26a. Gebhardt, Eric, Manfred Becker, and Erich Tranger. Über die Eigenschaften metallischer Schmelzen. X. Die innere Reibung flussiger Magnesium-Ble-Legierungen. Z. Metallk. 46:90. 1955.

26b. _____, _____ and Heinrich Sebastian. Uber die Eigenschaften metallischer Schmelzen. XI. Die innere Reibung flussiger Magnesium-Zinn-Legierungen. Z. Metallk. 46:669. 1955.

27. Baur, E. and R. Brunner. Dampfdruckmessung an hochsiedenden Metallen. Helv. Chem. Acta 17:958. 1934.

28. Langmuir, Irving. The Effect of Space Charge and Residual Gases on Thermionic Current in High Vacuum. Phys. Rev. 2:450. 1913.

29. Knudsen, Martin. Die Molekularstromung der Gase durch Offnungen und die Effusion. Ann. d. Physik 28:999. 1908.

30. Rudberg, Erik. The Vapor Pressure of Calcium between 500°C and 625°C. Phys. Rev. 46:863. 1934.

31. Erway, N. D. and R. L. Seifert. Vapor Pressure of Beryllium Oxide. U. S. Atomic Energy Commision Report MDDC-1030. [Manhattan District, Oak Ridge, Tenn.] 1947.

32. Daane, Adrian Hill. Vapor Pressures of Lanthanum and Prasedymium. Unpublished Ph.D. thesis. Ames, Iowa, Library, Iowa State University of Science and Technology. 1950.

33. Taylor, John Bradshaw and Irving Langmuir. Vapor Pressure of Caesium by the Positive Ion Method. Phys. Rev. 51:753. 1937.

34. Fox, Harold Gene. Ionization of Some Rare Earth Atoms at Metallic Surfaces. Unpublished M.S. thesis. Ames, Iowa, Library, Iowa State University of Science and Technology. 1959.

35. Jackson, D. M. and D. E. Hudson. An Ion Source for Molecular Effusion Studies. U. S. Atomic Energy Commission Report ISC-1175 [Ames Lab., Ames, Iowa.] 1959.

36. Kennard, Earle H. The Kinetic Theory of Gases. New York, N. Y., McGraw-Hill Book Company, Inc. 1938.

37. Clausing, P. Über die Strahlformung beider Molekularstromung. Ann. d. Physik 66:471. 1930.

38. Carlson, K. D. The Molecular and Viscous Effusion of Saturated Vapors. U. S. Atomic Energy Commission Report ANL-6156. [Argonne National Lab., Lemont, Ill.] 1960.

39. Schrage, Robert W. A Theoretical Study of Interphase Mass Transfer. New York, N. Y., Columbia University Press. 1953.

40. Darken, Lawrence S. and Robert W. Gurry. Physical Chemistry of Metals. New York, N. Y., McGraw-Hill Book Company, Inc. 1953.

41. Li, J. C. M. Thermodynamic Formulas for Two Phase Systems. J. Chem. Phys. 26:909. 1957.

42. Harteck, P. Dampfdruckmessungen von Ag, Au, Cu, Pb, Ga, Sn, und Berechnung der chemischen Konstanten. Z. physik. Chem. 134:1. 1928.

43. Hirth, J. and G. Pound. Evaporation of Metal Crystals. J. Chem. Phys. 26:1216. 1957.

44. Boteler, John Clarence. An Exploratory Study of a Mass Spectrometric Diffusion Technique. Unpublished M.S. thesis. Ames, Iowa, Library, Iowa State University of Science and Technology. 1961.

45. Peavler, Robert J. and Alan W. Searcy. Dependence of Dissociation Pressure Measurement by the Knudsen Effusion Method on Effusion Hole Area. Journal of the American Chemical Society 78:2706. 1956.

46. Knacke, O. and I. N. Stranski. The Mechanism of Evaporation. In Chalmers, B. and R. King, eds. Progress in Metal Physics. pp. 181-234. New York, N. Y., Pergamon Press, Ltd. 1956.

47. Stranski, I. N. and G. Wolff. Zur erzwungenen Kondensation beim Arsenik. Z. Elektrochemie 53:1. 1949.

48. Knacke, O., I. N. Stranski, and G. Wolff. Zur Theorie der Verdampfungsgeschwindigkeit. Z. phys. Chemie 198:197. 1951.

49. Knacke, O., G. Wolff, and I. N. Stranski. Probleme der Verdampfung. Z. Elektrochemie 56:476. 1952.

50. Ackerman, R. J., R. J. Thorn, and G. H. Winslow. Some Fundamental Aspects of Vaporization. [Mimeographed] Lemont, Illinois, Argonne National Laboratory, authors. 1959.

51. DeGroot, Sybren Purrds. Thermodynamics of Irreversible Processes. Amsterdam, North Amsterdam Publishing Company. 1952.

52. Sullivan, R. W., R. D. Siebel, and C. E. Lundin. Literature Survey of Selected Semiconductor Properties. U. S. Atomic Energy Commission Report AFCRL-4. [Air Force Cambridge Research Laboratories, Bedford, Mass.] 1960.

53. Hoch, Michael J. Heat of Formation of BaC_2. J. App. Phys. 29:1589. 1958.

54. Smith, J. F. and R. L. Smythe. Vapor Pressure Measurements Over Calcium, Magnesium, and Their Alloys and the Thermodynamics of Formation of $CaMg_2$. Acta Met. 7:261. 1959.

55. Winterbottom, W. L. and J. P. Hirth. The Diffusional Contribution to the Knudsen Cell Effusion Flux. U. S. Atomic Energy Commission Report AD 266 266. [Armed Services Tech. Inf. Agency, Arlington, Va.] 1962.

56. Kay, Eric and N. W. Gregory. Applicability of the Knudsen Effusion Method to the Study of Decomposition Reactions. J. Phys. Chem. 62:1079. 1958.

57. Trulson, Olof Conrad. A Mass Spectrometer Ion Detector. Unpublished M.S. thesis. Ames, Iowa, Library, Iowa State University of Science and Technology. 1956.

58. Topping, James. Errors of Observation and Their Treatment. London, The Institute of Physics. 1957.

59. Morris, Robert Cemmill. Semiconducting Properties of Mg_2Si Single Crystals. Unpublished Ph.D. thesis. Ames, Iowa, Library, Iowa State University of Science and Technology. 1957.

60. Kubaschewski, O. and E. L. Evans. Metallurgical Thermochemistry. London, Butterworth-Springer. 1951.

61. Brewer, Leo. The Thermodynamic and Physical Properties of the Elements. In Quill, L. L., ed. The Chemistry and Metallurgy of Miscellaneous Materials. New York, N. Y., McGraw-Hill Book Company, Inc. 1950.

62. Honig, R. E. Sublimation Studies of Silicon in the Mass Spectrometer. J. Chem. Phys. 22:1610. 1954.

63. JANAF Thermochemical Data. Midland, Mich., The Dow Chemical Company. 1960.

64. Honig, R. E. The Heats of Sublimation and Evaporation of Germanium. J. Chem. Phys. 22:1610. 1954.

65. Kubaschewski, O. The Problem of Stability of Intermetallic Phases. In The Physical Chemistry of Metallic Solutions and Intermetallic Compounds, Vol. 1. Chap. 3C. London, Her Majesty's Stationery Office. 1958.

66. Sanderson, R. T. Chemical Periodicity. New York, N. Y. Reinhold Publishing Corporation. 1960.

67. Margules, Max. Über die Zusammensetzund der gesattigten Dampfe von Mischungen. Sitzber. Akad. Wiss. Wien. 104:1243. 1895.

68. Spedding, F. H., J. J. Hanak, and A. H. Daane. The Preparation and Properties of Europium. Trans. Met. Soc. of Am. Inst. Met. Engrs. 212:379. 1958.

69. Schmahl, N. G. and P. Sieben. Vapor Pressures of Magnesium in Its Binary Alloys with Copper, Nickel, and Lead and Their Thermodynamic Evaluation. In The Physical Chemistry of Metallic Solutions and Intermetallic Compounds. Vol. 1. Chap. 2K. London, Her Majesty's Stationery Office. 1958.

70. Stull, D. R. and G. C. Sinke. The Thermodynamic Properties of the Elements in Their Standard States. Midland, Mich., The Dow Chemical Company. 1955.

71. Wilson, E. Bright. An Introduction to Scientific Research. New York, N. Y., McGraw-Hill Book Company, Inc. 1952.

72. Morris, R. G., R. D. Redin, and G. C. Danielson. Semiconducting Properties of Mg_2Si Single Crystals. Phys. Rev. 109:1909. 1958.

73. Redin, R. D., R. G. Morris, and G. C. Danielson. Semiconducting Properties of Mg_2Ge Single Crystals. Phys. Rev. 109:1916. 1958.

VIII. ACKNOWLEDGMENTS

The author is particularly grateful to his group leader, Dr. Donald E. Hudson, for his advice, criticism, and inspiration throughout the course of this work.

The materials used in this work were graciously furnished by Dr. Gordon C. Danielson of Experimental Physics Group VI. The author wishes to thank Dr. Marvin Heller of the same group for his assistance and advice on handling of the materials.

In the early phases of this work Dr. O. Conrad Trulson provided the assistance and guidance which are especially helpful to a beginning graduate student. Mr. Don M. Jackson, who built much of the equipment and familiarized the author with the mass spectrometer and wrote the necessary computer programs, deserves special thanks. The advice, encouragement, and assistance of my fellow graduate student Mr. Miles J. Dresser are gratefully acknowledged. Mr. Maynard Van Roekel was especially helpful in keeping the equipment operational.

The author has profited greatly by exchange of information and ideas with Mr. Donald Novotny. Mr. Novotny also contributed the weight loss data presented in Appendix B.

Mr. Garry Wells has been especially helpful in the design and construction of equipment. The spectroscopy group under Dr. V. A. Fassel and the analytical chemistry group under Dr. C. V. Banks contributed analyses of the various compounds. The computer group under Dr. D. R. Fitzwater assisted in the numerical calculations.

Dr. J. F. Smith, Dr. A. H. Daane, Dr. J. M. Keller, Dr. R. E. Rundle, Dr. R. H. Good, and Dr. K. Ruedenberg were helpful to the author in various phases of the theoretical work.

IX. APPENDIX A: SUBLIMATION FROM A BINARY SOLID

A. Introduction

In Section IIB it was shown that sublimation of one component of a binary compound can be described by an analogue of the Clausius equation if the sublimation does not appreciably deplete the solid of the volatile component. This section will discuss more general sublimation processes. As in Section IIB, the reaction of interest is

$$A_{n(1-\alpha)}\ B_{m(1-\beta)} \rightleftharpoons \alpha\, nA(v) + \beta\, mB(v) \ .$$

The methods to be examined are an approximate solution, a rigorous unpublished treatment, and a method unique to this thesis.

B. Approximate Solutions

The key to approximate solutions to the thermodynamics of the equilibrium described above is the van't Hoff equation:

$$\frac{d\ln K}{d(1/T)} = \frac{-\Delta H_R}{R} \ ,$$

where K is the equilibrium constant governing the reaction, ΔH_R is the heat of reaction, and R is the universal gas constant. The van't Hoff equation is rigorously true for ideal gases, ideal solutions, ideal solids, or equilibria among these ideal phases. The application of the equilibrium constant to the given equilibrium involves various assumptions which are beyond the scope of this discussion. These assumptions are discussed in detail by Darken and Gurry (40). Only the results of their analysis are given here. The equilibrium constant

method yields the Clausius-Clapeyron equation for the sublimation of an elemental solid. Indeed each subliming component, i, of a compound appears (by these methods) to be governed by an individual Clausius-Clapeyron equation

$$\frac{d\ln P_i}{d(1/T)} = -\frac{\Delta H_i}{R} ,$$

where ΔH_i is the change in partial molar enthalpy of component i during the sublimation.

C. The Method of Li

The number of thermodynamic variables in a two phase, multi-component system may be large. Dr. J. C. M. Li (41) has developed a general method whereby the partial derivatives which relate these variables can be obtained. Unfortunately the generality and power of Li's method was gained at great sacrifice of simplicity and physical insight. Each partial derivative is the quotient of two large determinants, the terms of which are, themselves, complicated entities. An exposition of Li's method is well beyond the scope of this thesis. The exact method of Li leads to the result

$$\frac{dP}{dT} = \frac{\alpha n \Delta S_A + \beta m \Delta S_B}{\alpha n \Delta V_A + \beta m \Delta V_B} \quad *$$

*Li, J. C. M., U. S. Steel Research Laboratories, Monroeville, Pennsylvania. Sublimation from two component solids. Private communication. 1962.

for constant α and β and for constant solid phase composition.

For variable α and β Li's equation is

$$\frac{dP}{dT} = \frac{(X_A'^2 F_{A'A'} - X_A^2 F_{A'A})\Delta S_A + (X_B'^2 F_{B'B'} - X_B^2 F_{B'B})\Delta S_B}{(X^2 F_{A'A'} - X^2 F_{A'A})\Delta V_A + (X_B'^2 F_{B'B'} - X^2 F_{B'B})\Delta V_B}$$

where the prime phase refers to the solid phase, the X's are mole fractions of the subscripted component, $F_{AA'} = \left(\frac{\partial F_A}{\partial X_A'}\right)_{T,P}$, etc.

In Li's work F is the symbol for total Gibbs free energy of the phase, so

$$F_{A'} = \mu_A^s \text{, etc.}$$

D. A New Method

It is possible to derive a very general equation governing the sublimation from a binary compound under Knudsen conditions. This method is especially useful because it explicitly displays all of the assumptions involved and because it yields a result of great generality.

For any phase the total Gibbs free energy G is given by

$$G = \Sigma n_i \mu_i ,$$

where the n's and μ's are defined as in Section IIB. Small changes dP and dT will result in a change in G given by

---

*Li, J. C. M., U. S. Steel Research Laboratories, Monroeville, Pennsylvania. Sublimation from two component solids. Private communication. 1962.

$$dG = -SdT + VdP + \Sigma \mu_i dn_i$$

$$\equiv n_i(-S_i dT + V_i dP) + \Sigma \mu_i dn_i$$

The equation which results from the subtraction of the two equations for dG is

$$\Sigma n_i(-S_i dT + V_i dP - d\mu_i) = 0.$$

This last equation must apply in both phases. Suppose the solid AnBm contains n_A^s moles of A and n_B^s moles of B in the ratio $n_A^s/n_B^s = n/m$. Then

$$n_A^s(-S_A^s dT + V_A^s dP - d\mu_A) + n_B^s(-S_B^s dT + V_B^s dP - d\mu_B) = 0.$$

If ϵ moles of A were added to the solid, then

$$(n_A^s + \epsilon)(-S_A^{s'} dT + V_A^{s'} dP - d\mu_A') + n_B^s(-S_B^{s'} dT + V_A^{s'} dP - d\mu_B') = 0,$$

where the primes indicate the values associated with the new solid (A enriched AnBm). For example

$$S_A^{s'} - S_A^s = \frac{\partial S_A^s}{\partial n_A^s}\epsilon + \tfrac{1}{2}\frac{\partial^2 S_A^s}{\partial n_A^{s2}}\epsilon^2 + \cdots$$

But $\partial S_A^s/\partial n_A^s$ is the derivative of an intensive variable with respect to an extensive variable, so the value of $\partial S_A^s/\partial n_A^s$ can be made as small as desired by having sufficiently large values of n_A^s and n_B^s. If n_A^s and n_B^s are chosen properly

$$S_A^{s'} - S_A^s = 0(\epsilon^2),$$

where $0(\epsilon^2)$ is a function which approaches 0 at a rate proportional to ϵ^2. Similarly for properly chosen n_A^s and n_B^s,

$$(n_A^s + \epsilon)\left[-S_A^s dT + V_A^s dP - d\mu_A + 0(\epsilon^2)\right]$$
$$+ n_B^s\left[-S_B^s dT + V_B^s dP - d\mu_B + 0(\epsilon^2)\right] = 0$$

Therefore

$$\epsilon(-S_A^s dT + V_A^s dP - d\mu_A) + 0(\epsilon^2) = 0$$

or

$$d\mu_A = -S_A^s dT + V_A^s dP + 0(\epsilon).$$

So to good accuracy

$$d\mu_A = -S_A^s dT + V_A^s dP$$

in reactions in which the number of A atoms involved is very small compared with the number originally present in the solid. This condition obtains during Knudsen effusion. Similarly

$$d\mu_B \cong -S_B^s dT + V_B^s dP.$$

For a vapor containing n_A^v moles of A and n_B^v moles of B,

$$n_A^v(-S_A^v dT + V_A^v dP - d\mu_A) + n_B^v(-S_B^v dT + V_B^v dP - d\mu_B) = 0.$$

Using the expressions just derived for $d\mu_A$ and $d\mu_B$, one obtains

$$\frac{dP}{dT} = \frac{n_A^v \Delta S_A + n_B^v \Delta S_B}{n_A^v \Delta V_A + n_B^v \Delta V_B}.$$

In particular if (as in the case of Mg_2X) $n_A^v >> n_B^v$, then

$$\frac{dP_A}{dT} = \frac{\Delta S_A}{\Delta V_A} .$$

However the general formula for dP/dT is applicable in any situation in which n_A^v/n_B^v is known.

E. The Duhem-Margules Equation

As shown earlier

$$G = \Sigma n_i \mu_i, \text{ so}$$

$$dG = \Sigma n_i d\mu_i + \Sigma \mu_i dn_i .$$

Also

$$dG = -SdT + VdP + \Sigma \mu_i dn_i .$$

Hence at constant T and P,

$$\Sigma n_i d\mu_i = 0.$$

For a two component, two phase system, say sublimation of Mg_2X, $\Sigma n_i d\mu_i = 0$ becomes, for the gaseous phase,

$$n_{Mg}^v d\mu_{Mg}^v + n_X^v d\mu_X^v = 0,$$

or dividing by $n_{Mg}^v + n_X^v$,

$$X_{Mg}^v d\mu_{Mg}^v + X_X^v d\mu_X^v = 0. \quad (43)$$

If both the Mg vapor and the X vapor are ideal, then their chemical potentials are

$$\mu^{v}_{Mg} = \mu^{o}_{Mg} + RT\ \ln P_{Mb} \text{ and } \mu^{v}_{X} = \mu^{o}_{X} + RT\ \ln P_{X}.$$

Thus $d\mu^{v}_{Mg} = RT\ d\ln P_{Mg}$ and $d\mu^{v}_{X} = RT\ d\ln P_{X}$.

Equation 43 then becomes

$$X^{v}_{Mg}\ d\ln P_{Mg} + X^{v}_{X}\ d\ln P_{X} = 0. \tag{44}$$

Dividing Equation 44 by dX^{v}_{Mg} we obtain

$$X^{v}_{Mb}\ \frac{d\ln P_{Mg}}{dX^{v}_{Mg}} + X^{v}_{X}\ \frac{d\ln P_{X}}{dX^{v}_{Mg}} = 0. \tag{45}$$

But $X^{v}_{Mg} + X^{v}_{X} = 1$, so $dX^{v}_{Mg} = -dX^{v}_{X}$. Equation 45 transforms into the Duhem-Margules equation for Mg X sublimation

$$X^{v}\ \frac{d\ln P_{Mg}}{dX^{v}_{Mg}} = X^{v}_{X}\ \frac{d\ln P_{X}}{dX^{v}_{X}} \quad . \tag{46}$$

It is useful to consider the Margules' integration of the Duhem-Margules equation (67). In the following call the two phases 1 and 2. For $X_1 = 1$, $P \equiv P^{o}_{1}$ and for $X_2 = 1$, $P \equiv P^{o}_{2}$. Also we must have $d\ln P_1/d\ln X_1 = d\ln P_2/d\ln X_2$. It is easy to find solutions to this. For example $d\ln p_1/d\ln X_1 = C = d\ln P_2/d\ln X_2$ implies $P_1 = P^{o}_{1}\ X_1$ and $P_2 = P^{o}_{2}\ X_2$. There are other solutions to the Duhem-Margules equation and its boundary conditions. We must choose an equation with sufficiently many parameters to fit the rather complicated data that actually occur. Two such equations are $P_1 = P^{o}_{1}\ X_1^{\alpha_o}\left[e^{\alpha_1 X_2} + \frac{\alpha_2}{2}\ X_2^2 + \frac{\alpha_3}{3}\ X_2^3 + \cdots\right]$ and

$$P_2 = P^{o}_{2}\ X_2^{\beta_o}\left[e^{\beta_1 X_1} + \frac{\beta_2}{2}\ X_1^2 + \frac{\beta_3}{3}\ X_1^3 + \cdots\right]$$

The Duhem-Margules equation imposes the restrictions

$$\begin{aligned}
\beta_o &= \alpha_o - \alpha_1 \\
\beta_1 &= -\alpha_1 \\
\beta_2 &= \alpha_2 + \alpha_3 + \alpha_4 + \cdots \\
\beta_3 &= -\alpha_3 - 2\alpha_4 - 3\alpha_5 \cdots \\
&\cdots\cdots\cdots\cdots\cdots
\end{aligned}$$

Also $\frac{\partial P_1}{\partial X_1} = \frac{P_1^o}{X_1}\left[\alpha_o - \alpha_1 X_1 - \alpha_2 X_1 X_2 - \cdots\right]$ and

$$\frac{\partial P_2}{\partial X_2} = \frac{P_2^o}{X_2}\left[-\beta_o - \beta_1 X_2 - \beta_2 X_2 X_1 - \cdots\right],$$

So $\left(\frac{\partial P_1}{\partial X_1}\right)_{X_2=o} \cong P_1^o \cong P_1^o\,(\alpha_o - \alpha_1)$ and

$$\left(\frac{\partial P_2}{\partial X_2}\right)_{X_1=o} \cong P_2^o \cong P_2^o\,(\beta_1 - \beta_o)\,.$$

Thus $\alpha_o \cong \beta_o \cong 1$ and $\alpha_1 \cong \beta_1 \cong 0$. So far we have (with some redundancy in not having eliminated the β's)

$$P_1 = P_1^o X_1\, e^{\frac{\alpha_2}{2} X_2^2 - \frac{\alpha_3}{3} X_2^3 - \cdots} \quad \text{and}$$

$$P_2 = P_2^o X_2\, e^{\frac{\beta_2}{2} X_1^2 - \frac{\beta_3}{3} X_1^3 - \cdots}$$

For $\alpha_2 >> \alpha_3, \alpha_4, \ldots$, we have $\beta_2 \cong \alpha_2$ and thus $P_1 = P_1^o X_1\, e^{\alpha X_2^2}$ and $P_2 = P_2^o X_2\, e^{\alpha X_1^2}$

This is a form found to fit reasonably well for most binary alloys.

X. APPENDIX B: AUXILIARY EXPERIMENTS

This appendix contains information on experiments which did not measure ΔH_{Mg} but which were necessary in order to assure the validity of the ΔH_{Mg} results.

An experiment was performed in order to check the applicability of the equipment and technique of this thesis to the measurement of heats of sublimation. This experiment consisted of the measurement of ΔH for the sublimation of europium metal and the comparison of results with the ΔH values previously obtained for europium. The sample studied was obtained from Dr. Joseph Hanak of this laboratory who had analyzed the metal for impurities. This analysis showed faint trace amounts of Sm, Yb, Ca, and Fe. No other impurities appeared to be present. Seven runs were taken on one loading of europium metal. The results of these runs are summarized in Table 10. The weighted mean ΔH at 780°K was 41.39 kcal/mole. The net error in ΔH is given by

$$E_h^2 = (0.712)^2 + \frac{(2X41.4X2)^2}{780} = (0.84)^2 .$$

Thus the result of this experiment is

$$\Delta H_{780} = 41.4 \pm 0.8 \text{ kcal/mole.}$$

This compares with

$$\Delta H_{798} = 41.10 \pm 0.075 \text{ kcal/mole}$$

obtained by Spedding, Hanak, and Daane (68). Trulson (11) obtained

$$\Delta H_{727} = 42.04 \pm 0.41 \text{ kcal/mole.}$$

Table 10. Data compilation on europium metal

Run	Midrange temperature (^{o}K)	Experimental Δ H value ΔH_i (kcal/mole)	Normalized weight K_i
1A	778	41.44	0.072
1B	776	36.52	0.025
1C	784	42.83	0.086
1D	782	43.65	0.255
1E	779	40.84	0.326
1F	778	38.55	0.082
1G	784	41.46	0.155
Mean	781	41.41	0.143

$S_{bi}^2 = 5062/K_i (^{o}K^2)$

Expected standard deviation of mean, S_h^e	0.14 kcal/mole
Observed standard deviation of mean, S_h^o	0.71 kcal/mole
Instrumental error, e_n	0.21 kcal/mole
Net experimental error, E_h	0.84 kcal/mole
Orifice correction	-0.02 kcal/mole

Latent heat of sublimation, $\Delta H_{781} = 41.4 \pm 0.8$ kcal/mole

The result of this work lies between the results of the two previous observations and within the experimental error of both. Correction of all of Δ H's to the same temperature by the Kirchoff equation would not appreciably alter these results because the temperatures differ by only about 50^{o}K at 750^{o}K. A typical data plot is given in Figure 15, and the

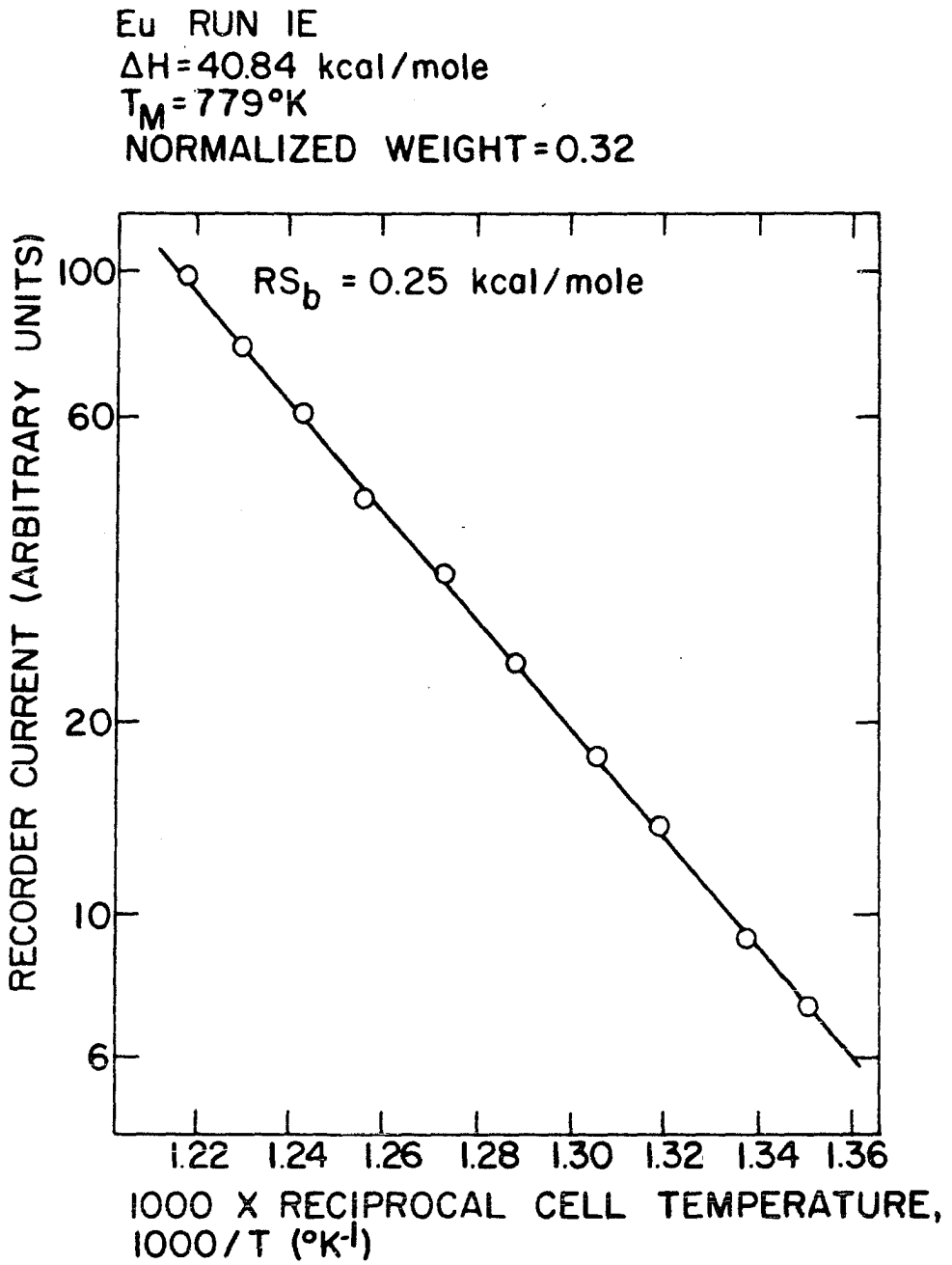

Figure 15. A typical europium data plot

original data are found in Appendix E.

Several experiments were performed to investigate the composition of the vapor above Mg_2X.

Mass spectrometric searches revealed no Mg_2^+, Mg_2X^+, or X^+ ion peaks. The apparent absence of these ion peaks is not conclusive evidence against the assumption that vapors other than Mg sublime from Mg_2X, so several additional experiments were performed.

The vapor subliming from Mg_2Ge at 870°K was allowed to condense on a cold aluminum plate. The condensed material was spectrographically analyzed. Ge was found to constitute "less than 0.1%" of the condensate. It is reasonable to expect the same to hold for the other members of the Mg_2X series.

The weight-loss method of studying effusion was described in Section IC. This method measures the total dP/dT for the sublimation, if the average molecular weight of the effusing gas is known. Mr. Donald Novotny of the Ames Laboratory consented to take measurements on Mg_2Ge taken from the sample used in this thesis by the weight-loss method. If it is assumed that the only species subliming is Mg, Mr. Novotny's dP/dT should be equal to the dP_{Mg}/dT measured in this experiment. The data from Novotny's weight-loss measurements (based on the monomer Mg assumption) are shown in Table 11. Analysis of these data by Novotny's method of lumping all of the data together yields

$$\Delta H_{Mg} = 48.97 \pm 1.14 \text{ kcal/mole} .$$

A plot of these data, Figure 16, suggests that the analysis of Section

Table 11. Weight-loss data on Mg_2Ge assuming average molecular weight = 24.32

Run No.	P (mm)	1000/T ($^oK^{-1}$)
1	$2.271X10^{-3}$	1.126
1	$7.905X10^{-3}$	1.078
1	$1.735X10^{-2}$	1.043
1	$4.006X10^{-2}$	1.008
1	$9.936X10^{-2}$	0.975
1	$6.842X10^{-2}$	0.988
1	$4.456X10^{-2}$	1.005
1	$1.872X10^{-2}$	1.055
1	$2.255X10^{-2}$	1.035
2	$1.347X10^{-2}$	1.055
2	$4.299X10^{-3}$	1.099
2	$5.422X10^{-3}$	1.090
2	$6.031X10^{-2}$	0.997
2	$3.915X10^{-2}$	1.009
2	$3.040X10^{-2}$	1.022
2	$2.150X10^{-2}$	1.037

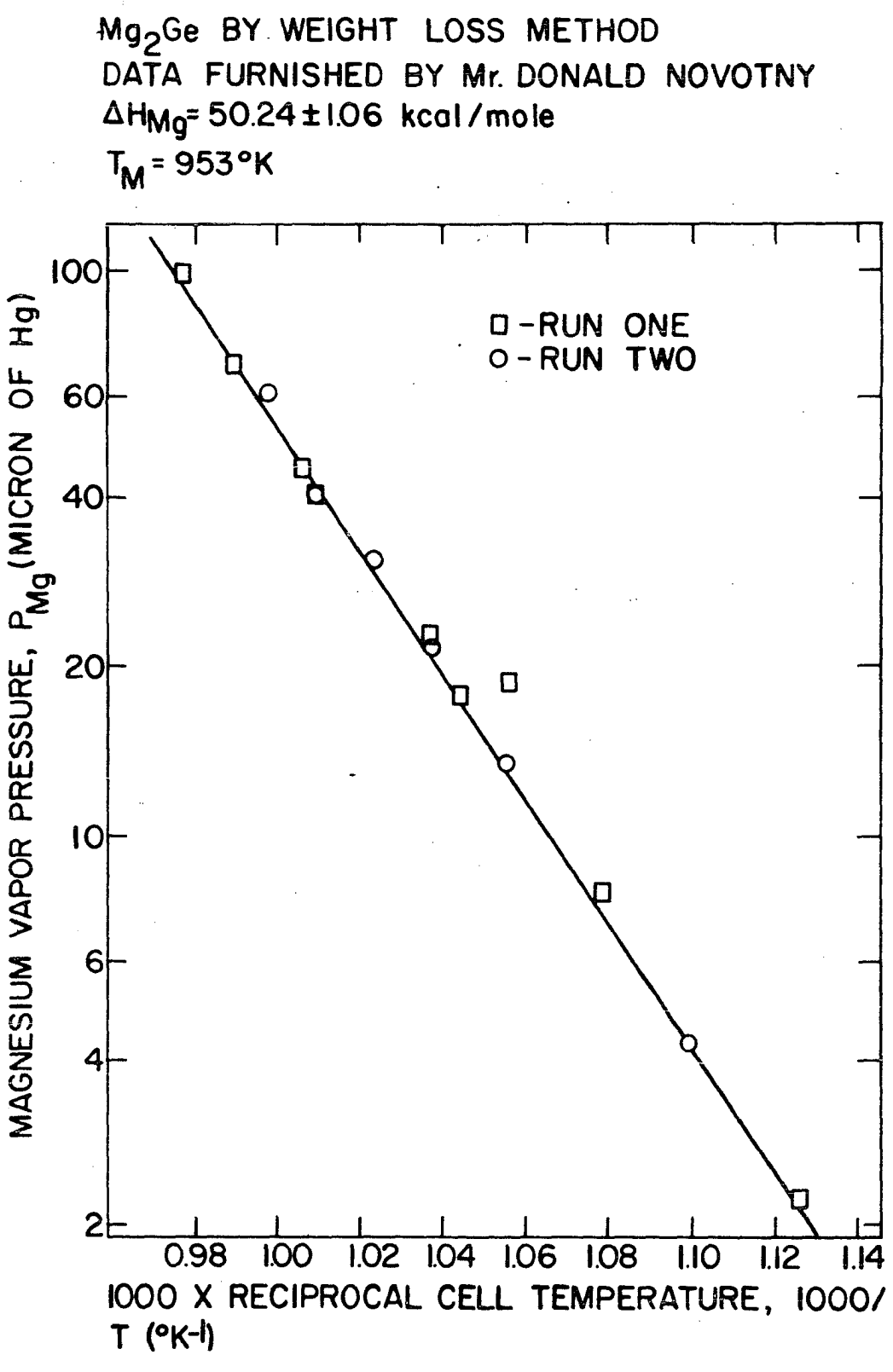

Figure 16. A plot of Knudsen effusive weight-loss data on Mg_2Ge

IV can be usefully applied. The result of such an analysis is ΔH^1_{Mg} = 48.13 kcal/mole and ΔH^2_{Mg} = 50.36 kcal/mole, but K_1 = 0.05294 and K_2 = 0.94706. Thus $\overline{\Delta H_{Mg}} = \Sigma K_1 \Delta H_i$ = 50.24 kcal/mole. Indeed the result, exclusive of instrumental error, is ΔH_{Mg} = 50.24 $\pm$ 1.06 kcal/mole at T_M = 953°K. This compares with ΔH_{Mg} = 54.4 $\pm$ 1.8 kcal/mole from Section V. While it is true these values do not have overlapping errors, they lack little more than 2% of overlapping. It is distinctly possible that further weight-loss data would move the H value in the desired direction. Furthermore weight loss is a reflection of depletion of the solid so the ΔH_{Mg} may change with time. In any case this is considered a confirmation of the hypothesis that the predominant subliming species is Mg.

Novotny's data on the absolute partial pressure of Mg above Mg_2Ge can be employed in the Margules integration of the Duhem-Margules equation as indicated in Appendix A. The resulting estimate of P_{Ge} at 1000°K is $P_{Ge} = 10^{-20}$ mm. This estimate could be off several orders of magnitude and still be support for the hypothesis of the predominance of the Mg vapor.

Schmahl and Sieben (69) measured Mg pressure over the melts of several Mg - Pb alloys including the compound Mg_2Pb(X_{Mg} = 0.667). Only on the two alloys of lowest Mg composition did they observe enough Pb vapor to make a quantitative estimate of P_{Pb}. Their data are shown in Table 12. Clearly two factors work in reducing P_{Pb} even below the values listed in Table 12, namely the increase in X_{Mg} from 0.441 to 0.667 and the decrease in temperature from 998 to 770°K. Note also that

Pb is the most volatile of the Group IV elements involved in these Mg_2X compounds, so if P_{Pb} is negligible certainly P_{Si}, P_{Ge}, and P_{Sn} will be also.

Table 12. Data of Schmahl and Sieben on Mg - Pb alloys

Mole fraction of Mg X_{Mg}	Temperature, T (^oK)	Partial pressure of Mg (mm)	Partial pressure of Pb (mm)
0.441	998	0.55	0.0077±0.009
	1114	3.34	0.074±0.009
0.274	865	0.49	0.0396
	1050	1.82	0.176

The effect on ΔH_{Mg} of the choice of the particular Mg_2X sample to be studied was investigated in an auxiliary experiment in which Mg_2Si from three different batches was used. That is the Mg_2Si was produced at separate times from separate supplies of Mg and Si. The absence of variation of ΔH_{Mg} from batch to batch indicated that H_{Mg} is a property of Mg_2Si in general and is not affected by small batch-to-batch differences (Section V). It is assumed that for all Mg_2X compounds ΔH_{Mg} will not vary with the sample studied.

In the vast majority of cases the cell was loaded with several small chunks of the solid; however Run 4 on Mg_2Si (Section V) was made on a powdered sample. No effect due to this on the ΔH_{Mg} values was observed.

Again the other Mg_2X compounds should show the same invariance of ΔH_{Mg} to the state of the sample. Powdering increases the surface area of the sample considerably, so the absence of effect on ΔH_{Mg} due to powdering suggests that the surface area of the unpowdered sample is large enough to eliminate error due to a/A effects or Kay and Gregory effects (Section IIE).

The first three runs (Section V) on Mg_2Si were taken at electron bombardment ionization energy 267 eV. The other Mg_2Si runs were taken with 144 eV ionizing electrons. The fact that ΔH_{Mg} appears to be independent of ionizing energy is assumed to hold for all Mg_2X compounds. The apparent Mg^+ ion beam can arise from any of three different ionization reactions, i.e.

$$Mg + e \rightarrow Mg^+ + 2e$$

$$Mg_2 + e \rightarrow Mg^+ + mg + 2e$$

$$Mg_2 + e \rightarrow Mg_2^{++} + 3e$$

The ion Mg_2^{++} contributes to the "Mg^+" beam, because the mass spectrometer analyzes mass-to-charge ratios, not just masses. The other two reactions contribute directly to the Mg^+ ion current. The apparent current of Mg^+ is

$$I_{Mg} = \alpha P_{Mg} + \beta P_{Mg_2} + \gamma P_{Mg_2},$$

where α, β, and γ are quantities proportional to the ionization efficiencies of the three ionization processes involved. Note that α, β, and γ will each depend on the ionization energy in a different way.

For different ionization electron energies E_1 and E_2, the measured ΔH_{Mg} values depend on

$$d(\alpha_1 P_{Mg} + \beta_1 P_{Mg_2} + \gamma_1 P_{Mg_2})/dT \text{ and}$$

$$d(\alpha_2 P_{Mg} + \beta_2 P_{Mg_2} + \gamma_2 P_{Mg_2})/dT.$$

Clearly ΔH_{Mg} can be invariant to E, in general, only if the gaseous phase has only one component. So lack of variation of ΔH_{Mg} with ionizing energy shows that only one ionization process contributes significantly to the Mg^+ beam. The simplest ionization process to assume is $Mg + e \rightarrow Mg^+ + 2e$. Also this ionization process is believed to occur because the Mg_+ vapor above pure Mg metal is known to be essentially monatomic (70). Mg_2Si was used in other studies of the ionization mechanism. The Mg^+ beam height was found to vary linearly with both EBIS trap current and emission current for a given vacuum. Within the range of vacuua used in this experiment the Mg^+ beam height for a given cell temperature depended on the trap current only, the emission-current-to-trap-current ratio being a function of the vacuum. Data were taken throughout the range from 22 to 270 eV ionizing energy using constant filament current and constant V_c (see Figure 9). For a given cell temperature, the Mg current rose sharply from V_A = 22v to V_A = 144v. At V_A = 144v there appeared to be a flat peak of width about 20v. Thereafter an increase in V_A resulted in a decrease of the Mg^+ current. Various instrumental uncertainties and insensitivity made extrapolation to the appearance potential of very dubious value.

XI. APPENDIX C: KINETIC THEORY AND IRREVERSIBLE THERMODYNAMICS

A. Introduction

This appendix will describe the extension of the Carlson treatment (Section IIC) of the gas kinetics of Knudsen effusion to the case $\alpha = \beta < 1$. Also some effects of temperature gradients are discussed in terms of irreversible thermodynamics.

B. Modified Carlson Correction

The derivation of Carlson (38) is exact for the case in which adsorption coefficient, α, is equal to unity. This section will employ Carlson's method to the case $\alpha < 1$. This treatment is expected to be meaningful only to one who has read pp. 38-88 of Carlson's paper. The definitions and explanations from those fifty pages are too numerous and involved for inclusion in this appendix. Symbols will be used in exact agreement with Carlson, and only new quantities will receive explicit definitions. Escape from the orifice is governed by the equation

$$n(dS_o)dS_o = \alpha \int_{S_1} g(10)\,dS_1 dS_o + \int_{S_2} n(dS_2)\,g(20)\,dS_2 dS_o + (1-\alpha)\int_{S_1} n(dS_1)\,g(10)\,dS_1 dS_o,$$

which yields

$$\frac{Z(S_o)S_o}{Z_e S_1} \equiv W(L,R_o,R_1) = \frac{\alpha}{S_1}\int_{S_1}\int_{S_o} g(10)\,dS_1 dS_o +$$

$$\int_{\rho_o} nW\,\frac{2}{R_1}\left[\frac{1}{2\pi}\int_{S_o}\int_{\beta_2} g(20)\,dS_o\,d\beta_2\right]d\rho + \frac{(1-\alpha)}{S_1}\int_{S_1}\int_{S_o} n(r_1)\,g(10)\,dS_1 dS_o.$$

By the mean value theorem $\int_{S_1}\int_{S_o} n(r_1)g(10)dS_1dS_o = n(\tilde{r_1})\int_{S_1}\int_{S_o} g(10)dS_1dS_o$, where $0 \leq \tilde{r_1} \leq R_1$. But n is normalized and is reasonably insensitive to r_1, so $0 \leq n(\tilde{r_1}) \leq 1$. Indeed since $R_1 \to 0$ implies $n(r_1) \to 1$, $n(\tilde{r_1}) = 0.9$ seems a safe assumption. Now $W(H\ P,1) = \left[\alpha + 0.9(1-\alpha)\right]\frac{1}{S}\int_{S_1}\int_{S_o} g(10)dS\ dS + \int_{\rho} n(\rho)\frac{2}{R_1}\left[\frac{1}{2\pi}\int_{S_1}\int_{S_o} g(20)dS_o d\beta_2\right]d1$.

By Carlson (5,4-2) we have $2k(H,P,1) + 2\int_0^H n(\eta)\frac{K(H-\eta,P,1)}{\partial\eta}d\eta = 2K(0,P,1) - 2\int_0^H \delta(\eta)\frac{K(H-\eta,P,1)}{\partial\eta}d\eta$. Also Carlson (5,3-18) yields $\frac{1}{S_1}\int_{S_1}\int_{S_o} g(10)dS_1dS_o = 2K(H,P,1)$. Therefore it follows that $W(H,P,1) = 2K(0,P,1) - 0.2(1-\alpha)K(H,P,1) - 2\int_0^H \delta(\eta)\frac{\partial K(H-\eta,P,1)}{\partial\eta}d\eta$, where $K(0,P,1) = \frac{1}{2}P^2 = \frac{1}{2}\frac{S_o}{S_1}$. As before (5,4-5) $\frac{dn}{dt} = Z_e\ S_1\ W(H,P,1) = Z_e\ S_o\left[1 - \Delta - 0.2(1-\alpha)\frac{S_1}{S_o}K(H,P,1)\right]$.

Or $P(0) = P_e\left[1 - \Delta - 0.2(1-\alpha)\frac{K(H,P,1)}{P^2}\right]$. For H = 2 and P = 0.1, it can be shown that $\Delta = 0.054$ and K = 0.001. Thus $P(0) = P_e\left[0.946 - 0.02(1-\alpha)\right]$. For H = 2 and P = 0.01, it follows that $P(0) = P_e\left[0.99 - 0.02\ (1-\alpha)\right]$.

C. Temperature Gradients

It was observed in Section IIC that temperature gradients can arise at various places within the Knudsen cell and its contents from imperfect heating and from cooling of the solid surface due to the sublimation. This appendix consists of two distinct discussions of the effect of temperature gradients at the surface of the solid. Both

discussions are based on the Onsager relationships as formulated by DeGroot (51).

A common approach to sublimation is to consider that the atoms near the surface are moving about more or less freely. When an atom strikes the sublimation barrier it escapes if its energy is sufficient. That is sublimation is assumed to be rate limited by the movement of particles from a gas layer adjacent to the surface into the gas in the cell proper. The resulting let the temperature of the adjacent layer be T_1 and the temperature within the cell be T_2. The symbols S, μ, n, and H will have the same meanings as they have had throughout this thesis (e.g. Section IIB). U is the internal energy. The quantity T_1-T_2 is called ΔT. It is assumed that

$$\Delta T << T ,$$

where by definition,

$$T = \tfrac{1}{2}(T_1+T_2) .$$

The gas is assumed to be ideal. The entropy change can still be determined from

$$dS = \frac{dU}{T} - \frac{\mu}{T} dn.$$

The thermodynamic forces are chosen to be

$$X_n = -\Delta\left(\frac{\mu}{T}\right) \text{ and}$$

$$X_U = \Delta\left(\frac{1}{T}\right).$$

The conjugate fluxes are

$$J_n = -L_{11}\,\Delta\left(\frac{\mu}{T}\right) + L_{12}\,\Delta\left(\frac{1}{T}\right) \text{ and}$$

$$J_U = L_{22}\,\Delta\left(\frac{1}{T}\right) - L_{21}\,\Delta\left(\frac{\mu}{T}\right).$$

The quantities L_{ij} are Onsager's phenomenologic coefficients. Onsager's reciprocal relation is

$$L_{12} = L_{21}.$$

The quantity $\Delta\left(\frac{1}{T}\right)$ can be approximated by

$$\Delta\left(\frac{1}{T}\right) = -\frac{\Delta T}{T^2}.$$

The quantity $\Delta\left(\frac{\mu}{T}\right)$ is approximately

$$\Delta\left(\frac{\mu}{T}\right) = -\frac{\mu}{T^2}\Delta T + \frac{T\,\Delta\mu}{T^2}.$$

From elementary thermodynamics (e.g. Appendix A)

$$\Delta\mu = V\Delta P - S\Delta T, \text{ so}$$

$$\Delta\left(\frac{\mu}{T}\right) = -\frac{\mu}{T^2}\Delta T + \frac{V\Delta P}{T} - \frac{TS}{T^2}\Delta T = -\left(\frac{\mu+TS}{T^2}\right)\Delta T + \frac{V}{T}\Delta P.$$

But by definition

$$\mu + TS = H, \text{ so}$$

$$\Delta\left(\frac{\mu}{T}\right) = -\frac{H}{T^2}\Delta T + \frac{V}{T}\Delta P.$$

Therefore the fluxes can be rewritten

$$J_n = -\frac{L_{11}}{T}V\Delta P + \frac{L_{11}H - L_{12}}{T^2}\Delta T \text{ and } J_U = -\frac{L_{21}}{T}V\Delta P + \frac{L_{21}H - L_{22}}{T^2}\Delta T.$$

For $\Delta T = 0$ these reduce to

$$J_n = -\frac{L_{11}}{T} V \Delta P \text{ and } J_U = -\frac{L_{21}}{T} V \Delta P, \text{ so } J_U = \frac{L_{21}}{L_{11}} J_n .$$

This last equation relates the rate of energy transfer to the rate of mass flow. Therefore L_{21}/L_{11} is the average internal energy carried across a line by a mole of gas. For a gas with a Boltzmann velocity distribution L_{21}/L_{11} is given by

$$L_{21}/L_{11} = 2RT .$$

But by Onsager's reciprocal relation

$$L_{12}/L_{11} = 2RT .$$

For an ideal monomer gas

$$H = \frac{5}{2} RT .$$

Therefore one can write

$$\frac{J_n(\Delta T \neq 0)}{J\ (\Delta T = 0)} = 1 - \left(\frac{H - L_{12}/L_{11}}{RT^2}\right) \Delta T$$

$$= 1 - \frac{(5/2 - 2)R}{RT^2} \Delta T$$

$$= 1 - \tfrac{1}{2}(\Delta T/T) .$$

For the experiments reported in this thesis T is about 800°K. Therefore a temperature difference $\Delta T = 1.6°K$, the error in sublimation rate will be 0.1%.

(Ackerman, Thorn, and Winslow (50) have applied a similar analysis

to the case in which the sublimation rate is governed by direct passage of particles from the solid to the gas. Their equation is

$$J_n = \left[\frac{J_m - L_{11}\Delta(1/T)}{-\Delta(\mu/T)}\right]\Delta(1/T) + L_{22}\left[-\Delta(\mu/T) + H\Delta(1/T)\right], \text{ so}$$

$$\frac{J_n\left(\Delta(1/T) \neq 0\right)}{J_n\left(\Delta(1/T) = 0\right)} = 1 + \left[\frac{J_m - L_{11}\Delta(1/T)}{-\Delta(\mu/T)}\right] + L_{22}H\Delta(1/T).$$

Here J_n is the heat flux and J_m is the mass flux. The coefficient of $\Delta(1/T)$ is difficult to evaluate, so the equation is of no immediate use quantitatively.)

XII. APPENDIX D: MASS SPECTROMETER PARAMETERS

The mass spectrometer was described in detail in Section IIIB. This appendix will present the values of various parameters whose values were not critical to the success of the experiment. That is the experiments related in this thesis should be repeatable on many mass spectrometers, but the particular characteristics of the spectrometer employed in this work are presented here for completeness.

The ion optics can be described by reference to Figure 5. The voltages on the various plates were as follows:

Plate E, V = 0 volts

Plate D, V = 1300 volts

Plate C, V = 1600 volts

Plate B, V = 1900 volts

The slit widths were as follows:

Plate E, 0.003 inches

Plate D, 0.012 inches

Plate C had a 0.25 inches diameter circular hole instead of a slit. The distance between D and E was 1.25 inches, the distance between B and C was 0.125 inches, and the distance between C and D was 0.25 inches. Mr. Peter Sivgals of this laboratory has experimented with the effect of the voltages between B and C and between C and D. His tentative best focusing of Mg occurs with the voltages as follows:

Plate E, V = 0 volts

Plate D, V = 1550 volts

Plate C, V = 1775 volts

Plate B, V = 1900 volts

However Mr. Sivgals emphasizes the qualitative nature of his results so far.

The slit which served as an entrance to the multipliers was 0.013 inches wide.

The quantity A such that $M = AB^2$ relates the mass, M, of a singly charged ion to the field, B, which brought that ion into focus, was determined empirically. For this mass spectrometer $A \simeq 6$ amu/(k G)^2. That is Mg^{24} appeared at about 2 kilogauss.

The EBIS filament current was about 5 amperes. Typical values for the emission current and trap current for EBIS were 400 microamperes and 150 microamperes respectively. The accelerating voltage for the EBIS electrons was always of the order of 150-200 volts. Experiments on the effects of accelerating voltage on ΔH_{Mg} are discussed in Appendix B.

XIII. APPENDIX E: STATISTICAL EVALUATION OF THE ANALYSIS

This appendix will discuss various ways of analyzing the raw data obtained in this work. The final "best value" of Δ H might be estimated in many ways. For ease of discussion, these analyses may be grouped under two types, unweighted means and weighted means. Discussion will be facilitated by a typical example, Mg_2Ge (Table 3).

A. Unweighted Means

If there is no reason to count one of these Δ H (in this section the subscript Mg will be omitted for convenience) values more heavily than any other one, one is confronted with twelve measured values from which a "best value" is to be estimated. The choice of that best value will depend on the assumptions that are made as to the reason for the observed fluctuations in the measured values of Δ H. If these fluctuations arise as the result of four or more independent causes of roughly equal magnitude, each cause being distributed arbitrarily, then it can be shown (71) that the Gaussian distribution law describes the measurements quite accurately. The Gaussian (or normal) law of errors has been the subject of many extensive theoretical investigations, so powerful methods are available for analyzing Gaussian data. Also the given set of data points can be tested for normality. The best estimate of the true Δ H from this set of values is $\overline{\Delta H} = 1/n\left(\sum_{i=1}^{n} \Delta H_i\right) = 54.7$ kcal/mole if a Gaussian distribution is assumed. The best estimate of the variance, σ^2, is $\sigma^2 = \left(1/n-1\right)\sum (\Delta H_i - \overline{\Delta H})^2$. This estimate of σ^2 involves 12 Δ H values and one restriction, i.e. $\sum (\Delta H_i - \overline{\Delta H}) = 0$. Thus

it is said that σ^2 involves 12-1 = 11 degrees of freedom. For Mg_2Ge, $\sigma^2 = 13.2(\text{kcal/mole})^2$. Another estimate of the variance can be obtained by averaging the variances from loadings one and two. For loading one, $\overline{\Delta H_1} = 56.7$ kcal/mole and $\sigma_1^2 = 12.3(\text{kcal/mole})^2$ with three degrees of freedom. Similarly $\overline{\Delta H_2} = 53.7$ kcal/mole and $\sigma_2^2 = 10.1(\text{kcal/mole})^2$ with seven degrees of freedom. Hence $\overline{\sigma^2} = \frac{1}{2}(12.3 + 10.1) = 11.2(\text{kcal/mole})^2$ with ten degrees of freedom. A third estimate of σ^2 can be obtained from the two "data points" $\overline{\Delta H_1}$ and $\overline{\Delta H_2}$. In this case $\overline{\overline{\sigma^2}} = 5.03(\text{kcal/mole})^2$. Clearly other groupings of the given values could lead to other variance estimates, but these three estimates will suffice for the two tests that follow. It is a matter of simple algebra to show that these three estimates of σ^2 are not independent.

The distribution for the ratio of two independent estimates of the variance of a single Gaussian distribution can be calculated with the degrees of freedom of the two estimates as parameters. The probability that these variance ratios will exceed a given number is tabulated (71).

Consider $\sigma^2/\overline{\sigma^2} = 13.2/11.2 = 1.18$. The degrees of freedom of the numerator and denominator are eleven and ten respectively. 10% of the time this ratio could be expected to exceed 2.30 for a Gaussian population, so the analysis of variance does not contradict the normal distribution hypothesis. If indeed the distribution were normal, the effect of the parameter changed from loading one to loading two could be determined. In this case the factor varied was the orifice area. The $\overline{\overline{\sigma^2}}$ estimated from the scatter between the two loadings (5.03) is

compared with the $\overline{\sigma}^2$ estimated from the scatter within each run (11.2). The variance ratio is 5.03/11.2 = 0.449 with one and ten degrees of freedom in the numerator and denominator respectively. 10% of the time this ratio could be expected to exceed 3.29, so no correlation between orifice area and ΔH appears to be present.

The range of the ΔH values is $(\Delta H)_{MAX} - (\Delta H)_{MIN}$ = 60.58-49.52 = 11.06 kcal/mole. For a sample of 12, we expect (71) $\sigma \approx$ 0.3 x range = 3.32 kcal/mole for a Gaussian distribution. This compares with the best estimate $\sigma = \left[\frac{1}{n-1}\Sigma(\Delta H_i - \overline{\Delta H})^2\right]^{\frac{1}{2}}$ = 3.63 kcal/mole. This again does not refute the Gaussian hypothesis.

Although one cannot exclude the possibility of a Gaussian distribution on the basis of these statistics, other distributions are also possible. If one or two factors were the main causes of the fluctuations, then a highly non-normal distribution might result. This distribution might well be operative in these data. At least the statistics do not exclude that possibility. It would appear to be useful to ascertain as much information as possible without any assumption on the nature of the distribution, however in practice such generality can be gained only at great sacrifice of efficiency.

It is found that if subgroups of n members each are drawn from the original population, the means of the subgroups are far more likely to be normally distributed than are the members of the original population. Here it is necessary that n be at least 3 or 4. In the case of Mg_2Ge, the twelve runs can be partitioned into three groups of four in $0.665X10^7$ ways. It can be partitioned into four groups of three

2.00×10^7 ways.

Consider the grouping (1B, 1C, 1D), (1E, 2A, 2C), (2D, 2E, 2F), (2G, 2H, 2I). The mean $\overline{\Delta H}$ values are 56.03, 56.28, 54.26, and 52.30 kcal/mole. Thus the best $\overline{\Delta H}$ = 54.72 kcal/mole and σ = 1.85 kcal/mole. The grouping (1B, 1C, 1D, 1E), (2A, 2C, 2D, 2E), (2F, 2G, 2H, 2I) yields $\overline{\Delta H}$ = 54.72 kcal/mole and σ = 1.74 kcal/mole.

Clearly any such grouping will yield $\overline{\Delta H}$ = 54.72 kcal/mole but σ will vary with the grouping. An average σ would appear to be about 1.80 kcal/mole.

Strictly, the quantity $\left[\frac{1}{n-1}\Sigma(\Delta H_i - \overline{\Delta H})^2\right]^{\frac{1}{2}}$ should be labeled s rather than σ to distinguish s from the true σ which characterizes the normal distribution. However it is possible to get confidence intervals from s as described in Wilson (71). Thus for twelve samples the 95% confidence interval is $\overline{\Delta H} \pm 0.63\underline{s}$.

The interesting fact about the unweighted means is that in every case the best value of ΔH is $\overline{\Delta H} = \frac{1}{n}\Sigma \Delta H$ = 54.72 kcal/mole. The error involved seems to depend quite strongly on how that error is calculated.

B. Weighted Means

The unweighted means do not utilize all of the available information. An example of unutilized data is the number of points taken in each run. If the data consisted of one run with two points and another run of 100 points, it would not seem reasonable to count the two runs equally. In the case of Mg_2Ge the number of points per run varies from 15 to 36. One reasonable way of taking this into account is to weight each run by the number of points it contains. In this case the result of this

procedure is $\overline{\Delta H} = 55.24$ kcal/mole. The weighted σ is 0.99 kcal/mole.

Finally if it is assumed that the factors which cause run-to-run variations are also the factors that cause scatter within each run, the scatter of the run is related to the accuracy with which that run reflects the true ΔH. In this case the analysis of Section IVC applies, and $\overline{\Delta H} = 54.4 \pm 1.1$ kcal/mole.

It is thus apparent that the mean and the statistical error are functions of the method of analysis. From the data taken on Mg_2Ge the $\overline{\Delta H}$ values 54.7 ± 3.6, 54.7 ± 1.8, 55.2 ± 1.0, and 54.4 ± 1.1 kcal/mole could all be obtained by some sort of analysis. All of the analyses are of types applied to similar data in the literature.

The choice of statistical analysis represented by Section IVC was made in the belief that the greater the internal consistency of the run the greater the accuracy of the resulting ΔH. This has not been proved. Rather it is what appears to this author to be the most plausible assumption.

XIV. APPENDIX F: DATA FOR GRAPHS AND DISCUSSION

This appendix contains the data points used in plotting the typical runs for Mg_2Si, Mg_2Ge, Mg_2Sn, Mg_2Pb, and Eu, as well as the temperature ranges for Mg_2Sn and Mg_2Pb.

Table 13. Mg Si - Run 1A

Point number	I (arbitrary units)	T (^oK)
1	97.7	909
2	88.6	907
3	76.2	902
4	69.3	898
5	61.8	895
6	56.5	891
7	51.3	887
8	45.3	883
9	39.9	879
10	35.3	874
11	29.7	869
12	25.1	863
13	20.8	856
14	17.3	850
15	14.3	844
16	11.6	836
17	9.2	829
18	7.2	822
19	58.8	895

Table 14. Mg_2Ge - Run 2H

Point number	I (arbitrary units	T (^oK)
1	92.9	904
2	85.3	900
3	73.7	897

Table 14. (Continued)

Point number	I (arbitrary units)	T (^{o}K)
4	63.9	892
5	56.7	888
6	47.8	883
7	41.5	879
8	34.9	875
9	31.9	870
10	25.6	865
11	22.6	861
12	20.1	858
13	17.7	854
14	15.1	850
15	13.7	846
16	11.1	841
17	9.3	837

Table 15. Mg_2Sn - Run 3D

Run number	I (arbitrary units)	T (^{o}K)
1	252	869
2	195	861
3	144	849
4	113	842
5	88	831
6	67.1	823
7	50.5	814
8	37.6	804
9	28.9	796
10	19.1	785

Table 16. Mg_2Pb - Run 1C

Run number	I (arbitrary units)	T (^oK)
1	154	809
2	145	807
3	124	803
4	86.5	787
5	74.2	780
6	60.4	775
7	53.8	770
8	91.2	788
9	77.1	782
10	67.5	778
11	54.4	769
12	45.1	763
13	40.9	758
14	33.8	752
15	29.3	747
16	24.0	740
17	21.4	735
18	17.9	728
19	16.1	723
20	15.5	722
21	13.5	719
22	9.9	709

Table 17. Eu - Run 1E

Run number	I (arbitrary units)	T (^oK)
1	99.2	822
2	78.3	814
3	59.9	805
4	46.5	797
5	33.6	786
6	24.5	777
7	17.4	766
8	13.5	758
9	9.0	748
10	7.1	741

Table 18. Temperature ranges for Mg_2Sn runs in descending order

Run number	Temperature range (°K)	ΔH_{Mg} (kcal/mole)
1A	104	54.57
2A	93	41.26
3D	84	42.29
2B	83	41.16
2C	83	38.62
3C	82	43.92
3B	81	38.38
3E	81	41.85
3A	80	41.40
1C	80	46.25
1D	78	50.84
1E	74	39.50
1B	66	47.71

Table 19. Temperature ranges for Mg_2Pb runs in descending order

Point number	Temperature range (°K)	ΔH_{Mg} (kcal/mole)
1C	100	31.98
1A	98	39.34
1B	86	32.70
2A	83	36.78
1G	79	35.98
1F	78	32.30
1H	78	31.49
1D	77	34.67
2C	74	36.21
1E	73	32.68
2B	72	32.54
1I	71	35.27
1J	63	33.30

EXPERIMENTAL PHYSICS GROUP V

Sample Mg_2Ge Run 2D Isotope Mg 24 Field 1.99 KG
Orifice diameter 30 mils Pressure $8X10^{-7}$ mm EBIS 60 a
Multiplier Voltage 2.03 KV Experimentalist H.J.C. Date 1/17/61

EXPERIMENTAL DATA

Point no.	Upper reading	Lower reading	Upper-lower	t' (mv)	t (°C)	T (°K)	1000/T (°K^{-1})
1	85.2	3.1	82.1	5.955	635	908	1.101
2	74.2	2.2	72.0	5.906	630	903	1.107
3	67.3	2.1	65.2	5.860	626	899	1.112
4	60.0	1.6	58.4	5.816	622	895	1.117
5	53.4	0.9	52.5	5.768	618	891	1.122
6	45.2	0.9	44.3	5.720	614	887	1.127
7	40.8	0.7	40.1	5.660	609	882	1.134
8	33.4	0.4	33.0	5.608	604	877	1.140
9	31.0	0.6	30.4	5.559	600	873	1.145
10	24.8	0.3	24.5	5.501	594	867	1.153
11	22.3	0.2	22.1	5.450	590	863	1.159
12	17.8	0.3	17.5	5.393	585	858	1.166
13	14.6	0.1	14.5	5.341	580	853	1.172
14	12.0	0.1	11.9	5.281	575	848	1.179
15	69.1	1.8	67.3	5.868	627	900	1.111

Figure 17. Sample data sheet